LITHOS

The nature of the mantle beneath La Grille volcano (Grande Comore Island, western Indian Ocean) as revealed by mineral chemistry, noble gas geochemistry, CO2 abundance and radiogenic isotopes of ultramafic mantle xenoliths

--Manuscript Draft--

Manuscript Number:	
Article Type:	VSI:EMAW2022
Keywords:	Comoros Archipelago, mantle xenoliths, mineral chemistry, noble gases, fluid inclusions, radiogenic isotopes
Corresponding Author:	Barbara Faccini, Ph.D University of Ferrara Ferrara, Ferrara ITALY
First Author:	Claudio Ventura Bordenca
Order of Authors:	Claudio Ventura Bordenca
	Barbara Faccini, Ph.D
	Antonio Caracausi
	Massimo Coltorti
	Andrea Di Muro
	Raphaël Pik
	Andrea Luca Rizzo
	Marco Liuzzo
	Alessandro Aiuppa
Abstract:	Petrology and geochemistry of fluid inclusions (FI) are increasingly used in tandem to constrain the compositional features and evolution of the lithospheric mantle. In this study, we combine petrography and mineral chemistry with analyses of noble gases (He, Ne and Ar) and CO2 in olivine-, opx- and cpx-hosted FI, as well as radiogenic isotope (Sr-Nd-Pb) systematics of ultramafic xenoliths collected at La Grille volcano in Grande Comore Island, aiming at better characterizing one of the most controversial portions of the western Indian Ocean lithospheric mantle. Xenoliths have been divided in three groups on the basis of their textural features: Group 1 (Opx-bearing), characterized by protogranular to porphyroclastic texture overprinted by metasomatic reactions; Group 2 (Opx-free), with ad-cumulitic, infiltrated characteristics, and Group 3 (Cumulate), showing ortho-cumulitic texture. Overall, petrographic observations and mineral phase compositions indicate that the sampled lithospheric portion experienced variable degrees of melting (from 5% to 35%), recorded by Group 1 most refractory harzburgites and lherzolites, as well as modal metasomatic processes as evidenced by the severe crystallization of cpx at the expenses of opx in Group 1 fertile lherzolites and wehrlite and by Group 2 xenoliths. Crystallization of slightly oversaturated basic silicate melts seems also to have occurred, as shown by Group 3 xenolith. The calculated equilibration temperatures range from 930 ◦C to 1180 ◦C with oxygen fugacity values between −0.93 and +0.71 ΔlogƒO2 [FMQ], with Group 1 tending to be the most reduced and the coldest. A positive trend between temperature and ƒO2 can be envisaged, with Group 2 and 3 xenoliths testifying for hotter and more oxidised conditions than Group 1. The variability of the 4He/40Ar* ratio (0.02-0.39) in Group 1, significantly below typical values of a fertile mantle (4He/40Ar* = 1-5), can be explained by the variable degrees of partial melting coupled to metasomatism enrichment that may account for modifying 4He/40Ar*, as also indicated by the mineral composition. He-Ar-CO2 relationships support the presence of a metasomatic CO2-rich process post-dating the melt extraction and the cumulite formation event and affecting their relative abundances, as suggested by Coltorti et al. (1999). The air-corrected 3He/4He isotopic ratios (6.30 to 7.36 Ra) are intermediate between the MORB mantle signature (8±1Ra, Mid-Ocean Ridge Basalt) and the SCLM (6.1±0.9Ra, Sub-Continental Lithospheric Mantle). The Ne and Ar isotopic signatures (20Ne/22Ne, 21/Ne/22Ne and

	40Ar/36Ar) are consistent with mixing between an air-derived component and a MORB-like mantle, supporting the hypothesis for a lithospheric origin of the Comoros magmas, and arguing against any deep mantle plume-related contribution. This is also corroborated by combining Ne with He isotopes, showing that La Grille ultramafic xenoliths are far from the typical plume-type compositions. Sr-Nd-Pb isotope systematics in Opx and Cpx from La Grille additionally support a MORB-type signature for the lithospheric mantle beneath La Grille. In summary, our investigation reveals that the La Grille ultramafic xenoliths record variable degrees of partial melting (Group 1) of a MORB-type mantle and metasomatic processes (all Groups), without necessarily requiring the influence of a deep mantle plume beneath the Comoros Archipelago as previously inferred.
Suggested Reviewers:	Ray Burgess The University of Manchester Department of Earth and Environmental Sciences ray.burgess@manchester.ac.uk Expert in noble gases
	Patrick Bachèlery University of Clermont Auvergne P.Bachelery@opgc.fr Familiar with the geology of the studied area
	Rita Parai Washington University in St Louis parai@wustl.edu Expert in noble gases isotopic geochemistry
	Cornelia Class Lamont-Doherty Earth Observatory class@ldeo.columbia.edu Expert of the studied area
Opposed Reviewers:	

The nature of the mantle beneath La Grille volcano (Grande Comore Island, western Indian Ocean) as revealed by mineral chemistry, noble gas geochemistry, CO_2 abundance and radiogenic isotopes of ultramafic mantle xenoliths

Claudio Ventura Bordenca [a,1], Barbara Faccini [b,*], Antonio Caracausi [c], Massimo Coltorti [b,c], Andrea Di Muro [d,e], Raphaël Pik [f], Andrea Luca Rizzo [c,g], Marco Liuzzo [b,c], Alessandro Aiuppa [a]

[a] Dipartimento di Scienze della Terra e del Mare (DiSTeM), Università di Palermo, Via Archirafi 36, 90143 Palermo, Italy
[b] Department of Physics and Earth Sciences, University of Ferrara, Via Saragat 1, 44121 Ferrara, Italy
[c] Istituto Nazionale di Geofisica e Vulcanologia, Sezione di Palermo, Via Ugo La Malfa 153, 90146 Palermo, Italy
[d] Institut de Physique du Globe de Paris, CNRS, Université de Paris, 75005 Paris, France
[e] Observatoire Volcanologique du Piton de la Fournaise, Institut de Physique du Globe de Paris, La Plaine des Cafres, 75005 Paris, France
[f] CRPG, UMR 7358 CNRS-Université de Lorraine, BP 20, 15 rue Notre-Dame des Pauvres, 54500 Vandœuvre-lès-Nancy, France
[g] Istituto Nazionale di Geofisica e Vulcanologia, Sezione di Milano, Via Alfonso Corti 12, 20133 Milano, Italy

[*] Corresponding author: barbara.faccini@unife.it (B. Faccini)

[1] **Present address:** Dipartimento di Fisica e Chimica "Emilio Segrè", Università di Palermo, Viale delle Scienze 90128, Palermo, Italy

Cover letter

Università degli Studi di Ferrara

DIPARTIMENTO DELL'AMBIENTE E DELLA PREVENZIONE
UNIVERSITÀ DI FERRARA
Dr. Barbara Faccini

Ferrara, January, 17th, 2023

Dear Editors

I am pleased to submit an original article entitled " **The nature of the mantle beneath La Grille volcano (Grande Comore Island, western Indian Ocean) as revealed by mineral chemistry, noble gas geochemistry, CO_2 abundance and radiogenic isotopes of ultramafic mantle xenoliths**" by Claudio Ventura Bordenca, Barbara Faccini, Antonio Caracausi, Massimo Coltorti, Andrea Di Muro, Raphaël Pik, Andrea Luca Rizzo, Marco Liuzzo and Alessandro Aiuppa for publication on the Lithos Special Issue "EMAW2022".

In this paper, we report a complete petrographic, petrological (major-element mineral chemistry) and first ever geochemical investigation of noble gases (He, Ne and Ar) and CO_2 in orthopyroxene-, clinopyroxene- and olivine-hosted fluid inclusions from ultramafic xenoliths collected at La Grille volcano, Grand Comore Island. Our investigation reveals that the La Grille ultramafic xenoliths record variable degrees of partial melting of a MORB-type mantle and metasomatic processes, without necessarily requiring the influence of a deep mantle plume beneath the Comoros Archipelago.

We suggest the following scientists that are competent on topics related to our work as reviewers:

Cornelia Class
Lamont-Doherty Earth Observatory of Columbia University, Palisades, New York 10964, USA.
Email: class@ldeo.columbia.edu

Ray Burgess
Department of Earth and Environmental Sciences, University of Manchester, Manchester, UK.
Email: ray.burgess@manchester.ac.uk

Patrick Bachèlery
Université de La Rèunion, Laboratoires GéoSciences Rèunion, F-97744, Saint-Denis, France.
Laboratiore Magma et Volcans, Université Clermont Auvergne – CNRS-IRD, OPGC, Campus Universitaire des Cézeaux, 6 Avenue Blaise Pascal, 63178 Aubière Cedex, France.

Email: P.Bachelery@opgc.fr

Rita Parai
Department of Earth and Planetary Sciences, and McDonnel Center for Space Sciences, Washington University in St. Louis, St. Louis, MO, USA.
Email: parai@wustl.edu

We remain at your disposal for any editorial requirements.
Thank you for your consideration.

Sincerely
For the authors
Barbara Faccini

The nature of the mantle beneath La Grille volcano (Grande Comore Island, western Indian Ocean) as revealed by mineral chemistry, noble gas geochemistry, CO_2 abundance and radiogenic isotopes of ultramafic mantle xenoliths

Claudio Ventura Bordenca [a,1], Barbara Faccini [b,*], Antonio Caracausi [c], Massimo Coltorti [b,c], Andrea Di Muro [d,e], Raphaël Pik [f], Andrea Luca Rizzo [c,g], Marco Liuzzo [b,c], Alessandro Aiuppa [a]

[a] Dipartimento di Scienze della Terra e del Mare (DiSTeM), Università di Palermo, Via Archirafi 36, 90143 Palermo, Italy
[b] Department of Physics and Earth Sciences, University of Ferrara, Via Saragat 1, 44121 Ferrara, Italy
[c] Istituto Nazionale di Geofisica e Vulcanologia, Sezione di Palermo, Via Ugo La Malfa 153, 90146 Palermo, Italy
[d] Institut de Physique du Globe de Paris, CNRS, Université de Paris, 75005 Paris, France
[e] Observatoire Volcanologique du Piton de la Fournaise, Institut de Physique du Globe de Paris, La Plaine des Cafres, 75005 Paris, France
[f] CRPG, UMR 7358 CNRS-Université de Lorraine, BP 20, 15 rue Notre-Dame des Pauvres, 54500 Vandœuvre-lès-Nancy, France
[g] Istituto Nazionale di Geofisica e Vulcanologia, Sezione di Milano, Via Alfonso Corti 12, 20133 Milano, Italy

[*] Corresponding author: barbara.faccini@unife.it (B. Faccini)

ABSTRACT

Petrology and geochemistry of fluid inclusions (FI) are increasingly used in tandem to constrain the compositional features and evolution of the lithospheric mantle. In this study, we combine petrography and mineral chemistry with analyses of noble gases (He, Ne and Ar) and CO_2 in olivine-, opx- and cpx-hosted FI, as well as radiogenic isotope (Sr-Nd-Pb) systematics of ultramafic xenoliths collected at La Grille volcano in Grande Comore Island, aiming at better characterizing one of the most controversial portions of the western Indian Ocean lithospheric mantle. Xenoliths have been divided in three groups on the basis of their textural features: Group 1 (Opx-bearing), characterized by protogranular to porphyroclastic texture overprinted by metasomatic reactions; Group 2 (Opx-free), with ad-cumulitic, infiltrated characteristics, and Group 3 (Cumulate), showing ortho-cumulitic texture. Overall, petrographic observations and mineral phase compositions indicate that the sampled lithospheric portion experienced variable degrees of melting (from 5% to 35%), recorded by Group 1 most refractory harzburgites and lherzolites, as well as modal metasomatic processes as evidenced by the severe crystallization of cpx at the expenses of opx in Group 1 fertile lherzolites and wehrlite and by Group 2 xenoliths. Crystallization of slightly oversaturated basic silicate melts seems also to have occurred, as shown by Group 3 xenolith. The calculated equilibration temperatures range from 930 °C to 1180 °C with oxygen fugacity values between −0.93 and +0.71 $\Delta\log fO2$ [FMQ], with Group 1 tending to be the most reduced and the coldest. A positive trend between temperature and fO_2 can be envisaged, with Group 2 and 3 xenoliths testifying for hotter and more oxidised conditions than Group 1. The variability of the $^4He/^{40}Ar^*$ ratio (0.02-0.39) in Group 1, significantly below typical

[1] **Present address:** Dipartimento di Fisica e Chimica "Emilio Segrè", Università di Palermo, Viale delle Scienze 90128, Palermo, Italy

values of a fertile mantle ($^4He/^{40}Ar^*$ = 1-5), can be explained by the variable degrees of partial melting coupled to metasomatism enrichment that may account for modifying $^4He/^{40}Ar^*$, as also indicated by the mineral composition. He-Ar-CO_2 relationships support the presence of a metasomatic CO_2-rich process post-dating the melt extraction and the cumulite formation event and affecting their relative abundances, as suggested by **Coltorti et al. (1999)**. The air-corrected $^3He/^4He$ isotopic ratios (6.30 to 7.36 Ra) are intermediate between the MORB mantle signature (8±1Ra, Mid-Ocean Ridge Basalt) and the SCLM (6.1±0.9Ra, Sub-Continental Lithospheric Mantle). The Ne and Ar isotopic signatures ($^{20}Ne/^{22}Ne$, $^{21}/Ne/^{22}Ne$ and $^{40}Ar/^{36}Ar$) are consistent with mixing between an air-derived component and a MORB-like mantle, supporting the hypothesis for a lithospheric origin of the Comoros magmas, and arguing against any deep mantle plume-related contribution. This is also corroborated by combining Ne with He isotopes, showing that La Grille ultramafic xenoliths are far from the typical plume-type compositions. Sr-Nd-Pb isotope systematics in Opx and Cpx from La Grille additionally support a MORB-type signature for the lithospheric mantle beneath La Grille.

In summary, our investigation reveals that the La Grille ultramafic xenoliths record variable degrees of partial melting (Group 1) of a MORB-type mantle and metasomatic processes (all Groups), without necessarily requiring the influence of a deep mantle plume beneath the Comoros Archipelago as previously inferred.

HIGHLIGHTS

- Petrography, mineral chemistry, noble gases and CO_2 in mineral-hosted fluid inclusions, and Sr-Nd-Pb systematics of ultramafic xenoliths from La Grille volcano have been combined to unravel the processes in the lithospheric mantle beneath Grande Comore Island.
- The lithospheric mantle experienced variable degrees of melting (from 5% to 35%), as well as modal metasomatic processes with crystallization of clinopyroxene at the expense of orthopyroxene, leading to wehrlite formation.
- He-Ar-CO_2 relationships support the presence of a metasomatic CO_2-rich process post-dating the melt extraction.
- The air-corrected $^3He/^4He$ isotopic ratios (6.30 to 7.36 Ra) are intermediate between the MORB mantle signature (8±1Ra) and the SCLM (6.1±0.9Ra).
- The features of the lithospheric mantle beneath La Grille can be explained without necessarily requiring the influence of a deep mantle plume.

The nature of the mantle beneath La Grille volcano (Grande Comore Island, western Indian Ocean) as revealed by mineral chemistry, noble gas geochemistry, CO_2 abundance and radiogenic isotopes of ultramafic mantle xenoliths

Claudio Ventura Bordenca [a,1], Barbara Faccini [b,*], Antonio Caracausi [c], Massimo Coltorti [b,c], Andrea Di Muro [d,e], Raphaël Pik [f], Andrea Luca Rizzo [c,g], Marco Liuzzo [b,c], Alessandro Aiuppa [a]

[a] Dipartimento di Scienze della Terra e del Mare (DiSTeM), Università di Palermo, Via Archirafi 36, 90143 Palermo, Italy
[b] Department of Physics and Earth Sciences, University of Ferrara, Via Saragat 1, 44121 Ferrara, Italy
[c] Istituto Nazionale di Geofisica e Vulcanologia, Sezione di Palermo, Via Ugo La Malfa 153, 90146 Palermo, Italy
[d] Institut de Physique du Globe de Paris, CNRS, Université de Paris, 75005 Paris, France
[e] Observatoire Volcanologique du Piton de la Fournaise, Institut de Physique du Globe de Paris, La Plaine des Cafres, 75005 Paris, France
[f] CRPG, UMR 7358 CNRS-Université de Lorraine, BP 20, 15 rue Notre-Dame des Pauvres, 54500 Vandœuvre-lès-Nancy, France
[g] Istituto Nazionale di Geofisica e Vulcanologia, Sezione di Milano, Via Alfonso Corti 12, 20133 Milano, Italy

[*] Corresponding author: barbara.faccini@unife.it (B. Faccini)

ABSTRACT

Petrology and geochemistry of fluid inclusions (FI) are increasingly used in tandem to constrain the compositional features and evolution of the lithospheric mantle. In this study, we combine petrography and mineral chemistry with analyses of noble gases (He, Ne and Ar) and CO_2 in olivine-, opx- and cpx-hosted FI, as well as radiogenic isotope (Sr-Nd-Pb) systematics of ultramafic xenoliths collected at La Grille volcano in Grande Comore Island, aiming at better characterizing one of the most controversial portions of the western Indian Ocean lithospheric mantle. Xenoliths have been divided in three groups on the basis of their textural features: Group 1 (Opx-bearing), characterized by protogranular to porphyroclastic texture overprinted by metasomatic reactions; Group 2 (Opx-free), with ad-cumulitic, infiltrated characteristics, and Group 3 (Cumulate), showing ortho-cumulitic texture. Overall, petrographic observations and mineral phase compositions indicate that the sampled lithospheric portion experienced variable degrees of melting (from 5% to 35%), recorded by Group 1 most refractory harzburgites and lherzolites, as well as modal metasomatic processes as evidenced by the severe crystallization of cpx at the expenses of opx in Group 1 fertile lherzolites and wehrlite and by Group 2 xenoliths. Crystallization of slightly oversaturated basic silicate melts seems also to have occurred, as shown by Group 3 xenolith. The calculated equilibration temperatures range from 930 °C to 1180 °C with oxygen fugacity values between −0.93 and +0.71 Δlog$f$O2 [FMQ], with Group 1 tending to be the most reduced and the coldest. A positive trend between temperature and fO_2 can

[1] **Present address:** Dipartimento di Fisica e Chimica "Emilio Segrè", Università di Palermo, Viale delle Scienze 90128, Palermo, Italy

be envisaged, with Group 2 and 3 xenoliths testifying for hotter and more oxidised conditions than Group 1. The variability of the $^{4}He/^{40}Ar^{*}$ ratio (0.02-0.39) in Group 1, significantly below typical values of a fertile mantle ($^{4}He/^{40}Ar^{*}$ = 1-5), can be explained by the variable degrees of partial melting coupled to metasomatism enrichment that may account for modifying $^{4}He/^{40}Ar^{*}$, as also indicated by the mineral composition. He-Ar-CO_2 relationships support the presence of a metasomatic CO_2-rich process post-dating the melt extraction and the cumulite formation event and affecting their relative abundances, as suggested by **Coltorti et al. (1999)**. The air-corrected $^{3}He/^{4}He$ isotopic ratios (6.30 to 7.36 Ra) are intermediate between the MORB mantle signature (8±1Ra, Mid-Ocean Ridge Basalt) and the SCLM (6.1±0.9Ra, Sub-Continental Lithospheric Mantle). The Ne and Ar isotopic signatures ($^{20}Ne/^{22}Ne$, ^{21}/Ne/^{22}Ne and $^{40}Ar/^{36}Ar$) are consistent with mixing between an air-derived component and a MORB-like mantle, supporting the hypothesis for a lithospheric origin of the Comoros magmas, and arguing against any deep mantle plume-related contribution. This is also corroborated by combining Ne with He isotopes, showing that La Grille ultramafic xenoliths are far from the typical plume-type compositions. Sr-Nd-Pb isotope systematics in Opx and Cpx from La Grille additionally support a MORB-type signature for the lithospheric mantle beneath La Grille.
In summary, our investigation reveals that the La Grille ultramafic xenoliths record variable degrees of partial melting (Group 1) of a MORB-type mantle and metasomatic processes (all Groups), without necessarily requiring the influence of a deep mantle plume beneath the Comoros Archipelago as previously inferred.

Keywords: *Comoros Archipelago, mantle xenoliths, mineral chemistry, noble gases, fluid inclusions, radiogenic isotopes*

1. Introduction

Oceanic and continental magmas allow characterizing mantle heterogeneities and their possible evolution since the Earth formation (**e.g., Broadley et al., 2021; Graham, 2002; Hilton et al., 2002; Marty et al., 2021**). Such mantle heterogeneities, and the processes that determine them, are still matter of debate and represent the target of multidisciplinary investigations (**e.g., Davies, 2009; Jackson et al., 2018, 2021**). Combining petrography, mineral chemistry and fluid inclusions (FI) composition (noble gases and CO_2) in minerals from ultramafic xenoliths has proven to be an efficient tool for constraining the geochemical characteristics and understanding the evolution of specific portions of the lithospheric mantle, as well as for identifying the chemical processes that affect its pristine composition such as melting and metasomatic events (**e.g., Correale et al., 2012, 2016, 2019; Faccini et al., 2020; Martelli et al., 2011; Rizzo et al., 2018, 2021**). In this regard, the Comoros Archipelago in the western Indian Ocean, where the characteristics of the local lithospheric mantle are intimately related to a complex and debated geodynamic setting (**e.g.**, **Bachelery et al., 2016; Famin et al., 2020**), offers an intriguing opportunity to use such an approach. The Comoros Archipelago is located in the northern edge of the Mozambique Channel between the northern tip of Madagascar and the eastern coast of Mozambique (**Fig.1a**), and includes four major volcanic islands (**Fig.1b**): from west to east, Grand Comore, Moheli, Anjouan and Mayotte, followed by a series of poorly known submarine volcanic banks and submerged reef platforms (**Daniel et al., 1972; Tzevahirtzian et al., 2021**). Grande Comore Island is a volcanic doublet composed by two main coalescing shields: La Grille, located in the north, and the large edifice of Karthala in the south (**Fig. 1c**). La Grille volcano, mostly active during the Pleistocene, is characterized by eroded and weathered lava flows associated with a series of large monogenetic scoria cones (**Bachelery et al., 2016; Bachelery and Coudray, 1990**), while Karthala is the second most active volcano of the Indian Ocean (after Piton de la Fournaise at the Reunion Island), with its most recent volcanic eruption in January 2007 (**Thivet et al., 2022**). Alkali basalts, including oceanites (olivine-rich basalts) and ankaramites (pyroxene-rich basalts), are the most common lithotypes at Karthala volcano, whereas La Grille products are markedly more silica-undersaturated, ranging from basanites to nephelinites (**Späth et al., 1996; Strong, 1972**). Subaerial Holocene volcanic activity, ranging in compositions from basanite to phonolite, has been documented in all four islands (**Bachélery et al., 2016; Berthod et al., 2021a, b; Quidelleur et al., 2022**). Lavas from La Grille often enclose abundant cm- to dm- sized ultramafic xenoliths (**Bachelery and Coudray, 1993; Coltorti et al., 1999; Strong, 1972**). In the present paper, we report on a complete petrographic, petrological (major-element mineral chemistry) and first ever geochemical investigation of noble gases (He, Ne and Ar) and CO_2 in orthopyroxene-, clinopyroxene- and olivine-hosted FI from ultramafic xenoliths collected at La Grille volcano. Previous investigations of La Grille lithotypes have been mainly focused on bulk samples and mineral separates from lavas (**Class et al., 1998; Class et al., 2005; Class and Goldstein, 1997**), although petrological and geochemical data from clinopyroxenes and glasses of ultramafic xenoliths from La Grille were discussed by **Coltorti et al., 1999**. The investigation of these ultramafic xenoliths can help to shed light and deepen our current knowledge on the compositional features of the mantle below

Grande Comore Island. A renewal of multidisciplinary investigations on the sources of the volcanic activity of this archipelago was also stimulated by the intense volcano-tectonic crisis starting in May 2018 and still ongoing, leading to the formation of a huge submarine (3.5 km depth bsl) volcanic edifice about 50 km offshore east of Mayotte (**Berthod et al., 2021a, b; Cesca et al., 2020; Feuillet et al., 2021; Lemoine et al., 2020; Liuzzo et al., 2021**). At Mayotte, magma differentiation in the upper mantle (1.2 GPa) has been recently suggested from phenocryst composition in basanitic to tephritic magmas. Ultramafic xenoliths, occurring both in basanite and phonolite lavas, record surprisingly low re-equilibration pressures (< 0.6 GPa), corresponding to that inferred for the local Moho depth (**Berthod et al., 2021a**). Finally, our detailed study aims also at contributing to define the geochemical dataset of the Comoros Archipelago with important implications for the development of geochemical monitoring of one of the most active and potentially hazardous regions of the Indian Ocean (**Liuzzo et al., 2021, 2022**).

2. Geodynamic context

The Comoros archipelago is one of the most active seismic and magmatic sectors of the western Indian Ocean (**Berthod et al., 2021a, b; Cesca et al., 2020; Deville et al., 2018; Famin et al., 2020; Feuillet et al., 2021; Franke et al., 2015; Heidbach et al., 2016; Lemoine et al., 2020; Michon et al., 2016; Rindraharisaona et al., 2013; Saria et al., 2014; Stamps et al., 2018; Thivet et al., 2022**), but its tectonic features are far from being unambiguously defined. In fact, the origin of the Comoros magmatism has been ascribed to either lithospheric migration above a relatively stationary plume-related hot spot (**Class et al., 1998; Claude-Ivanaj et al., 1998; Deniel, 1998; Emerick and Duncan, 1982; Hajash and Armstrong, 1972**) or to passive response of lithospheric break-up due to activation of a very slowly spreading ridge axis dissected by transform zones (**Courtillot et al., 2003; Nougier et al., 1986; Upton, 1982**). According to the latest interpretations, the volcanic alignment of the Comoros Archipelago would represent a NW-SE-trending tectonic boundary between the Somali plate and the Lwandle microplate and part of the SE prolongation of the East African Rift System, a broad deformation zone characterized by intense seismicity extending from the African coast in the west to the northern half of Madagascar in the east (**Cesca et al., 2020; Courgeon et al., 2018; Deville et al., 2018; Famin et al., 2020; Franke et al., 2015; Lemoine et al., 2020; Michon et al. 2016; Saria et al., 2014; Stamps et al., 2018, 2021**). The few absolute ages available in the literature from the emerged sector of the volcanic edifices indicate that magmatic activity of the

Comoros Archipelago began in the Mio-Pliocene and was diachronous in all four volcanic islands (Mayotte, 10.6 ± 0.5 Ma to ~6 ka; Anjouan, 11.1 ± 0.5 to 0.36 ± 0.09 Ma; Moheli, 5.0 ± 0.4 Ma to 0.48 ± 0.15 Ma; Grande Comore, 0.13 ± 0.02 Ma to present) (**Debeuf, 2004; Emerick and Duncan, 1982; Hajash and Armstrong, 1972; Montaggioni and Nougier, 1981; Nougier et al., 1986; Pelleter et al., 2014; Quidelleur et al., 2022; Zinke et al., 2003, 2005**). Based on magma production rate, **Michon, 2016** estimated the submarine onset of magmatic activity of the Comoros Archipelago at around 20 Ma ago in Mayotte and, almost simultaneously, 10 Ma ago in Anjouan, Moheli and Grande Comore. This magmatism is coeval with other volcanic provinces around the Mozambique Channel, i.e., East African Rift System and the central-northern Madagascar whose magmatic periods date back the upper Oligocene (**Cucciniello et al., 2011; Roberts et al., 2012**).

It is matter of debate whether volcanic activity in the Comoros Archipelago developed on either continental (**Esson et al., 1970; Flower and Strong, 1969; Lacroix, 1922; Lort et al., 1979**) or oceanic crust (**Cochran, 1988; Coffin and Rabinowitz, 1987; Phethean et al., 2016; Rabinowitz et al., 1983; Talwani, 1962**). Recently, new geophysical data strongly support a dual nature of the underlying crust in the region surrounding the Comoros Archipelago (**Dofal et al., 2021 and references therein**), and suggest the occurrence of continental crust in the form of thinned crustal slices in the western and southern sectors of the Comoros basin (**Roach et al., 2017; Vormann et al., 2020**), and oceanic crust in the northern part (**Klimke et al., 2016; Vormann et al., 2020**), thus casting further questions on the continental-oceanic transition in the northern Mozambique Channel.

3. Sampling and analytical methods

3.1 Sample preparation

Ultramafic xenoliths were collected on the north-eastern coast of Grande Comore Island (La Grille volcano; **Fig. 1c**) during two field campaigns (2017-2018). All the xenoliths were embedded within basanitic lavas. Samples were cut, sliced and polished in order to define modal composition, petrography and mineral chemistry. After crushing and sieving of the xenoliths, orthopyroxene, clinopyroxene and olivine (Opx, Cpx, and Ol) crystals larger than 0.5 mm size-fraction were handpicked with binocular microscope for noble gas (He, Ne, and Ar) and CO_2 analyses. Modal estimations were carried out by count-pointing under optical microscope (> 2000 points per section); modes were also determined by mass balance to the least square minimum between mineral phases, glass and whole rock composition for those samples whose larger dimensions allowed to obtain powders for X-Ray Fluorescence (XRF) analyses. Comparison between the two methods showed that the errors were on the first decimal of the percentages. The minerals selected for noble gas and CO_2 measurements were then ultrasonically immersed in 6.5% HNO_3 and 6.5% HCl, respectively, before being cleaned and rinsed with deionised water and acetone in ultrasonic bath to remove all the impurities.

3.2 Bulk and mineral chemistry analyses

Whole rock analyses. Whole-rock major chemistry was determined by means of an ARL Advant-XP automated X-Ray Fluorescence (XRF) spectrometer at the Department of Physics and Earth Sciences of the University of Ferrara. Full matrix correction procedure and intensities were carried out according to **Traill and Lachance, 1966**. Accuracy and precision were better than 2–5% for major elements and detection limits were 0.01 wt% for most of the major element concentrations.

Mineral major element. The major-element composition of orthopyroxene, clinopyroxene olivine and spinel minerals was determined using a CAMECA SX100 electron microprobe equipped with four WD and one ED spectrometers, at the Department of Lithospheric Research, University of Vienna. The operating conditions were: 15 kV accelerating voltage, 20 nA beam current, 20 s counting time on peak position with background counting times half of the peak counting time. In order to minimize Na and K loss, a 5 μm defocused beam and 10 s counting time on peak position was applied for glass analyses. Natural and synthetic standards were used for calibration and PAP corrections were applied to the intensity data (**Pouchou and Pichoir, 1991**). Detection limits were typically in the range of 0.02–0.06 wt%.

3.3 Noble gas (He-Ne-Ar) and CO_2 measurements in fluid inclusions

Elemental and isotopic analysis of noble gases (He, Ne, Ar) and CO_2 concentration in FI were performed at the Noble Gas Laboratory of Istituto Nazionale di Geofisica e Vulcanologia, Sezione di Palermo (Italy). The handpicked minerals (up to 1 gr) were loaded into a stainless-steel crusher capable of holding up to six different samples simultaneously for noble gas measurements. FI were released by in-vacuum single-step crushing of minerals by hydraulic press at about 200 bar. CO_2 concentration was quantified during crushing at the time of noble gas extraction. Firstly, the total gas pressure (CO_2 + N_2 + O_2 + noble gases) was measured, then the residual pressure of N_2 + O_2 + noble gases was subtracted after removing CO_2 using a "cold finger" immersed in liquid N_2 at − 196 °C. The released noble gases from FI were then cleaned in an ultra-high vacuum (10^{-9}-10^{-10} mbar) purification line by using four St 101 Zr-Al alloy getters (three kept at room temperature and one at about 400°C). All the unwanted species in the gas mixture were removed, so at the end of the purification procedure only He, Ne, Ar were in the line and ready for being analysed. Ar was trapped in a cold finger with active charcoal cooled by liquid nitrogen, whereas He and Ne were trapped and released separately by a cold-head cryogenic pump. Hence, Ar was released from the trap at room temperature after removing the liquid nitrogen and successively measured for its stable isotopes (^{36}Ar, ^{38}Ar, and ^{40}Ar) by a multi-collector mass spectrometer *Argus GVI*. He (^{3}He and ^{4}He) and Ne (^{20}Ne, ^{21}Ne and ^{22}Ne) isotopes were determined using two different split-flight-tube mass spectrometers (*Helix STF Thermo Scientific*). Helium isotope ratios ($^{3}He/^{4}He$) are expressed in R/Ra units (where R is the $^{3}He/^{4}He$ ratio of the samples and Ra is the $^{3}He/^{4}He$ ratio in air = 1.39 x 10^{-6}). The values of the Ne-isotope ratios ($^{20}Ne/^{22}Ne$ and $^{21}Ne/^{22}Ne$) are corrected for isobaric interferences at m/z values of 20 ($^{40}Ar^{2+}$) and 22 ($^{44}CO^{2+}$). The measurements of ^{20}Ne, ^{21}Ne, ^{22}Ne, ^{40}Ar and $^{44}CO_2$ during the same analysis allowed to perform corrections given that the $^{40}Ar^{2+}/^{40}Ar^{+}$ and $^{44}CO^{2+}/CO^{+}$ ratios were previously determined on the same Helix SFT that run FI samples. For each analytical session, at least one standard sample was analysed for He, Ne and Ar that had previously been purified from air and stored in tanks. The analytical uncertainty (1σ) values for $^{3}He/^{4}He$, $^{20}Ne/^{22}Ne$, $^{21}Ne/^{22}Ne$, $^{40}Ar/^{36}Ar$ were <0.94%, <0.07%, <0.3%, <0.05%, respectively. Typical blanks for He, Ne and Ar were $<10^{-15}$, $<10^{-16}$ and 10^{-14} mol, respectively. Additional details about sample preparation and analytical procedures can be found in **Rizzo et al., 2018 and 2021**. Considering that some of the samples showed the presence of an atmosphere-derived component (e.g., $^{4}He/^{20}Ne < 2$; the same ratio in air is 0.318 and in mantle-derived volatiles it is higher than 1000, **e.g.**, **Ozima & Podosek, 2002**), the measured $^{3}He/^{4}He$ ratios, ^{40}Ar and ^{21}Ne were corrected for atmosphere contamination. He isotope compositions were corrected on the basis of $^{4}He/^{20}Ne$ ratio and expressed as Rc/Ra using the following formula (**Ballentine et al. 2002**):

$$Rc/Ra = ((R_M/Ra)(He/Ne)_M – (He/Ne)_A)/((He/Ne)_M-(He/Ne)_A)$$

where (R_M/Ra) and $(He/Ne)_M$ represent the measured values and $(He/Ne)_A$ the atmospheric value (0.318; **Ozima & Podosek, 2002**), respectively.

^{40}Ar was corrected assuming an entire atmospheric origin of the measured ^{36}Ar as follows (**Graham, 2002**): $^{40}Ar^* = {}^{40}Ar_M – [{}^{36}Ar_M \text{ x } ({}^{40}Ar/{}^{36}Ar)_A]$

where $^{40}Ar^*$ is the corrected ^{40}Ar value, while $^{40}Ar_M$ and $^{36}Ar_M$ represent the measured values and $(^{40}Ar/^{36}Ar)_A$ the atmospheric value (298.56; **Lee et al., 2006**), respectively.

Finally, ^{21}Ne were corrected on the basis of the measured $^{20}Ne/^{22}Ne$ and $^{21}Ne/^{22}Ne$ ratios with the following relation (**Graham, 2002**): $^{21}Ne^* = {}^{21}Ne_M – [{}^{22}Ne_M \text{ x } ({}^{21}Ne/{}^{22}Ne)_A]$

where $^{21}Ne^*$ is the corrected ^{21}Ne value, while $^{21}Ne_M$ and $^{22}Ne_M$ represent the measured values and $(^{21}Ne/^{22}Ne)_A$ the atmospheric values (0.029; **Ballentine et al., 1991**), respectively.

3.4 Radiogenic isotope analyses (Sr-Nd-Pb)

Mineral powders (of approximately 100 mg) of opx and cpx separates were placed in Teflon beakers and dissolved in a mixture of 1.5 ml HF and 1.5 ml HNO_3 on a hot plate at 120°C for 72h. After evaporation, 3 ml of 6N HCL were added to the mineral residue at 120°C for 72h before evaporation to dryness, then digested samples were re-dissolved in 1 ml of HBr. Before purification each sample was split into two different aliquots for Sr-Nd and Pb extraction, respectively. Chromatographic separation was carried out on Teflon columns with exchange resin using a HBr-HCL-HNO_3 exchange procedure. Sr, Nd and Pb isotope analyses were performed at CRPG (Nancy, France). Sr isotope ratios were measured with thermal-ionization mass spectrometer (TIMS) *Thermo Scientific Triton*, whereas Nd and Pb isotope ratios were determined with multi-collector inductively coupled plasma mass spectrometer (MC-ICP-MS) *Thermo Scientific Neptune Plus*. Sr and Nd isotope ratios were corrected for mass fractionation by normalizing to $^{86}Sr/^{87}Sr = 0.11938$ and $^{146}Nd/^{144}Nd = 0.74049$. Over the course of this study, the NBS 987 Sr standard gave a mean value of $^{86}Sr/^{87}Sr = 0.710256 \pm 9$ ($2\sigma_m$, n = 5), and the La Jolla Nd standard gave a mean value of $^{146}Nd/^{144}Nd = 0.512097 \pm 6$ ($2\sigma_m$, n = 10). The NIST 981 Pb standard yielded average values of $^{206}Pb/^{204}Pb = 16.93 \pm 0.0054$, $^{207}Pb/^{204}Pb = 15.48 \pm 0.0074$, $^{208}Pb/^{204}Pb = 36.66 \pm 0.0083$.

4. RESULTS

4.1 Petrography and mineral chemistry of La Grille xenoliths

4.1.1 Petrographic outline

Ultramafic xenoliths from La Grille volcano (**Fig. 2**) include three lherzolites (NDR2, NDR6 and NDR7), three harzburgites (NDR9, NDR11 and NDR13), four wehrlites (NDR1, NDR5, NDR8 and NDR12), and two dunites (NDR14 and NDR16). Modal proportions and rock classification, together with a textural classification, are reported in **Table 1**. Based on their textural features, the xenoliths can be divided into three different groups:

Group 1 ("Opx-bearing group", **Fig. 2**, colour code: soft blue) includes all the harzburgites (NDR9, NDR11 and NDR13) and lherzolites (NDR2, NDR6 and NDR7), and one wehrlite (NDR5). All samples share a similar pre-metasomatic coarse-grained protogranular texture (**Mercier and Nicolas, 1978**), characterized by large primary olivines and orthopyroxenes (up to 25 and 20 mm across, respectively) with curvilinear boundaries (**Fig. 1A, B, C, D ESM**). The largest olivines typically show kink-banding, fractures and they are often altered to iddingsite to various degrees, although never completely (**Fig. 1B, D ESM**); orthopyroxenes have fine exolution lamellae at their cores. NDR7 has a texture transitional between protogranular and porphyroclastic (**Mercier and Nicolas, 1978**), with a band made up of mosaic equigranular smaller (up to 1.5 mm) olivines. Primary spinels, when preserved, have dark brown colour and lobate to vermicular shapes. Metasomatic textures, superimposed on the pre-metasomatic features, are widespread and include three Types similar to those already described by **Coltorti et al., 1999** for ultramafic xenoliths from La Grille volcano:

- Type A (**Fig. 2A, B ESM**) is set on primary orthopyroxenes, which show evidence of destabilization/reaction by losing their exolution lamellae at the rims, progressively becoming spongy and studded with FI. Secondary clinopyroxenes and olivines are replacing orthopyroxenes (**Fig. 2A ESM**) together with tiny idiomorphic spinels and rare yellowish glass. Clinopyroxenes related to this texture have a sieved appearance due to FI (**Fig. 2B ESM**) and are generally small, but they may reach large dimensions (up to 6 mm) in some cases. Indeed, orthopyroxenes have been almost totally replaced by clinopyroxene in wehrlite NDR5 (**Fig. 1D ESM**).

- Type B (**Fig. 2C ESM**) includes patches and veinlets of light to dark yellow glass that contain small euhedral to subhedral clinopyroxenes, olivines (up to 1 and 3 mm in size, respectively) and sub-millimetric spinels.
- Type C (**Fig. 2D ESM**) is somehow similar to Type B but it is characterized by the presence of secondary olivine and clinopyroxene grains grown aligned and/or in optical continuity within abundant yellowish glass; secondary spinels may also be present.

Both Type B and C often involve primary spinels that react and give rise to clusters of secondary black, micrometric euhedral spinel grains arranged in shapes that resemble those previously occupied by the former primary phase. All metasomatic textures can be present in the same sample, with Type A grading into, or being cut by, Type B and/or Type C. This co-existence is sometimes intricate to the point that envisaging a temporal sequence is impossible.

Group 2 (“Opx-free Group”, **Fig. 2**, colour code: pale yellow) includes wehrlites NDR1 and NDR8 and the two dunites NDR14 and NDR16 (**Table 1**). NDR1, NDR8 and NDR14 share a very similar texture, constituted by a backbone of large olivine grains (up to 20 mm across) that are characterized by irregular and/or lobate contacts, well-defined kink-banding and some fractures. These olivines often show dusty patches, incipient signs of iddingsitization **(Fig. 1E, F, G ESM).** Small secondary euhedral to subhedral olivine (up to 1 mm across) and spinel crystals, subhedral to anhedral clinopyroxenes (up to 4 mm in size) and dark yellow-brownish glass can be found in patches, pods and veinlets (**Fig. 2E, F ESM**) between the large olivines (**Fig. 1E, F ESM**). The secondary olivines have no kink-banding and may include spinel grains; the clinopyroxenes can be optically iso-oriented (**Fig. 2F ESM**) and often appear sieved-textured due to their high amount of FI. The proportions of secondary phases and their dimensions are variable between the three samples, as well as the amount of glass: NDR1 and NDR8 have more clinopyroxenes and less glass with respect to NDR14. Dunite NDR16 has a mosaic equigranular texture (**Mercier and Nicolas, 1978**) in which deformed remnants of large kink-banded olivines are mixed with slightly smaller (max 2 mm) polygonal individuals devoid of kinking and typically joined at a 120° angle (**Fig. 1G ESM**). The sample has been massively infiltrated by a melt through both veinlets and as porous flow between grains, resulting in the crystallization of the same secondary phases that are present in other samples of this group. In addition, acicular plagioclase is often found within the glass and the secondary clinopyroxenes (up to 0.3 mm in size) can be frequently observed as single grains at the olivine junctions. The infiltration textures closely resemble Type B and Type C textures.

Group 3 ("Cumulate Group", **Fig. 2**, colour code: magenta) is constituted only by wehrlite NDR12 (**Table 1**). Its texture is ortho-cumulitic, with euhedral olivine crystals as cumulus phase and anhedral clinopyroxenes and orthopyroxenes occupying the intercumulus spaces (**Fig. 1H ESM**). Olivines lack kink-banding; clinopyroxenes and orthopyroxenes sometimes have very thin sets of exolution lamellae while cleavage is almost absent. Micrometric globular spinel grains are often poikilitically enclosed in both olivines and pyroxenes. Trails of FI are abundant especially in clinopyroxenes. Melt infiltration, in the form of rare patches of dark glass with quenched acicular phases, can be observed between the grains, which, however, show no evidence of destabilization/reaction.

4.1.2 Bulk rock composition

The large size of some samples allowed to carry out bulk rock major element measurements (**Fig. 4 ESM, Table ESM1**). Group 1 xenoliths show variable degrees of depletion, according to their modal composition, with harzburgites having higher MgO (and mg#) and lower SiO_2, Al_2O_3, FeO and CaO with respect to the lherzolite (**Fig. 4a, b, c, d, e ESM**). The compositions of Group 1 xenoliths fit both the polybaric batch melting and fractional melting paths (< 5 GPa) of **Niu, 2004** and those proposed by **Herzberg, 2004** (**Fig. 4a, b, c, d ESM**). Group 1 harzburgites could represent peridotitic residua after 20-30% degree of melting (F) of a fertile source. Furthermore, these latter are similar to a cpx-free harzburgite sampled on Mayotte Island (sample MAY181215-14 of **Berthod et al., 2021a**), whose composition fits well with a refractory mantle that underwent polybaric (pressure < 2 GPa) fractional melting up to 25% (**Fig. 4a, b, c, d ESM**). On the other hand, Group 2 xenoliths are characterized by lower SiO_2 and mg# and higher FeO and CaO with respect to Group 1 samples (**Fig. 4a, b, c, d, e ESM**), and their compositional features are inconsistent with simple partial melting processes, but rather tend towards compositions of metasomatized rocks (**Fig. 4a, c and d ESM**).

4.1.3 Mineral chemistry

All mineral phases analyses are reported in the **Electronic Supplementary Materials** (**Tables ESM2**, **ESM3**, **ESM4**, **ESM5**).

4.1.3.1 Olivines

Primary olivines (ol1) in Group 1 xenoliths have large variation in Fo contents (87.5-91.6), with the more restitic compositions being found in harzburgites and the more fertile in lherzolites and wehrlite (**Fig. 4a ESM**). NiO content in lherzolites (0.41 to 0.28 wt%) shows a higher degree of variation with respect to harzburgites (0.41-0.32 wt%) and particularly with respect to the wehrlite (0.37-0.33 wt%). The range of Fo and NiO of ol1 in Group 2 xenoliths are similar to those of Group 1 ol1 (**Fig. 4a ESM**), but for wehrlite NDR1 that is characterized by lower Fo contents (86.3-87.3). CaO in ol1 of both Group 1 and 2 is generally low (< 0.1 wt%), with an increasing tendency at decreasing Fo (up to 0.24 in NDR1). As a whole, our data are comparable to those of **Coltorti et al., 1999** except for the lack of olivines with very low NiO contents (**Fig. 4a ESM**). Olivines of Group 3 have distinctly lower Fo (82.3-83.4) and NiO (0.24-0.18 wt%) (**Fig. 4a ESM**) and their CaO contents are globally higher than that of Group 1 and 2 ol1. Secondary olivines (ol2) in all metasomatic textures of Group 1 and Group 2 have lower NiO contents (0.37-0.19 wt%) with respect to ol1 at slightly lower or higher Fo values (84.9-91.6) (**Fig. 4a ESM**). In addition, their CaO contents are high (0.15-0.35). Olivines in Group 3 wehrlite generally have variable Fo at comparable NiO and CaO but show a large decrease in Fo and NiO when in contact with the glass (**Fig. 4a ESM**).

4.1.3.2 Orthopyroxenes

Similarly to olivines, orthopyroxenes in Group 1 xenoliths has higher mg# in harzburgites (90.7-92.3) than in lherzolites (88.4-90.7) and wehrlite (88.3-89.1) (**Fig. 4b ESM**). Analogously, Al_2O_3 contents are lower in harzburgites (0.90-4.09 wt%) than in lherzolites (2.01-5.73 wt%) and wehrlite (4.28-5.11 wt%). TiO_2 is rather low, being always below 0.21 wt%, while CaO are similar in all lithologies (0.50-0.97 wt%). Orthopyroxenes similar to those belonging to Group 1 have already been described by **Coltorti et al., 1999**. Orthopyroxenes in Group 3 have distinctly lower mg# (83.1-83.5), higher Al_2O_3 (5.27-7.06

wt%) (**Fig. 4b ESM**) and TiO_2 (0.20-0.48 wt%) than those in Group 1 xenoliths, at comparable CaO contents (0.95-1.61 wt%).

4.1.3.3 Clinopyroxenes

Clinopyroxene is the phase that shows the largest compositional variations in La Grille ultramafic xenoliths. In Group 1, clinopyroxenes in the three types of metasomatic textures have overlapping compositions and cannot be parted out, with the exception of one single grain poikilitically enclosed in spinel and two tiny acicular crystals quenched within the glass (**Fig. 4c, d, e ESM**). A decrease in mg# is coupled with increasing Al_2O_3 contents passing from clinopyroxenes in harzburgites (mg#: 91.3-93.5; Al_2O_3: 1.08-5.01 wt%) to those in lherzolites (mg#: 85.5-90.8; Al_2O_3: 3.41-7.48 wt%) and wehrlite (mg#: 84.1-86.2; Al_2O_3: 5.64-6.63 wt%) (**Fig. 4c ESM**). TiO_2 increases with rock fertility, from bdl to 0.91 wt%, while CaO and Cr_2O_3 show the opposite behaviour, reaching lower values in lherzolites and wehrlite with respect to harzburgites (CaO: 17.8-21.5 wt%, 18.4-21.1 wt% and 19.2-22.6 wt%; Cr_2O_3: 0.74-2.45 wt%, 0.74-1.66 wt% and 0.84-1.35 wt%, respectively) (**Fig. 4d, e ESM**). Clinopyroxenes in Group 2 xenoliths have distinct compositional characteristics depending on the lithology and, according to their petrographic features, they can be considered all of secondary origin. They have higher mg# and lower Al_2O_3 in the dunites (89.3-91.9 and 1.47-2.63 wt%, respectively) with respect to wehrlites (81.4-88.5 and 4.12-7.17 wt%, respectively) (**Fig. 4c, d ESM**). TiO_2 behaves like in Group 1, ranging from bdl up to 2.27 wt%, as well as CaO and Cr_2O_3 that decrease from dunites to wehrlites (CaO: 17.8-20.8 wt% in dunites, 20.3-23.2 wt% in wehrlites; Cr_2O_3: 1.34-3.52 wt% in dunites, 0.50-1.62 wt% in wehrlites). The acicular grains found in the glass of the dunites have a distinct composition, being enriched in Al_2O_3 and CaO and depleted in Cr_2O_3 with respect to the other clinopyroxenes (**Fig. 4c, d, e ESM**). Group 3 clinopyroxenes have Al_2O_3, CaO and Cr_2O_3 contents comparable to those of Group 2 wehrlites (5.64-6.63 wt%, 18.6-21.0 wt% and 0.80-1.45 wt%, respectively) but at lower mg# (84.1-86.2) (**Fig. 4c, d, e ESM**).

4.1.3.4 Spinels

Primary spinels in Group 1 have highly variable compositions in terms of mg# and cr# especially in the harzburgites, while the ranges are smaller for lherzolites and the wehrlite

(**Fig. 4f ESM**), these latter being more fertile (mg#: 59.7-74.4 in harzburgites, 67.6-76.1 in lherzolites, 68.8-70.75 in the wehrlite; cr#: 30.5-71.9 in harzburgites, 15.3-31.3 in lherzolites, 21.2-27.0 in the wehrlite). Cr_2O_3 contents increases in secondary and recrystallized spinels in Type B and C metasomatic textures, while maintaining comparable mg#. Spinels in Group 2 are all secondary phases and have more chromiferous compositions in dunites (mg#: 50.5-54.7, cr#: 81.8-81.9) with respect to wehrlites (mg#: 59.7-62.2, cr#: 30.9-36.2) (**Fig. 4f ESM**). Comparison between our data and those of spinels analysed in La Grille ultramafic xenoliths by **Coltorti et al., 1999** shows partial overlap only for the highly restitic compositions. Group 3 spinels are very different from those in the other two Groups, being typified by rather constant mg# (68.2-68.9) and very low cr# (3.70-4.49) (**Fig. 4f ESM**).

4.2 Redox and thermal state of the mantle beneath La Grille Volcano

The Mg and Fe equilibrium exchange between peridotite minerals allows the evaluation of mineral pairs equilibrium (**Brey and Köhler, 1990**). The Fe/Mg exchange between olivine and orthopyroxene of Group 1 samples reproduces, within the experimental error, the slope of olivine-orthopyroxene lines calculated for temperatures varying between 627 and 1127 °C (900–1400 °K) in the pressure range of 1.5–2.0 GPa. On the other hand, olivine-clinopyroxene (both primary and secondary phases) and orthopyroxene-clinopyroxene pairs do not always reflect the ideal Fe/Mg equilibrium in the same temperature and pressure range; this is particularly evident for Group 2. These non-equilibrated mineral pairs were discarded from temperature and oxygen fugacity calculations. Equilibrium between primary olivine and spinel was also evaluated, using the method described in **Faccini et al., 2013**. Equilibration temperatures of La Grille ultramafic xenoliths were estimated using both the olivine-spinel exchange thermometer of **Ballhaus et al., 1991** and orthopyroxene-clinopyroxene exchange thermometer by **Brey and Köhler, 1990**, this latter only for opx-bearing samples (**Table 1**). Minerals in metasomatic reaction textures were excluded from computation. A constant average input pressure of 1.5 Gpa has been used. When homogeneous, both core and rim compositions of the grains (this latter were acquired at approximately 20–40 μm from the crystal edges to avoid potential effects of diffusion) were used for calculations. Temperatures for the xenoliths were averaged from multiple olivine-spinel and orthopyroxene-clinopyroxene pairs within the same grain. The differences in calculated T were small and had negligible influences on the results of oxygen fugacity computations, which are referenced to the FMQ (Fayalite-Magnetite-Quartz) buffer to minimise the effects of T uncertainties (see below). Irrespective of the lithology, Group 1 xenoliths yielded a larger range of temperatures (933-1142°C; **Ballhaus et al., 1991**; 930-1139°C, **Brey and Köhler, 1990**); lherzolite NDR2 showed a systematic increase in temperature from cores to rims of olivine and spinel (**Table 1**). As a general rule, temperatures obtained from the two-pyroxene thermometer tend to be higher than those calculated from olivine-spinel equilibria but, in both cases, they are comparable to the temperatures reported by **Coltorti et al., 1999** for La Grille lherzolites (**Fig. 5 ESM**). The oxygen fugacity (fO_2) recorded by spinel peridotites can be determined using any of the calibrated heterogeneous chemical equilibria (e.g., $2Fe_3O_4 + 3Fe_2Si_2O_6 = 6Fe_2SiO_4 + O_2$ or $2Fe_3O_4 + 3SiO_2 = 3Fe_2SiO_4 + O_2$), with the most sensitive compositional parameter being the spinel ferric/ferrous iron ratio. The Fe^{3+} content of spinels from the xenoliths was calculated from microprobe data assuming perfect stoichiometry; comparison of stoichiometric versus Mössbauer spectroscopy $Fe^{3+}/\Sigma fe$ ratios in spinels indicated that this method yields comparable results (**Canil and O'Neill, 1996**). Oxygen fugacity was calculated relative to the FMQ buffer based on the olivine-spinel oxygen barometer of **Ballhaus et al., 1991**. This formulation was selected as it can be applied to opx-free samples; however, for validation, fO_2s for opx-bearing samples have also been calculated using the **Miller et al., 2016** method that has the major advantage of solving several reactions simultaneously by the least-squares method, providing a robust estimate within an accuracy of about ±0.3–0.6 log units. The results from the different methods here used are generally in good agreement (**Table 1**). As for temperatures, $\Delta\log fO_2$ [FMQ] for the xenoliths are averages determined from multiple olivine-spinel-orthopyroxene sets. Differences in calculated fO_2 are generally small (within or slightly above 0.1 log units), suggesting redox equilibrium between the minerals. The calculated $\Delta\log fO_2$ [FMQ] values varied between -0.93 and 0.05 for Group 1 xenoliths (with all samples but one lying below FMQ) and between 0.09 and 0.71 for Group 2 xenoliths. Group 3 sample yielded a $\Delta\log fO_2$ [FMQ] of -0.65 (**Fig. 5 ESM**). A positive trend between temperature and fO_2 can be envisaged, with Group 2 xenoliths tending to be hotter and less reduced than Group 1 and 3. A comparison between the fO_2 ranges of values computed in this work and those from **Coltorti et al., 1999** has been carried out (**Fig. 5 ESM**). These latter were calculated using different methods (**O'Neill and Wall, 1987** and **Wood et al., 1990**) that, however, yield results consistent with those obtained with the **Ballhaus et al., 1991** equation within an accuracy of ± 0.5 log units (**Wood, 1991**). A similarity can be envisaged between Group 1 and the lherzolites from **Coltorti et al., 1999**; however, Group 2 differ significantly from the two groups of wehrlites (Wh 1 and Wh 2) previously recognized (**Fig. 5 ESM**). All samples fall within both the ridge peridotite and the MORB ranges reported by **Davis and Cottrell, 2021**, although Group 1 and 3 sit slightly below the averages.

4.3. Noble gas geochemistry and CO_2 abundance

Noble gas (^{4}He, ^{21}Ne* and ^{40}Ar*) and CO_2 concentrations in FI hosted in La Grille minerals are illustrated in **Fig. 4** and **Table ESM6**. The concentrations of ^{4}He in Ol, Opx and Cpx are 3.64×10^{-13}-1.45×10^{-11}, $1.10 \times 10^{-11} – 4.30 \times 10^{-11}$, and $1.38 \times 10^{-12} – 3.84 \times 10^{-11}$ mol/g, respectively (**Fig. 4a, b, c**). The ^{40}Ar* contents in Ol, Opx and Cpx are $3.55 \times 10^{-12} – 2.40 \times 10^{-10}$, $4.90 \times 10^{-11} – 1.14 \times 10^{-9}$, and $1.12 \times 10^{-11} – 1.22 \times 10^{-10}$ mol/g, respectively (**Fig. 4a**). The abundance of ^{21}Ne* in Ol, Opx and Cpx are $8.30 \times 10^{-19} – 1.15 \times 10^{-17}$, $2.96 \times 10^{-18} – 4.02 \times 10^{-17}$, $4.60 \times 10^{-19} – 2.31 \times 10^{-18}$ mol/g, respectively (**Fig. 4c**). Finally, CO_2 is the most abundant gas species with concentrations varying from 2.77×10^{-10} to 1.42×10^{-7} in Ol, from 5.50×10^{-7} to 1.27×10^{-6} in Opx, and from 8.92×10^{-8} to 1.08×10^{-6} in Cpx mol/g (**Fig. 4b**). In general, within the same xenolith Opx and Cpx are more gas-rich than Ol.
The measured ^{3}He/^{4}He ratio not corrected for air contamination (R/Ra) is 5.67-7.34 in Ol, 6.57-7.01 in Opx, and 6.46-7.25 in Cpx (**Fig. 5; Table ESM6**). The ^{4}He/^{20}Ne ratios are in the range 2.82-125 in Ol, 46.6-572.82 in Opx, and 77.47-1859.82 in Cpx, (**Fig. 5; Table ESM6**). The ^{20}Ne/^{22}Ne and ^{21}Ne/^{22}Ne ratios are respectively 9.81-9.90 and 0.0291- 0.0304 in Ol, 9.93-10.36 and 0.0299-0.0347 in Opx, and 9.80-10.38 and 0.0292-0.0345 in Cpx (**Table ESM6**). The ^{40}Ar/^{36}Ar ratio is 310.30-1501.54 in Ol, 1860.89-7747.47 in Opx, and 501.39-3161.71 in Cpx (**Table ESM6**). The ^{3}He/^{4}He ratio corrected for air contamination is 6.30-7.36 in Ol, 6.60-7.01 in Opx, and 6.48-7.25 in Cpx (**Table ESM6**). Finally, the ^{4}He/^{40}Ar* ratios range between 0.02 and 0.42 in Ol, 0.04 and 0.21 in Opx, and 0.005 and 0.39 in Cpx (**Table ESM6**), and are significantly below than the typical mantle production values (^{4}He/^{40}Ar= 1-5; **Graham, 2002; Marty, 2012**).

4.4 Radiogenic isotopes

Sr, Nd and Pb isotope ratios for Opx and Cpx crystals are given in **Table ESM7**. The ^{87}Sr/^{86}Sr ratios vary between 0.703225 and 0.703449, and 0.703457 and 0.703551 in Cpx and Opx, respectively, while ^{143}Nd/^{144}Nd ratios range between 0.512807 and 0.512865, and 0.51279 and 0.51286 in Cpx and Opx, respectively. The ^{206}Pb/^{204}Pb, ^{207}Pb/^{204}Pb and

$^{208}Pb/^{204}Pb$ ratios are 18.63-19 and 18.24-18.70, 15.62-15.66 and 15.63-15.81, and 38.60-38.93 and 38.47-38.87 in Cpx and Opx, respectively.

5. Discussion

In the discussion below, we integrate the information obtained from the petrographic and petrologic evidence with abundance and isotope signature of noble gases and CO_2 concentration in FI, with the aim to shed light into the geochemical characteristics of the mantle source beneath La Grille volcano.

5.1 Atmosphere-derived component

Due to distinctive isotopic signatures of the different Erath's reservoirs, the isotope ratios of He, Ne, and Ar can provide useful information on the origin of these noble gases trapped within the FI. The $^{4}He/^{20}Ne$ ratios, together with Ne ($^{20}Ne/^{22}Ne$ and $^{21}/Ne/^{22}Ne$) and Ar ($^{40}Ar/^{36}Ar$) isotopes in FI from La Grille mantle xenoliths, suggest variable extents of addition of an atmospheric component, with olivine being generally more contaminated than Opx and Cpx. Overall, the $^{4}He/^{20}Ne$ and R/Ra values fall along the binary mixing curve between air and mantle end-members, and overlap with the compositional fields of ultramafic xenoliths from other localities such as European SCLM, West Antarctic Rift Systems (WARS) and Kenya Rift Graben (**Fig. 5**). In the Ne three-isotope plot (**Fig. 6**), our data fall in correspondence of the two-component mixing between air and a MORB-like mantle assuming $^{20}Ne/^{22}Ne = 12.5$ and $^{21}/Ne/^{22}Ne = 0.06$ as MORB end-member values (**Moreira et al., 1998; Sarda et al., 1988**). Similar indications are provided by coupling helium isotopes with argon isotopes (**Fig. 7**). These show that La Grille xenoliths fall along the theoretical mixing trend between air and $^{40}Ar/^{36}Ar$ isotope ratios expected for the regional mantle (**Hopp et al., 2007**) assuming ~ 44000 as the MORB-like $^{40}Ar/^{36}Ar$ signature of the pristine upper mantle (**Moreira et al., 1998**) and $^{3}He/^{36}Ar$ between 2.45 and 0.002 (**Fig. 7**). In this respect, $^{20}Ne/^{22}Ne$, $^{21}Ne/^{22}Ne$ and $^{40}Ar/^{36}Ar$ isotope ratios in La Grille xenoliths are found significantly below the typical mantle values (**Burnard, 1997; Moreira et al., 1998**), supporting the evidence of a certain contamination by atmosphere-derived fluids. The presence of an atmospheric component in mantle-derived materials can reflect either a source signature or shallow-level contamination, as it has been widely observed in mantle xenoliths worldwide both in oceanic (e.g., Samoa [**Poreda and Farley,**

1992], Kerguelen [**Valbracht et al., 1996**], La Reunion [**Hopp and Trieloff, 2005**]) and continental settings (e.g., Europe [**Buikin et al., 2005; Correale et al., 2012; Gautheron et al., 2005; Martelli et al., 2011; Rizzo et al., 2018, 2021**], Africa [**Halldórsson et al., 2014; Hopp et al., 2007**], Antarctica [**Correale et al., 2019**], central America [**Sandoval-Velasquez et al., 2021, 2022**]). To date, three hypothetic scenarios have been set out to unfold the origin of the atmospheric signature incorporated in the FI of ultramafic mantle xenoliths: **1)** recycling of atmospheric volatiles due to dehydration during subduction of hydrated oceanic slabs and their sedimentary cover (i.e., **Faccini et al., 2020; Hopp and Ionov, 2011; Matsumoto et al., 2001; Rizzo et al., 2018, 2021; Sandoval-Velasquez et al., 2021, 2022; Sarda, 2004; Yamamoto et al. 2004**), **2)** syn- or post-eruptive air entrapment in mineral micro-cracks (i.e., **Correale et al., 2012; Martelli et al., 2011; Nuccio et al., 2008**), and **3)** air contamination due to melt/volatile percolation during ascent of xenolith-bearing magmas (i.e., **Buikin et al., 2005; Gautheron et al., 2005**). As far as concern the first hypothesis, if air contamination resulted from recycling of atmospheric noble gases introduced into the mantle via subducting slabs, then a positive correlation between primordial (e.g., ^{3}He) and air components (e.g., ^{36}Ar) should be expected (**Matsumoto et al., 2001**). However, no correlation between ^{3}He and ^{36}Ar concentrations is observed (**Fig. 4d**), thus suggesting that recycling process as dominant origin of the air-derived component in our xenoliths seems unlikely. However, it is worth pointing out that the lack of correlation between ^{3}He and ^{36}Ar is a necessary but not sufficient condition to rule out the hypothesis of a (fossil) subduction, whose effects would be distant in the geological time and thus far from the current geodynamic context. The lithospheric mantle beneath La Grille in fact has not been recently affected by subduction and, on the basis of the latest investigations, the Comorean volcanism has been interpreted as a result of plate boundary processes (see section Geodynamic context). At the current state of our knowledge, we argue that La Grille mantle minerals may have entrapped air-derived volatiles in crystal micro-cracks due to surface exposure to the atmosphere during or after xenolith emplacement, or, alternatively, by percolation of melts and volatiles from the host magma into the entrained xenoliths en route to the surface. The petrographic evidence of melt infiltration in the form of veinlets and glass patches observed between the mineral grains suggest that air-addition from the host basalt may represents the most likely hypothesis to explain the atmospheric component in our xenoliths.

5.2 Mantle processes

5.2.1 Mineral chemistry constrains

The major-element composition of the minerals in the studied ultramafic mantle xenoliths can provide precious information on melt extraction and metasomatic history affecting the sampled lithospheric portions below La Grille volcano. Nearly all of the Group 1 La Grille xenoliths fall within the area defined by hydrous melting paths at 1 GPa and water content ranging from 0.5 to 1 wt. % H_2O (**Fig. 2**), whereas Group 2 and 3 lay outside any partial melting trend. Interestingly, clinopyroxene phenocrysts from Mayotte basanites record a maximum pressure of 1.2 GPa, while ultramafic xenoliths record lower pressure (≤0.6 GPa), close to that expected at the Moho depth (**Berthod et al., 2021a**). The whole rock chemical variations (**Fig. 3 ESM**), together with compositional variability of MgO and Al_2O_3 in Opx and Cpx (**Fig. 3a, b**) and the evolution of Fo content in Ol and Cr# of spinel (**OSMA diagram in Fig. 3c**) provide important clues on the partial melting and/or metasomatic processes experienced by this lithospheric portion. In particular, Opx and Cpx of Group 1 harzburgites show compositions ranging from refractory (i.e., depleted in Al_2O_3 and enriched in MgO) to relatively more fertile (i.e., enriched in Al_2O_3) recording a variable partial melting degree ranging between 15% and 35% (**Fig. 3a, b**) consistent with both whole rock compositions (**Fig. 3 ESM b, c**) and olivine-spinel pairs showed in the OSMA diagram (**Fig. 3c**). Opx and Cpx of Group 1 lherzolites display a more fertile composition with lower degrees of melt extraction (5-20%) with respect to harzburgites and low Cr# composition. On the other hand, pyroxenes in the Group 1 wehrlite (sample NDR 5) are rich in Al_2O_3 and have low MgO contents (**Fig. 3a, b**) that may indicate low degrees of partial melting (≤15%). However, its high clinopyroxene modal content (**Fig. 1 ESM; Table 1**), along with low Fo and spinel Cr# composition (placing it almost outside the OSMA field, **Fig. 3c**), rather suggest a different origin, probably due to a metasomatic process that modified the pyroxene modal abundance increasing Cpx at the expenses of Opx starting from a harzburgitic lithology. Group 2 xenoliths show high compositional variability. Cpx in dunites have high MgO and low Al_2O_3, while Cpx in wehrlite display higher Al_2O_3 and lower MgO contents. In both cases, this phase, does not fit the model partial melting trends, irrespective of the selected PM clinopyroxenes composition (**Fig. 3b**). In the OSMA diagram (**Fig 3c**), Group 2 xenoliths fall outside the mantle field, following instead fractional crystallization trends. This, together with the total lack of equilibrium between Ol and Cpx in these lithologies, suggests that Group 2 xenoliths most likely originated as cumulates and, subsequently, they were variously modally metasomatized by a percolating melt that crystallized the Cpx within a dunitic matrix. The $\Delta \log f O_2$ [FMQ] always above 0 (**Fig. 5 ESM; Table 1**) likely indicates the oxidizing nature of the metasomatic melt (relative to the ambient peridotite). Group 3 xenolith (NDR12) show mineral compositions typical of cumulate rocks, with high Al_2O_3 and low MgO abundances in pyroxenes (**Fig. 3a, b**) in accordance with low Fo content and Cr# in olivine and spinel (**Fig 3c**). This sample may have been originated from the crystallization of a slightly oversaturated basic melt en route from the mantle to the surface.

5.2.2 Noble gas and CO_2 constrains

The information obtained from mineral chemistry of La Grille xenoliths are coupled to noble gas elemental ratios in FI in order to shed light on possible partial melting and/or metasomatic events occurring in the mantle. The $^4He/^{40}Ar^*$ ratio has been previously used as an index for assessing the effect of mantle processes on volatiles in FI retained in the residual mantle (**Burnard, 2004; Correale et al., 2012, 2016, 2019; Faccini et al., 2020; Rizzo et al., 2018, 2021; Yamamoto et al., 2009**). Due to their incompatibility in mantle minerals, noble gases in fact tend to be preferentially partitioned into the melt phase during melt extraction or magma migration within the mantle (**Burnard, 2004; Yamamoto et al., 2009**). The different crystal-melt partition coefficients between ^4He and ^{40}Ar, with that of He being one order of magnitude higher than that of Ar (**Heber et al., 2007**) would lead to a fractionation of these two isotopes, resulting in a decrease of $^4He/^{40}Ar^*$ ratios in the mantle source. According to **Burnard, 2004**, the noble gases diffuse out of the solid mantle into fast diffusion routes such as fractures or melt channels during melt extraction. **Yamamoto et al., 2009** attributed the low $^4He/^{40}Ar^*$ ratios in olivines and pyroxenes in their mantle xenoliths study to isotope fractionation due to noble gas diffusion from mantle minerals towards magma channels crossing the mantle.

In the case of diffusive loss of helium, a kinetic $^3He/^4He$ isotope fractionation should be expected due to the different diffusion coefficients of ^3He and ^4He among mantle minerals (D_{3He}/ D_{4He} = 1.15; **Burnard, 2004; Trull and Kurz, 1993; Yamamoto et al., 2009**) leading to a decreasing of Rc/Ra isotope ratio. However, Rc/Ra vs. $^4He/^{40}Ar$ ratios (**Fig. 8**) shows no appreciable variations of the $^3He/^4He$ values with the isotope ratio varying over a relatively narrow range.

As evidenced in Section 4.3, $^4He/^{40}Ar^*$ values of FI in La Grille xenoliths are up two orders of magnitude lower than the ^{4}He/^{40}Ar* ratio of a typical fertile mantle (ranging from 1 to 5; **Graham, 2002; Marty, 2012**), which is based on the (U+Th)/K production ratio (**e.g.**, **Jochum et al., 1983; Yamamoto et al., 2009**). Moreover, ^{4}He/^{40}Ar* values below the mantle production range paralleled by small variations of ^{3}He/^{4}He ratios could be an indication of elemental fractionation of noble gas atomic species due to magma generation in the mantle instead of low (U+Th)/K ratios (**Yamamoto et al., 2009**).

Both partial melting and melt infiltration events can be invoked to explain the observed variability in the ^{4}He/^{40}Ar* geochemistry in our samples. The variability of the ^{4}He/^{40}Ar* ratio (0.005-0.42), significantly below typical production values of a fertile mantle, can be explained by the variable degrees of partial melting, as also indicated by the mineral compositions. The occurrence of metasomatic enrichment, overimposed to melt extraction processes, may account for the ^{4}He/^{40}Ar* ratios which tend to reach again fertile mantle values (**Fig. 8**). Hence, in order to unravel the processes able to modify the primordial composition of the mantle portion beneath La Grille volcano, we plotted Mg# in Ol, Opx and Cpx versus ^{4}He/^{40}Ar* and Rc/Ra ratios in FI (**Fig. 9a, b**).

Taking into account the ^{4}He/^{40}Ar* ratios of mantle minerals, the three groups of xenoliths show quite variable compositions and partially overlapping values (**Fig. 8**). Group 1 harzburgites exhibit a relatively narrow ^{4}He/^{40}Ar* values (**Fig. 8 and 9a**) and characterized by the highest Mg# relative to the other samples (**Fig. 9a, b**). These values are compatible with high degrees of partial melting as estimated by mineral chemistry. Group 1 lherzolites display the highest ^{4}He/^{40}Ar* variation from fertile (0.39 in Cpx) to depleted values (0.02 in Ol) (**Fig. 8 and 9a**) and Mg# lower than harzburgite (**Fig. 9a, b**), consistent with variable (and lower) degrees of melt extraction or with a metasomatic episode that progressively added Cpx to a harzburgitic matrix, thus matching the information arising from mineral chemistry. In this context, Group 1 wehrlite (NDR 5) showing ^{4}He/^{40}Ar* values decreasing from 0.23 (Cpx) to 0.06 (Ol) together with Mg# threshold values (**Fig. 8 and 9a, b**), would be the end result of the metasomatic process.

Group 2 xenoliths show ^{4}He/^{40}Ar* values which partially overlap those from Group 1 (**Fig. 8 and 9a, b**). In particular, Group 2 dunites show ^{4}He/^{40}Ar* values from 0.05 in ol to 0.005 in cpx that are among the lowest ratios in the studied xenoliths (**Fig. 8 and 9a**) paralleled by Mg# values intermediate between harzburgites and lherzolites of Group 1(**Fig. 9a, b**). Group 2 wehrlites have variable ^{4}He/^{40}Ar* ratio from 0.18 to 0.02 in ol (**Fig. 8 and 9a**) and are characterized by low Mg# values, falling in the cumulate quadrant (**Fig. 9a, b**).

However, the compositional features arising from major element (**Fig. 3a, b, c, d, e ESM**), combined with observed variability of both dunites and wehrlites in terms of $^4He/^{40}Ar^*$ ratios with respect to the Mg# of the host minerals (**Fig. 9a**), are not consistent with a trend of partial melting processes but instead indicate the occurrence of metasomatic processes which most likely led to the recrystallisation of Cpx from an initial dunite cumulate lithology. The positive correlation between fO_2 and temperature observed in **Fig. 5 ESM** is in agreement with this hypothesis.

Finally, Group 3 wehrlite (NDR 12) is distinct both for the highest $^4He/^{40}Ar^*$ values (from 0.36 in cpx to 0.42 in ol) (**Fig. 8 and 9a**), which are close to the fertile mantle ratio ($^4He/^{40}Ar$= 1-5; **e.g.**, **Graham, 2002; Marty, 2012**), and the lowest Mg# (<88) indicating a cumulitic origin for this rock (**Fig. 9 a, b**).

A comprehensive comparison of all mantle minerals from the three different groups was however prevented by the low amount of opx in harzburgite NDR 11 and wehrlite NDR 5 of Group 1, cpx in harzburgite NDR 13 of Group 1, dunite NDR 14, wehrlites NDR 1 and 8 of Group 2, and opx in wehrlite NDR 12 of Group 3, which did not permit us to hand-pick enough mineral material for noble gas measurements. Furthermore, optical observation often revealed the presence of microscopic crystals of Cpx adhering to the surface of Opx minerals, thus making the separation procedure impossible.

When plotting He, Ar and CO_2 abundance vs. $^4He/^{40}Ar^*$ ratio (**Fig. 10**) reveals that La Grille xenoliths show a rather scattered distribution of the data points. According to the approach used in **Rizzo et al., 2018**, we have modelled the partial melting trends for both batch and fractional melting of a pristine mantle considering both the crystal-melt partition coefficients of noble gases for Ol and Cpx (**Heber et al., 2007**) and the He, Ar and CO_2 concentrations inferred for the mantle (**Fig. 10**). Interestingly, La Grille xenoliths fall by and large between batch and fractional melting trends and, in accordance with bulk rock chemistry (**Fig. 3 ESM**), fail to unequivocally fit with a unique partial melting model. This behaviour suggests that the observed chemical variability of the mantle minerals is not caused by a single process but instead that the studied xenoliths could record a combination of competing processes including both depletion and metasomatism that affect the pristine composition of upper mantle below La Grille volcano as previously inferred by the Rc/Ra vs $^4He/^{40}Ar^*$ ratios (**Fig. 8**). Previous investigations have shown the occurrence of metasomatic processes beneath this region. In fact, in their study of worldwide mantle peridotites, **Schiano and Clocchiatti, 1994** reported direct evidence of metasomatism from La Grille and other intraplate oceanic and continental settings by investigating the composition of fluid and melt inclusions trapped in minerals of ultramafic xenoliths. Furthermore, **Class and Goldstein, 1997** and **Class et al., 1998** argued that the presence of amphibole in the source of La Grille lavas indicates derivation from a metasomatized oceanic lithospheric mantle below Grande Comore. On the basis on petrological and geochemical constrains, **Coltorti et al., 1999** showed evidence of the occurrence of a pervasive metasomatic episode in the oceanic mantle beneath La Grille volcano. These authors argue that the variable compositions in terms of trace elements of Cpx phenocrysts and glasses extracted from La Grille spinel lherzolite and wehrlite xenoliths were due to an "ephemeral" alkali-rich carbonatite metasomatizing agent with compositions very close to those of natural carbonatites such as those found at Oldoinyo Lengai volcano. This metasomatic episode could have been responsible for the recrystallization of Cpx at the expenses of Opx in Group 1 lherzolites and wehrlite and Group 2 xenoliths. Furthermore, considering that CO_2 concentrations are generally higher in Cpx and Opx than in Ol, this would be consistent with the influence of a carbonatite metasomatizing agent enriched in CO_2.

5.3 Mantle features beneath Grande Comore: plume or plate boundary?

As shown in **Fig. 11** the relatively uniform Rc/Ra values in FI of Ol, Opx and Cpx suggest that the sampled lithospheric portion below La Grille is rather homogeneous in terms of helium isotope signature, and plots in a range between the lower limit of MORB mantle signature (8±1Ra, **Graham, 2002**) and the higher values of SCLM (6.1±0.9Ra; **Gautheron and Moreira, 2002**). The $^{3}He/^{4}He$ isotope ratios of La Grille xenoliths show similarities with those measured at the Kenya Rift Graben, WARS and European SCLM, and are also in good agreement with olivines from La Grille lavas (**Class et al., 2005**), but systematically higher than those from Karthala lavas (**Class et al., 2005**) and gases (**Liuzzo et al., 2021**). Moreover, the $^{3}He/^{4}He$ isotope ratios are significantly lower than those measured in plume-influenced mantle xenoliths such as Ethiopia (Afar; **Halldórsson et al., 2014**) and La Reunion (**Boudoire et al., 2020; Hopp and Trieloff, 2005**)

The mantle source below Grande Comore Island remains controversial and still strongly debated. Previous petrological investigations have inferred the influence of a deep mantle plume beneath this region to explain the isotope and trace element systematics of Karthala and La Grille lavas (**Class et al., 1998; Class et al., 2005**). However, recent seismic tomography fails to detect low-velocity features unequivocally attributable to the presence of a deep-rooted plume below the Comoros Archipelago (**French and Romanowicz 2015**).

The combination between He and Ne isotopes can be used to unravel any possible plume contribution on the isotope systematics of La Grille ultramafic xenoliths. We have therefore evaluated the relationship between $^{3}He/^{4}He$ ratios and the extrapolated Ne isotope ratio expressed as $^{21}Ne/^{22}Ne_{EX}$, i.e., the air-free mantle $^{21}Ne/^{22}Ne$ ratio (**Halldórsson et al., 2014; Hopp et al., 2007**). In order to extrapolate the air trend for each xenolith to the $^{20}Ne/^{22}Ne$ ratio of 12.5 (solar Ne or Ne-B; **Ballentine et al., 2005; Black, 1972**) we used the calculation proposed by **Graham, 2002** and **Halldórsson et al., 2014** and compared the $^{21}Ne/^{22}Ne_{EX}$ to those computed for the European SCLM, West Antarctic Rift Systems (WARS), Kenya Rift Graben, Ethiopia (Afar) and La Reunion. From **Fig. 12**, it is evident that our samples exhibit $^{4}He/^{3}He$ values between a MORB-like upper mantle and SCLM end-members. This evidence is similar to that observed in other portions of SCLM on Earth such us European SCLM, WARS and Kenya Rift Graben and significantly higher than the Ethiopia (Afar) and La Reunion that clearly show both $^{21}Ne/^{22}Ne_{EX}$ and $^{4}He/^{3}He$ values close to the plume end-member composition. On the basis of these results, along with those from the Ne isotopes systematic (**Fig. 6**) and the $^{40}Ar/^{36}Ar$ vs $^{3}He/^{36}Ar$ ratios (**Fig. 7**), the presence of a dominating MORB component in the upper mantle below La Grille can be envisaged, supporting the hypothesis for the lithospheric origin of the Comoros magmatism rather than plume-related hot-spot track

5.2.3 Information from radiogenic isotope signature (Sr-Nd-Pb)

Overall, both Opx and Cpx of La Grille mantle xenoliths show relatively homogenous compositions in terms of Sr-Nd-Pb isotope signatures (**Fig. 13 a, b**). As a whole, Sr-Nd isotopic ratios of Opx and Cpx from La Grille xenoliths fall along a trend between DMM and a relatively enriched component with a composition that straddles between the most and the least Sr radiogenic values of La Grille and Karthala lavas (**Fig. 13a**). Sr and Nd isotope ratios of Opx and Cpx are in good agreement with those of La Grille bulk lavas as well as with those of the other Comorean volcanic islands (Mayotte, Moheli, and Anjouan) (**Fig. 13a**). As opposed to the general similarity of Sr and Nd between La Grille mantle xenoliths and La Grille bulk lavas, the Pb isotope compositions of Opx and Cpx show significantly unradiogenic $^{208}Pb/^{204}Pb$ and $^{206}Pb/^{204}Pb$ ratios with respect to all Comoros bulk lavas (**Fig 13b**) pointing towards depleted MORB mantle (DMM) end-member composition.

Plotting helium vs. radiogenic isotopes (**Fig. 14 a, b, and c**) reveals that the La Grille mantle xenoliths fit well the binary mixing array defined by La Grille and Karthala end-members. The He-Sr, He-Nd and He-Pb isotopic relationships (**Fig. 14 a, b, and c**) show that the highest He isotopic ratios (R/Ra) are associated with the most radiogenic Nd and relatively unradiogenic Pb and Sr isotopic ratios, thus suggesting that the lithospheric mantle beneath La Grille volcano has geochemical features similar to the source of MORB. Moreover, our samples extend to the lowest $^{208}Pb/^{204}Pb$ and $^{206}Pb/^{204}Pb$ reported in Comorean magmatism (**Fig. 13b and 14c**), thus redefining the isotope signature of the depleted end-member of the La Grille mantle source. The measured Sr-Nd-Pb isotopic signature of the La Grille xenoliths could reflect depleted isotopic composition at the source. The unradiogenic Pb, relatively unradiogenic Sr and radiogenic Nd isotope ratios suggest a mantle source with relatively low time-integrated U/Pb, Th/Pb, Rb/Sr, and high Sm/Nd parent/daughter ratios. Previous investigations of the Sr-Nd-Pb isotopic relationships have shown mantle heterogeneity below Grand Comore Island (**Class et al., 1998**). The different isotopic signatures of Karthala and La Grille lava suites have been attributed to different mantle sources in their formation (**Class et al., 1998**).

CONCLUSIONS

We have carried out an integrated investigation using petrography, mineral phase analysis and noble gas isotopes together with the CO_2 abundance in mineral-hosted FI from ultramafic xenoliths to define the main geochemical features of the lithospheric mantle below La Grille volcano in Grande Comore Island (western Indian Ocean). The main results of this study can be synthetized below:

- The studied xenoliths are classified as harzburgites, lherzolites, wehrlites, and dunites. Based on their textural features, they are divided in three different groups: Group 1 (Opx-bearing) showing protogranular to porphyroclastic texture overprinted by type A, B and C metasomatic reactions (**Coltorti et al., 1999**), Group 2 (Opx-free) with ad-cumulitic, infiltrated characteristics, and Group 3 (Cumulitic) showing ortho-cumulitic texture. Group 1 shows refractory (harzburgite) to relatively more fertile (lherzolite) to modally metasomatized lithologies (wherlite). In particular, Group 1 harzburgites represent the most restitic portion of La Grille mantle with highly forsteritic olivine, high Mg#, low-Al pyroxene, variable Cr# and low $^{4}He/^{40}Ar^{*}$ ratios compatible with high extents of partial melting (up to 35%). The identification of such a high degree of melting in the mantle might contribute to explain the process of accumulation and also evolution of magma at mantle level as recently shown by the Mayotte volcanic event (**Berthod et al., 2021b**). Group 1 lherzolites show a more fertile composition with lower Mg#, high-Al pyroxene, low Cr# and variable $^{4}He/^{40}Ar^{*}$ ratios consistent with either lower degrees of melt extraction (up to 20%) or metasomatic event that led to the recrystallization of Cpx starting from a harzburgitic composition of which the Group 1 wehrlite would represent the final stage. Group 2 xenoliths show highly variable compositions in terms of Fo content, Mg#, MgO and Al_2O_3 abundance in Cpx, and have among the lowest $^{4}He/^{40}Ar^{*}$ ratios in the La Grille xenoliths. These characteristics are not consistent with typical partial melting trends but suggest the presence of percolating metasomatizing melts that added Cpx to an initial dunite cumulate matrix. Lastly, Group 3 xenolith displays typical cumulate composition (low Fo, low MgO, high Al_2O_3, low Cr# contents and the highest $^{4}He/^{40}Ar^{*}$ values) indicating crystallization from a slightly oversaturated basic melt en route to the surface.

- Consistent with the bulk rock composition, the relation between He, Ar and CO_2 concentrations show that the geochemical features of La Grille Group 1 xenoliths cannot be explained by a single partial melting model only (batch or fractional melting), but needed metasomatic episode(s) post-dating melt extraction presumably related with the circulation of carbonatite metasomatizing agents as previously documented in the mantle beneath La Grille volcano (**Coltorti et al., 1999**).
- The $^{3}He/^{4}He$ isotopic signature (from 6.30 to 7.36Ra) overlaps the mantle MORB (8±1Ra) and SCLM (6.1±0.9Ra) end-members.
- The $^{20}Ne/^{22}Ne$, $^{21}Ne/^{22}Ne$ and $^{40}Ar/^{36}Ar$ isotope systematics plot along a mixing between an atmosphere-derived component and compositions with MORB-like affinities. This result, together with the indications provided when combining He isotopes with the calculated air-free mantle Ne (Ne_{EX}), show a MORB-type mantle below the La Grille volcano.
- Sr-Nd-Pb systematics in Opx and Cpx from La Grille xenoliths fall along the binary mixing array defined by La Grille and Karthala end-members and supports that the lithospheric mantle beneath La Grille volcano has geochemical affinities to MORB source.
- Overall, the optical observations combined with mineral phase composition indicate that La Grille xenoliths experienced both variable degrees of mantle melting (from

as low as 5% to as high as 35% melt extraction) recorded by Group 1 harzburgites and lherzolites, which can be considered representative of the refractory nature of the sampled lithospheric portion beneath La Grille volcano, as well as modal metasomatic processes as evidenced by the recrystallization of Cpx at the expenses of Opx in Group 1 wehrlite and Group 2 xenoliths. Finally, crystallization of oversaturated basic silicate melts seems also to have occurred within the sampled lithosphere as shown by Group 3 cumulitic xenolith (**Fig. 15**).

- In summary, our investigation reveals that the La Grille ultramafic xenoliths record variable degrees of partial melting and metasomatic processes of a MORB-type upper mantle, without necessarily claiming for the involvement of a deep mantle plume beneath the sampled portions of the Grande Comore Island in the Comoros Archipelago as previously inferred.
- These results contribute to highlight the geochemical features of Grande Comore volcanic system (La Grille-Karthala) and its relationship with the underlying mantle, providing useful tools for future geochemical monitoring of an active, dangerous and very poorly explored natural system.

Acknowledgements

This work is part of the PhD (XXXII cycle) of Claudio Ventura Bordenca at the University of Palermo funded by Istituto Nazionale di Geofisica e Vulcanologia (Sezione di Palermo, Italy) and Centre de Recherches Pétrographiques et Géochimiques (CRPG-CNRS, Nancy, France) as well as by PRIN 2017 Coltorti, Prot. 20178LPCCPW "Micro to macro - how to unravel the nature of the Large Magmatic Events" and 2017LMNLAW.

We thank Mariano Tantillo, Mariagrazia Misseri and Kevin Palmeri for helping in sample preparation and noble gases analysis performed in the Noble Gas laboratory of INGV-Palermo. We are grateful to prof. Theodoros Ntaflos for assistance during electron microprobe and XRF analysis for mineral phase and bulk rock composition. We are also indebted with Christophe Cloquet for his precious guidance in radiogenic isotope analyses at CRPG in Nancy.

REFERENCES

- **Amhed, A.H., Moghazi, A.K.M., Moufti, M.R., Dawoo, Y.H., Ali, K.A., 2016.** Nature of the lithospheric mantle beneath the Arabian Shield and genesis of Al-spinel micropods: Evidence from the mantle xenoliths of Harrat Kishb, Western Saudi Arabia. Lithos 240–

243, 119–139

- **Bachelery, P. and Coudray, J., 1990.** La Grande Comore et son volcan actif: Le Karthala, Journal de la Nature 2, pp. 32-48. ISSN 0985-0856
- **Bachelery, P. and Coudray, J., 1993.** Carte geologique des Comores: Carte volcano-tectonique de la Grande Comore (Ngazidja), Laboratoire de Cartographie et d'informations geographiques, Cultures Annuelles, St. Denis de la Reunion, 1993.
- **Bachelery P., and Hémond, C., 2016.** Geochemical and Petrological Aspects of Karthala Volcano. In: Bachelery, P., Lénat, J. F., Di Muro, A. and Michon, L. (Eds.), Active Volcanoes of the Southwest Indian Ocean: Piton de la Fournaise and Karthala, Springer-Verlag, pp. 333-344
- **Ballentine, C.J., O'Nions, R.K., Oxburgh, E.R., Horvath, F., and Deak, J., 1991.** Rare gas constrains on hydrocarbon accumulation, crustal degassing and groundwater flow in the Pannonian Basin. Earth and Planetary Science Letters, 105, pp. 229-246
- **Ballentine, C.J., 1997.** Resolving the mantle He/Ne and crustal $^{21}Ne/^{22}Ne$ in well gases. Earth Planetary Science Letters 152, 233–249. https://doi.org/10.1016/s0012-821x(97) 00142-8.
- **Ballentine, C.J., Burgess, R. and Marty, B., 2002**. Tracing fluid origin, transport and interaction in the crust. Noble Gases in Geochemistry and Cosmochemistry: Rev. Mineral. Geochem., 47, Porcelli D., Ballentine C.J., Wieler R. (Eds.), pp. 539-614.
- **Ballentine, C.J., Mart, B., Lollar, B.S., Cassidy, M., 2005.** Neon isotopes constrain convection and volatile origin on the Earth's mantle. Nature, 433, 33-38. https:// doi.org/10.1038/nature03182.
- **Ballhaus, C., Berry, R.F., Green, D.H., 1991**. High pressure experimental calibration of the olivine-orthopyroxene-spinel oxygen geobarometer: implications for the oxidation state of the upper mantle. Contrib. Mineral. Petrol. 107, 27–40. https:// doi.org/10.1007/BF00311183
- **Bénard, A., Woodland, A.B., Arculus, R.J., Nebel, O., McAlpine, S.R.B., 2018.** Variation in sub-arc mantle oxygen fugacity during partial melting recorded in refractory peridotite xenoliths from the West Bismarck Arc. Chemical Geology 486, 16–30. https:// doi.org/10.1016/j.chemgeo.2018.03.004.
- **Berthod, C., Médard, E., Di Muro, A. Hassen Ali T., Gurioli L., Chauvel C., Komorowski J-C., Bachelery P., Peltier A., Benbakkar M., Devidal J-L., Besson P., Le Friant A., Deplus C., Nowak S., Thinon I., Burckel P., Hidalgo S., Feuillet N., Jorry S., Fouquet Y., 2021a.** Mantle xenolith-bearing phonolites and basanites feed the active volcanic ridge of Mayotte (Comoros archipelago, SW Indian Ocean). Contributions to Mineralogy and Petrology 176, 75. https://doi.org/10.1007/s00410-021-01833-1
- **Berthod, C., Médard, E., Bachelery P., Gurioli L., Di Muro, A., Peltier A., Komorowski J-C., Benbakkar M., Devidal J-L., Langlade J., Besson P., Boudon G., Rose-Koga E., Deplus C., Le Friant A., Bickert M., Nowak S., Thinon I., Burckel P., Hidalgo S., Kaliwoda M., Jorry S.,, Fouquet Y., Feuillet N., 2021b**. The 2018-ongoing Mayotte submarine eruption: Magma migration imaged by petrological monitoring, Earth and Planetary Science Letters, Volume 571, 117085, https://doi.org/10.1016/j.epsl.2021.117085.
- **Black, D.C., 1972.** On the origins of trapped helium, neon and argon isotopic variations in meteorites – I. Gas-rich meteorites, lunar soil and breccia. Geochimica et Cosmochimica Acta 36 (3), 347-375. https://doi.org/10.1016/0016-7037(72)90028-2.
- **Boudoire, G., Rizzo, A.L., Arienzo, I., Di Muro, A. 2020.** Paroxysmal eruptions tracked by variations of helium isotopes: inferences from Piton de la Fournaise (La Réunion island). Scientific Reports 10:9809, https://doi.org/10.1038/s41598-020-66260-x

- **Brey, G.P., Köhler, T., 1990**. Geothermobarometry in the four-phase lherzolites II. New Thermobarometers and practical assessment of existing thermobarometers. Journal of Petrology 31, 1353–1378.
- **Broadley, M.W., Barry, P.H., Bekaert, D.V., Caracausi, A., Ballentine, C.J., Marty, B., 2020**. Identification of chondritic krypton and xenon in Yellowstone gases and the timing of terrestrial volatile accretion. Proceedings of the National Academy of Sciences, PNAS, 117 (25) 13997-14004, https://doi.org/10.1073/pnas.2003907117
- **Buikin, A., Trieloff, M., Hopp, J., Althaus, T., Korochantseva, E., Schwarz, W. H., Altherr R., 2005.** Noble gas isotopes suggest deep mantle plume source of late Cenozoic mafic alkaline volcanism in Europe. Earth Planetary Science Letters 230, 143-162. https://doi.org/10.1016/j.epsl.2004.11.001
- **Burnard, P., 1997.** Vesicle-specific noble gas analyses of ‘’Popping Rock’’: implications for primordial noble gases in Earth. Science 276, 568-571. https://doi.org/10.1126/science.276.5312.568.
- **Burnard, P., 2004.** Diffusive fractionation of noble gas and helium isotopes during mantle melting. Earth Planetary Science Letters 220, 287-295. https://doi.org/10.1016/S0012-821X(04)00060-3.
- **Canil, D., O’Neill, H.S.C., 1996.** Distribution of ferric iron in some upper-mantle assemblages. Journal of Petrology 37, 609–635. https://doi.org/10.1093/petrology/37.3.609
- **Cesca, S., Letort, J., Razafindrakoto, H.N.T., Heimann S., Rivalta E., Isken M. P., Nikkhoo M., Passarelli L., Petersen G. M., Cotton F., Dahm T., 2020.** Drainage of a deep magma reservoir near Mayotte inferred from seismicity and deformation. Nature Geoscience 13, 87–93. https://doi.org/10.1038/s41561-019-0505-5
- **Class, C., Goldstein, S. L. and Kurtz, M. D., 1996**. Significance of lower mantle entrainment or plume–lithosphere interaction in oceanic islands basalts: helium isotope evidence from Grande Comore, Goldschmidt Conference, Journal of Conference Abstracts 1, 112.
- **Class, C., & Goldstein, S. L., 1997.** Plume-lithosphere interactions in the ocean basins: Constraints from the source mineralogy. Earth and Planetary Science Letters, 150, 245–260. https://doi.org/10.1016/s0012-821x(97)00089-7
- **Class, C., Goldstein, S. L., Altherr, R., & Bachèlery, P., 1998.** The process of plume—Lithosphere interactions in the Ocean Basins—The case of Grande Comore. Journal of Petrology, 39 (5), 881–903. https://doi.org/10.1093/petroj/39.5.881
- **Class, C., Goldstein, S. L., Stute, M., Kurz, MD., & Schlosser, P., 2005.** Grand Comore Island: A well-constrained “low 3He/4He”. Earth and Planetary Science Letters, *233*, 391–409. https://doi.org/10.1016/j.epsl.2005.02.029
- **Claude-Ivanaj, C., Bourdon, B., & Allègre, C. J., 1998.** Ra-Th-Sr isotope systematic in Grande Comore Island: A case study of plume-litho-sphere interaction. Earth and Planetary Science Letters, 164, 99–117. https://doi.org/10.1016/s0012-821x(98)00195-2
- **Cochran, J.R., 1988**. Somali basin, chain ridge, and origin of the northern Somali basin gravity and geoid low. Journal of Geophysical Research 93 (B10), 11985 - 12008. https://doi.org/ 10.1029/JB093iB10p11985.
- **Coffin, M.F., Rabinowitz, P.D., 1987**. Reconstruction of Madagascar and Africa: evidence from the Davie fracture zone and western Somali basin. Journal of Geophysical Research Solid Earth 92 (B9), 9385-9406. https://doi.org/10.1029/JB092iB09p09385.
- **Coltorti, M., Bonadiman, C., Hinton, R. W., Siena, F. Upton, B. 1999.** Carbonatite metasomatism of the oceanic upper mantle: evidence from clinopyroxenes and glasses in ultramafic xenoliths of Grande Comore, Indian Ocean, Journal of Petrology 40, pp. 133-165

- **Correale, A., Martelli, M., Paonita, A., Rizzo, A., Brusca, L., Scribano, V., 2012**. New evidence of mantle heterogeneity beneath the Hyblean Plateau (Southeast Sicily, Italy) as inferred from noble gases and geochemistry of ultramafic xenoliths. Lithos 132–133, 70–81. https://doi.org/10.1016/j.lithos.2011.11.007.
- **Correale, A., Rizzo, A.L., Barry, P.H., Lu, J., Zheng, J., 2016.** Refertilization of lithospheric mantle beneath the Yangtze craton in south-East China: evidence from noble gases geochemistry. Gondwana Research 38, 289–303. https://doi.org/10.1016/j.gr.2016.01.003.
- **Correale, A., Pelorosso, B., Rizzo, A.L., Coltorti, M., Italiano, F., Bonadiman, C., Giacomoni, P.P., 2019**. The nature of the West Antarctic Rift System as revealed by noble gases in mantle minerals. Chemical Geology 524, 104–118. https://doi.org/10.1016/j.chemgeo.2019.06.020.
- **Courgeon, S., Bachelery, P., Jouet, G., Jorry, S.J., Bou, E., BouDagher-Fadel, M.K., Revillon, S., Camoin, G., Poli, E., 2018**. The offshore east African rift system: new insights from the Sakalaves seamounts (Davie Ridge, SW Indian Ocean). Terra Nova 30 (5), 380–388. https://doi.org/10.1111/ter.12353.
- **Courtillot, V., Davaille, A., Besse, J., Stock, J**., **2003.** Three distinct types of hotspots in the Earth's mantle, Earth and Planetary Science Letters, Volume 205, Issues 3–4, pp. 295-308, https://doi.org/10.1016/S0012-821X(02)01048-8.
- **Cucciniello, C., Melluso, L., Morra, V., Storey, M., Rocco, I., Franciosi, L., Grifa, C., Petrone, CM., Vincent, M., 2011**. New Ar ages and petrogenesis of the Massif d' Ambre volcano, northern Madagascar. In: Beccaluva L, Bianchini G, Wilson M (eds) Volcanism and evolution of the African lithosphere, vol 478. Spec Pap Geol Soc Am, pp 257‑281
- **Daniel, J., Dupont, J., Jouannic, Ch., 1972.** Relations Madagascar-Archipel des Comores (Nord-Est du Canal du Mozambique). Sur la nature volcanique du Banc de Leven. C R Acad Sci Paris 274, pp. 1874-1877
- **Davies, G. F., 2009.** Reconciling the geophysical and geochemical mantles: Plume flows, heterogeneities, and disequilibrium, Geochemistry Geophysics Geosystems, 10, DOI: 10.1029/2009GC002634.
- **Davis, F.A., Cottrell, E., 2021**. Partitioning of Fe_2O_3 in peridotite partial melting experiments over a range of oxygen fugacities elucidates ferric iron systematics in mid‑ ocean ridge basalts and ferric iron content of the upper mantle. Contributions to Mineralogy and Petrology 176:67, :67, https://doi.org/10.1007/s00410-021-01823-3
- **Debeuf, D., 2004.** Etude de l'évolution volcano-structurale et magmatique de Mayotte (Archipel des Comores, Océan Indien): approches structurale, petrographique, geochimique et geochronologique., PhD Thesis, La Réunion Univ., p277
- **Deniel, C., 1998.** Geochemical and isotopic (Sr, Nd, Pb) evidence for plume-lithosphere interactions in the genesis of Grande Comore magmas (Indian Ocean). Chemical Geology, 144, 281–303. https://doi.org/10.1016/S0009-2541(97)00139-3
- **Deville, E., Marsset, T., Courgeon, S., Jatiault, R., Ponte, J.P., Thereau, E., Jouet, G., Jorry, S.J., Droz, L., 2018.** Active fault system across the oceanic lithosphere of the Mozambique Channel: implications for the Nubia–Somalia southern plate boundary. Earth Planetary Science Letters. 502 https://doi.org/10.1016/j.epsl.2018.08.052.
- **Dofal, A., Fontaine, F.R., Michon, L., Barruol, G., Tkalčić, H., 2021**. Nature of the crust beneath the islands of the Mozambique Channel: Constraints from receiver functions, Journal of African Earth Sciences, Volume 184, 104379, https://doi.org/10.1016/j.jafrearsci.2021.104379.
- **Emerick, C. M., & Duncan, R. A. 1982.** Age progressive volcanism in the Comoros

archipelago, eastern Indian Ocean and implications for Somali plate tectonics. Earth and Planetary Science Letters, 60 (3), 415–428. https://doi.org/10.1016/0012-821x(82)90077-2

- **Esson, J., Flower, M.F.J., Strong, D.F., Upton, B.G.J., Wadsworth, W.J., 1970.** Geology of the Comores Archipelago, Western Indian Ocean. Geological Magazine 107 (06), 549‑557.
- **Faccini, B., Bonadiman, C., Coltorti, M., Grégoire, M., Siena, F., 2013.** Oceanic material recycled within the sub-Patagonian lithospheric mantle (Cerro del Fraile, Argentina). Journal of Petrology 54, 1211‑1258.
- **Faccini, B., Rizzo, A.L., Bonadiman, C., Ntaflos, T., Seghedi, I., Gregoire, M., Ferretti, G., Coltorti, M., 2020**. Subduction-related melt refertilisation and alkaline metasomatism in the Eastern Transylvanian Basin lithospheric mantle: evidence from mineral chemistry and noble gases in fluid inclusions. Lithos 364–365, 105516. https://doi.org/10.1016/j.lithos.2020.105516.
- **Famin, V., Michon, L., & Bourhane, A. 2020.** The Comoros archipelago: A right-lateral transform boundary between the Somalia and Lwandle plates. Tectonophysics, 789, 228539. https://doi.org/10.1016/j.tecto.2020.228539
- **Feuillet, N., Jorry, S., Crawford, W.C. Deplus C., Thinon I., Jacques E., Saurel J.M., Lemoine A., Paquet F., Satriano C., Aiken C., Foix O., Kowalski P., Laurent A., Rinnert E., Cathalot C., Donval J-P., Guyader V., Gaillot A., Scalabrin C., Moreira M., Peltier A., Beauducel F., Grandin R., Ballu V., Daniel R., Pelleau P., Gomez J., Besançon S., Geli L., Bernard P., Bachelery P., Fouquet Y., Bertil D., Lemarchand A., Van der Woerd J., 2021.** Birth of a large volcanic edifice offshore Mayotte via lithosphere-scale dyke intrusion. Nature Geoscience **14,** 787–795, https://doi.org/10.1038/s41561-021-00809-x
- **Flower, M. F. J., and Strong, D. F., 1969**. The significance of sandstone inclusions in lavas of the Comores archipelago. Earth Planetary Science Letters 7:47–50
- **Franke, D., Jokat, W., Ladage, S., Stollhofen, H., Klimke, J., Lutz, R., Mahanjane, E.S., Ehrhardt, A., Schreckenberger, B., 2015**. The offshore East African Rift System: Structural framework at the toe of a juvenile rift. Tectonics 34, 2086‑2104. https://doi.org/10.1002/2015TC003922.
- **French, S.W., Romanowicz, B., 2015.** Broad plumes rooted at the base of the Earth's mantle beneath major hotspots. Nature, 525 (7567), 95-99. https://doi.org/10.1038/nature14876.
- **Gautheron, C., Moreira, M. 2002.** Helium signature of the sub-continentallithospheric mantle. Earth Planetary Science Letters, 199, 39–47. https:// doi.org/10.1016/S0012-821X(02)00563-0.
- **Gautheron, C., Moreira, M., Allègre, C. J., 2005.** He, Ne and Ar composition ofthe European lithospheric mantle. *Chemical Geology* 217, 97–112. https://doi.org/10.1016/j.chemgeo.2004.12.009.
- **Graham, D.W, 2002.** Noble Gases Isotope Geochemistry of Mid-Ocean Ridge and Ocean Island Basalts: Characterization of mantle Source Reservoirs. Noble Gases in Geochemistry and Cosmochemistry, Reviews in Mineralogy & Geochemistry, vol., 47, Porcelli D., C.J. Ballentine. R., Wieler (Eds.), pp. 247-317
- **Hajash, A., & Armstrong, R. L. 1972.** Paleomagnetic and radiometric evidence for the age of the Comoros Islands, West Central Indian Ocean. Earth and Planetary Science Letters, 16, 231–236. https://doi.org/10.1016/0012-821x(72)90195-1
- **Halldórsson, S.A., Hilton, D.R., Scarsi, P., Abebe, T., Hopp, J. 2014.** A common mantle plume source beneath the entire East African Rift System revealed by coupled

Helium-Neon systematics: Helium-Neon isotopes in the ears. Geophysical Research Letters 41, 2304-2311. https://doi.org/10.1002/2014GL059424

- **Heber, V.S., Brooker, R.A., Kelley, S.P., Wood, B.J. 2007.** Crystal-melt partitioning of noble gases (helium, neon, argon, krypton, and xenon) for olivine and clinopyroxene. Geochimica et Cosmochimica Acta 71, 1041-1061. https://doi.org/10.1016/j.gca.2006.11.010.
- **Heber, V.S., Wieler, R., Baur, H., Olinger, C., Friedmann, T.A., Burnett, D.S., 2009.** Noble gas composition of the solar wind as collected by the Genesis mission. Geochimica et Cosmochimica Acta 73, 7414–7432. https://doi.org/10.1016/j.gca.2009.09.013.
- **Heidbach, O., Rajabi, M., Reiter, K., Ziegler, M., WSM Team 2016**. World Stress Map Database Release 2016. V. 1.1. GFZ Data Services. https://doi.org/10.5880/WSM.2016.001
- **Herzberg, C. (2004)**. Geodynamic information in peridotite petrology. Journal of Petrology 45, 2507-2530.
- **Hilton, D.R., Fisher, T.P., Marty, B., 2002**. Noble gases and volatiles recycling at subduction zones. Noble Gases inGeochemistry and Cosmochemistry, Reviews in Mineralogy & Geochemistry, vol., 47, Porcelli D., C.J. Ballentine. R., Wieler (Eds.), pp. 320-370.
- **Hofmann, A.W., 2014.** Sampling Mantle Heterogeneity through Oceanic Basalts: Isotopes and Trace Elements. In: Turekian, H.D.H.K. (Ed.), Treatise on Geochemistry (Second Edition). Elsevier, Oxford, pp. 67-101
- **Hopp, J., Trieloff, M., Altherr, R., 2004.** Neon isotopes in mantle rocks from the Red Sea region reveal large-scale plume–lithosphere interaction. Earth and Planetary Science Letters 219, 61–76. https://doi.org/10.1016/S0012-821X(03)00691-5.
- **Hopp, J., Trieloff, M., 2005.** Refining the noble gas record of the Reunion mantle plume source: Implications on mantle geochemistry. Earth and Planetary Science Letters 240, 573-588. https://doi.org/10.1016/j.epsl.2005.09.036
- **Hopp, J., Trieloff, M., Altherr, R., 2007.** Noble gas compositions of the lithospheric mantle below the Chyulu Hills volcanic field. Kenya. Earth and Planetary Science Letters 261, 635-648. https://doi.org/10.1016/j.epsl.2007.07.027
- **Hopp, J., Ionov, D.A., 2011.** Tracing partial melting and subduction-related metasomatism in the Kamchatkan mantle wedge using noble gas compositions. Earth and Planetary Science Letters 302, 121-131. https://doi.org/10.1016/j.epsl.2010.12.001.
- **Jackson, M.G., Becke,r T.W., Konter, J.G., 2018.** Evidence for a deep mantle source for EM and HIMU domains from integrated geochemical and geophysical constraints, Earth and Planetary Science Letters, Vol. 484, pp. 154-167, ISSN 0012-821X, https://doi.org/10.1016/j.epsl.2017.11.052.
- **Jackson, M. G., Becker, T. W., & Steinberger, B., 2021**. Spatial characteristics of recycled and primordial reservoirs in the deep mantle. Geochemistry, Geophysics, Geosystems, 22, e2020GC009525. https://doi.org/10.1029/2020GC009525
- **Jochum, K.P., Hofmann, A.W., Ito, E., Seufert, H.M., White, W.M., 1983.** K, U and Th in mid-ocean ridge basalt glasses and heat production, K/U and K/Rb in the mantle. Nature 306, 431-436. https://doi.org/10.1038/306431a0.
- **Johnson, K.T.M., Dick, H.J.B., Shimizu, N., 1990**. Melting in the oceanic upper mantle: an ion microprobe study of diopsides in abyssal peridotites. Journal of Geophysical Research 95, 2661–2678. https://doi.org/10.1029/JB095iB03p02661.
- **Klimke, J., Franke, D., Gaedicke, C., Schreckenberger, B., Schnabel, M., Stollhofen, H., et al., 2016.** How to identify oceanic crust—Evidence for a complex break-up in the Mozambique Channel, off East Africa. Tectonophysics, 693, 436–452.

https://doi.org/10.1016/j. tecto.2015.10.012

- **Lacroix, A., 1922**. La constitution lithologique de l'archipel des Comores. C R XIIIème congrès Int Géol Bruxelle 2:949–979
- **Lee, J. Y., Marti, K., Severinghaus, K., Kawamura, K., Yoo, H. S., Lee, J. B. and Kim, J. S., 2006.** A redetermination of the isotopic abundances of atmospheric Ar. Geochimica et Cosmochimica Acta 70, 4507–4512.
- **Lemoine, A., Briole, P., Bertil, D., Roull´e, A., Foumelis, M., Thinon, I., Raucoules, D., de Michele, M., Valty, P., Hoste Colomer, R., 2020.** The 2018–2019 seismo-volcanic crisis east of Mayotte, Comoros islands: seismicity and ground deformation markers of an exceptional submarine eruption. Geophysical Journal International 223, 22–44.
- **Liuzzo, M., Di Muro, A., Rizzo, A. L., Caracausi, A., Grassa, F., Fournier, N., Shafik B., Boudoire G., Coltorti M., Moreira M, Italiano F. 2021.** Gas geochemistry at Grande Comore and Mayotte volcanic islands (Comoros archipelago), Indian Ocean. Geochemistry, Geophysics, Geosystems, *22*, e2021GC009870. https://doi.org/10.1029/2021GC009870
- **Liuzzo, M., Di Muro, A., Rizzo, A. L., Grassa, F., Coltorti M., Ader M., 2022.** The compositions of gas emissions at Petite Terre (Mayotte, Comoros): inferences on magmatic fingerprints. Comptes Rendus. Géoscience, online first (2022), pp. 1-24, doi: 10.5802/crgeos.148
- **Lort, J.M., Limond, W.Q., Segoufin, J., Patriat, Ph, Delteil, J.R., Damotte, B., 1979**. New seismic data in the Mozambique Channel. Marine Geophysical Research 4 (1), 71–89. https:// doi.org/10.1007/BF00286146.
- **Martelli, M., Bianchini, G., Beccaluva, L., Rizzo, A., 2011.** Helium and argon isotopic compositions of mantle xenoliths from Tallante and Calatrava. Spain. Journal of Volcanology and Geothermal Research 200, 18–26. https://doi.org/10.1016/j.jvolgeores.2010.11.015.
- **Martelli, M., Rizzo, A. L., Renzulli, a., Ridolfi, F., Arienzo, I., Rosciglione, A., 2014.** Noble-gas signature of magmas from a heterogeneous mantle wedge: the case of Stromboli volcano (Aeolian Islands, Italy). Chemical Geology, *vol.* 368, pp. 39–53.
- **Marty, B., Pik R., Gezahegn Y., 1996.** Helium isotopic variations in Ethiopian plume lavas: Nature of magmatic sources and limit on lower mantle contribution, Earth and Planetary Science Letters 144, 223–237.
- **Marty, B., 2012**. The origins and concentrations of water, carbon, nitrogen and noble gases on Earth. Earth and Planetary Science Letters 313–314, 56–66. https://doi.org/10.1016/j. epsl.2011.10.040
- **Marty, B., Almayrac, M., Barry, P.H., Bekaert, D.V., Broadley, M.W., Byrne, D.J., Ballentine, C.J., Caracausi, A., 2020**. An evaluation of the C/N ratio of the mantle from natural CO2-rich gas analysis: Geochemical and cosmochemical implications. Earth and Planetary Science Letters, https://doi.org/10.1016/j.epsl.2020.116574.
- **Matsumoto, T., Chen, Y., Matsuda, J., 2001.** Concomitant occurrence of primordial and recycled noble gases in the Earth's mantle. Earth and Planetary Science Letters 185, 35-47. https://doi.org/10.1016/S0012-821X(00)00375-7
- **Mercier, J-C. C., Nicolas, A., 1975**. Textures and fabrics of upper mantle peridotites as illustrated by xenoliths from basalts. Journal of Petrology 16, 454–487.
- **Michon, L., 2016.** The volcanism of the Comoros archipelago integrated at a regional scale. In P. Bachèlery, J.-F. Lénat, A. Di Muro, & L. Michon (Eds.), Active volcanoes of the Southwest Indian Ocean: Piton de La Fournaise and Karthala (pp. 333–344). Springer-Verlag, Berlin and Heidelberg. https://doi.org/10.1007/978-3-642-31395-0_21

- **Miller, W.G.R., Holland, T.J.B., Gibson, S.A., 2016.** Garnet and spinel oxybarometers: New internally consistent multi-equilibria models with applications to the oxidation state of the lithospheric mantle. Journal of Petrology 57, 1199–1222. https://doi.org/10.1093/petrology/egw037
- **Montaggioni, L. F., J. Nougier J., 1981**. Les enclaves de roches detritiques dans les Volcans d'Anjouan (Archipel des Comores); Origine et interpretation dans le cadre de l'evolution du Canal de Mozambique, Bull. Soc. Géol. France, 7 (1981), pp. 595-601
- **Moreira, M., Kunz, J., Allegre C., 1998.** Rare gas systematics in popping rocks: Isotopic and elemental composition in the upper mantle. Science 279, 1178-1181. https://doi.org/10.1126/science.279.5354.1178
- **Morin, J., 2012.** Gestion institutionnelle et réponses des populations face aux crises volcaniques: études de cas à La Réunion et en Grande Comore. PhD thesis, University of La Réunion, p 358 + annexes
- **Mukhopadhyay, S., 2012.** Early differentiation and volatile accretion recorded in deep-mantle neon and xenon - Nature 486 (7401), 101
- **Niu, Y., Langmuir, C.H., Kinzler, R.J., 1997**. The origin of abyssal peridotites: a new perspective. Earth and Planetary Science Letters 152, 251–265. https://doi.org/10.1016/s0012- 821x(97)00119-2.
- **Niu, Y., 2004.** Bulk-rock Major and Trace Element Compositions of Abyssal Peridotites: Implications for Mantle Melting, Melt Extraction and Post-melting Processes Beneath Mid-Ocean Ridges. Journal of Petrology 45, 2423-2458.
- **Nougier, J., Cantagrel, J. M., Karche, J. P., 1986.** The Comoros archipelago in the western Indian Ocean: Volcanology, geochronology and geodynamic setting. Journal of African Earth Sciences, 5 (2), 135–145. https://doi.org/10.1016/0899-5362(86)90003-5
- **Nuccio, P.M., Paonita, A., Rizzo, A., Rosciglione, A., 2008.** Elemental and isotope covariation of noble gases in mineral phases from Etnean volcanics erupted during 2001-2005, and genetic relation with peripheral gas discharges. Earth and Planetary Science Letters 272, 683-690. https://doi.org/10.1016/j.epsla.2008.06.007
- **O'Neill, H. St. C., Wall, V. J., 1987.** The olivine–orthopyroxene–spinel oxygen geobarometer, the nickel curve, and the oxygen fugacity of the Earth's upper mantle. Journal of Petrology 28, 1169–1191.
- **Ozima, M., Podosek, F.A., 2002.** Noble Gas Geochemistry. Second Edition. Cambridge University Press, Cambridge, UK
- **Palme, H., O'Neill, H.S.C., 2003.** Cosmochemical estimates of mantle composition. In: Carlson R.W. (ed) Treatise on Geochemistry, Vol. 2, The Mantle and Core, pp. 1-38. Oxford: Elsevier-Pergamon.
- **Pelleter, A.A., Caroff, M., Cordier, C., Bachelery, P., Nehlig, P., Debeuf, D., Arnaud, N., 2014.** Melilite-bearing lavas in Mayotte (France): an insight into the mantle source below the Comores. Lithos (208–209), 281–297. https://doi.org/10.1016/j. lithos.2014.09.012.
- **Phethean, J. J. J., Kalnins, L. M., van Hunen, J., Biffi, P. G., Davies, R. J., & McCaffrey, K. J. W., 2016.** Madagascar's escape from Africa: A high-resolution plate reconstruction for the Western Somali Basin and implications for supercontinent dispersal. Geochemistry, Geophysics, Geosystems, 17, 5036–5055. https://doi.org/10.1002/2016GC006624
- **Poreda, R.J., Farley K.A., 1992.** Rare gases in Samoan xenoliths. Earth and Planetary Science Letters 113, 129-144. https://doi.org/10.1016/0012-821X(92)90215-H
- **Pouchou, J.-L., Pichoir, F., 1991.** Quantitative analysis of homogeneous or stratified microvolumes applying the Model "PAP,". In: Heinrich, K.F.J., Newbury, D.E. (Eds.),

Electron Probe Quantitation. Springer US, Boston, MA, pp. 31–75. https://doi.org/10.1007/978-1-4899-2617-3_4.

- **Quidelleur, X., Michon, L., Famin, V., Geffray, M-C, Danišík, M., Gardiner, N., Rusquet, A., Zakaria, M.G., 2022.** Holocene volcanic activity in Anjouan Island (Comoros archipelago) revealed by new Cassignol-Gillot groundmass K–Ar and 14C ages, Quaternary Geochronology, Volume 67, 101236, https://doi.org/10.1016/j.quageo.2021.101236.
- **Rabinowitz, P. D., Coffin, M. F., Falvey, D., 1983.** The separation of Madagascar and Africa. Science, 220, 67–69. https://doi.org/10.1126/ science.220.4592.67
- **Rindraharisaona, E.J., Guidarelli, M., Aoudia, A, Rambolamanana, G, 2013.** Earth structure and instrumental of Madagascar: implications on the seismotectonics. Tectonophysics 594:165–181. doi:10.1016/j.tecto. 2013.03.033
- **Rizzo, A.L., Pelorosso, B., Coltorti, M., Ntaflos, T., Bonadiman, C., Matusiak-Małek, M., Italiano, F., Bergonzoni, G., 2018.** Geochemistry of noble gases and CO2 in fluid inclusions from lithospheric mantle beneath wilcza gora (Lower silesia, Southwest Poland). Frontiers in Earth Science 6, 215. https://doi.org/10.3389/feart.2018.00215.
- **Rizzo, A.L., Faccini B., Casetta F., Faccincani L., Ntaflos T., Italiano F., Coltorti M., 2021.** Melting and metasomatism in West Eifel and Siebengebirge Sub-Continental Lithospheric Mantle: Evidence from concentrations of volatiles in fluid inclusions and petrology of ultramafic xenoliths. Chemical Geology, Volume 581, 120400, https://doi.org/10.1016/j.chemgeo.2021.120400.
- **Roach, P., Milsom, J., Toland, C., Matchette-Downes, C., Budden, C., Riaroh, D., & Houmadi, N., 2017.** New evidence supports presence of continental crust beneath the Comoros: PESGB/HGS Africa Conference.
- **Roberts, E.M., Stevens, N.J., O'Connor, P.M., Dirks, P.H.G.M., Gottfried, M.D., Clyde, W.C., Armstrong, R.A., Kemp, A.I.S., Hemming, S., 2012.** Initiation of the western branch of the East African Rift coeval with the eastern branch. Nature Geoscience 5(4):289–294. doi:10.1038/ngeo1432
- **Sandoval-Velasquez A., Rizzo A.L., Frezzotti M.L., Saucedo R., Aiuppa A., 2021.** The composition of fluids stored in the central Mexican lithospheric mantle: Inferences from noble gases and CO_2 in mantle xenoliths. Chemical Geology 576, 120270. https://doi.org/10.1016/j.chemgeo.2021.120270
- **Sandoval-Velasquez, A., Rizzo, A.L., Aiuppa, A., Straub, S., Gomez-Tuena, A., Espinasa-Perena, R., 2022.** The heterogeneity of the Mexican lithospheric mantle: Clues from noble gas and CO_2 isotopes in fluid inclusions. Frontiers in Earth Science 10:973645. doi: 10.3389/feart.2022.973645
- **Sarda, P**., **Staudacher, T., Allegre, C. J., 1988**. Neon isotopes in submarine basalts. Earth and Planetary Science Letters 91, 73-88 https://doi.org/10.1016/0012-821X(88)90152-5
- **Sarda, P., 2004.** Surface noble gas recycling to the terrestrial mantle. Earth Planet. Sci. Lett., 228, 49-63. https://doi.org/10.1016/j.epsl.2004.09.026
- **Sarda, P., Moreira, M., Staudacher, T., Schilling, J-G, Allègre, C. J., 2000.** Rare gas systematics on the southernmost Mid-Atlantic Ridge: constraints on the lower mantle and the Dupal source. Journal of Geophysical Research: Solid Earth105:5973-5996, http://doi.org/10.1029/1999JB900282
- **Saria, E., Calais, E., Stamps, D.S., Delvaux, D., Hartnady, C.J.H., 2014**. Present-day kinematics of the East African Rift. Journal of Geophysical Research: Solid Earth 119, 3584–3600. https://doi.org/10.1002/2013JB010901

- **Schiano, P., Clocchiatti, R., 1994.** Worldwide occurrence of silica-rich melts in sub-continental and sub-oceanic mantle minerals. Nature 368, 621–624. https://doi.org/10.1038/368621a0.
- **Späth, A., Le Roex, A. P., Duncan, R. A., 1996.** The geochemistry of lavas from the Comores Archipelago, Western Indian Ocean: petrogenesis and mantle sourceregion characteristics, Journal of Petrology 37, pp. 961-991
- **Stamps, D.S., Saria, E., Kreemer, C., 2018**. A geodetic strain rate model for the east African rift system. Scientific Reports 8, 732. https://doi.org/10.1038/s41598-017-19097-w.
- **Stracke, A., 2012.** Earth's heterogeneous mantle: A product of convection-driven interaction between crust and mantle, Chemical Geology 330-331, pp. 274-299
- **Streckeisen, A., 1976.** To each plutonic rock its proper name. Earth-Science Reviews 12, 1–33. https://doi.org/10.1016/0012-8252(76)90052-0.
- **Strong, D. F., 1972** – The petrology of the lavas of Grande Comore, Journal of Petrology 13, pp. 181-217.
- **Talwani, M., 1962.** Gravity measuremants on HMS acheron in south Atlantic and Indian oceans. Geol. Soc. Am. Bull. 73 (9), 1171–1182. https://doi.org/10.1130/0016-7606 (1962)73[1171:GMOHAI]2.0.CO, 2.
- **Thivet, S., Carlier, J., Gurioli, L., Di Muro, A., Besson, P., Smietana, M., Boudon, G., Bachèlery, P., Eychenne, J., Nedelec, J-M., 2022**. Magmatic and phreatomagmatic contributions on the ash-dominated basaltic eruptions: Insights from the April and November–December 2005 paroxysmal events at Karthala volcano, Comoros, Journal of Volcanology and Geothermal Research, Volume 424, 107500, https://doi.org/10.1016/j.jvolgeores.2022.107500.
- **Traill, R.J., Lachance, G.R., 1966.** A practical solution to the matrix problem in X-ray analysis. II. Application to a multicomponent alloy system. Canadian Spectroscopy, 11, 63-71.
- **Trieloff, M., Kunz, J., Clague, D.A., Harrison, D., Allegre, C.J., 2000.** The nature of pristine noble gases in mantle plumes. Science, 288, 1036-1038.
- **Trull, T.W., Kurz, M.D., 1993.** Experimental measurements of 3He and 4He mobility in olivine and clinopyroxene at magmatic temperatures. Geochimica et Cosmochimica Acta 57, 1313-1324. https://doi.org/10.1016/0016-7037(93)90068-8
- **Tzevahirtzian, A., Zaragosi, S., Bachèlery, P., Biscara, L., & Marchès, E., 2021.** Submarine morphology of the Comoros volcanic archipelago. Marine Geology, *432*, 106383. https://doi.org/10.1016/j.margeo.2020.106383
- **Upton, B.G.J., 1982**. Oceanic Islands. In: Nairn, P., Stehli, F. (Eds.), Ocean Basins and their Margins, Indian Ocean, 6 (13). Plenum Press, New York, pp. 585–648.
- **Upton, B.G.J., Downes, H., Kirstein, L.A., Bonadiman, C., Hill, P.G., Ntaflos, T., 2011.** The lithospheric mantle and lower crust–mantle relationships under Scotland: a xenolithic perspective. J. Geol. Soc. Lond. 168, 873–886. https://doi.org/10.1144/ 0016-76492009-172.
- **Valbracht, P.J., Honda, M., Matsumoto, T., Mattielli, N., McDougall, I., Ragettli, R., Weis, D. 1996.** Helium, neon and argon isotope systematics in Kerguelen ultramafic xenoliths: implications for mantle source signatures. Earth and Planetary Science Letters 138, 29-38. https://doi.org/10.1016/0012-821X(95)00226-3
- **Vlastelic, I., Pietruszka, A. J., 2016.** A review of the recent geochemicalevolution of Piton de la Fournaise volcano (1927-2010) - In: Bachelery, P., Lénat, J.F., Di Muro, A. and Michon, L. (Eds.), Active Volcanoes of the Southwest Indian Ocean: Piton de la Fournaise and Karthala, Springer-Verlag, pp. 185-201

- **Vormann, M., Franke, D., Jokat, W., 2020**. The crustal structure of the southern Davie Ridge offshore northern Mozambique – a wide-angle seismic and potential field study. Tectonophysics 778, 228370. https://doi.org/10.1016/j.tecto.2020.228370.
- **Zindler, A., Hart, S., 1986.** Chemical geodynamics. Ann. Rev. Earth Planet.Sci. 14**:** 493 – 571.
- **Zinke, J., Reijmer, J.J.G., Dullo, W.-Ch., Thomassin, B.A., 2003**. Systems tracts sedimentology in the lagoon of Mayotte associated with the Holocene transgression. Sedimentary Geology 160, 57–79.
- **Zinke, J., Reijmer, J.J.G., Taviani, M., Dullo, W.-Chr., Thomassin, B.A., 2005**. Facies and faunal assemblage changes in response to the Holocene transgression in the Holocene transgression in the Lagoon of Mayotte (Comoro Archipelago, SW Indian Ocean). Facies 50, 391‑408. https://doi.org/10.1007/s10347-004-0040-7.
- **White, W., 2005.** Geochemistry, Wiley-Blackwell
- **Wood, B. J., Bryndzia, L. T., Johnson, K. E., 1990.** Mantle oxidation state and its relationship to tectonic environments and fluid speciation. Science 248, 337–345.
- **Wood, B.J. 1991.** Oxygen barometry of spinel peridotites. Reviews in Mineralogy, 25, 417–431
- **Yamamoto, J., Kaneoka, I., Nakai, S., Kagi, H., Prikhod'ko, V.S., Arai, S., 2004.** Evidence for subduction-related components in the subcontinental mantle from low 3He/4He and 40Ar/36Ar ratio in mantle xenoliths from Far Eastern Russia. Chemical Geology 207, 237-259., https://doi.org/10.1016/j.chemgeo.2004.03.007
- **Yamamoto, J., Nishimura, K., Sugimoto, T., Takemura, K., Takahata, N., Sano, Y., 2009.** Diffusive fractionation of noble gases in mantle with magma channels: Origin of low He/Ar in mantle-derived rocks. Earth and Planetary Science Letters 280, 167-174. https://doi.org/10.1016/j.epsl.2009.01.029.

FIGURE CAPTIONS

Fig. 1 – a) Location of the Comoros Archipelago in the western Indian Ocean; **b)** location of Grande Comore Island in the Comoros Archipelago **c)** Simplified volcanological map of Grande Comore Island modified from **Bachelery et al., 2016**. Yellow star indicates the sampling location. The proposed plate boundaries in dashed white lines are from **Saria et al., 2014, Stamps et al., 2018, Famin et al., 2020** and **Lemoine et al., 2020**.

Fig. 2. Olivine (Ol) – orthopyroxene (Opx) – clinopyroxene (Cpx) classification diagram (**Streckeisen, 1976**) for La Grille ultramafic xenoliths. Colour code is different for each of the three textural groups as described in chapter 4 of the main text: soft blue symbols, Group 1; pale yellow symbols, Group 2; magenta, Group 3. Grey asterisks are Grande Comore xenoliths from **Coltorti et al. (1999)**. Black square indicates Primordial Mantle (PM) modal composition from **Johnson et al. (1990)**. Dotted red and purple lines are anhydrous melting paths at 2 and 1 GPa, respectively (**Niu et al., 1997**) while fuchsia, violet and light blue lines are hydrous melting paths at 1 GPa and 0.1, 0.5 and 1 % of H_2O, respectively (**Bènard et al., 2018**).

Fig. 3. MgO vs Al_2O_3 of orthopyroxenes (a) and clinopyroxenes (b) in La Grille ultramafic xenoliths, divided by textural groups. Thick black lines show the melting paths for orthopyroxenes (in a) and clinopyroxenes (in b) according to the model of **Upton et al.**

(2011), with starting compositions fitting the **Palme and O'Neill (2003)** (PMa) and **McDonough and Sun (1995)** (PMb) bulk silicate Earth estimates. Olivine-Spinel Mantle Array (OSMA) diagram (c) shows the evolution of Fo content in olivine and cr# [molar Al/(Al+Cr)] of spinel with increasing partial melting (F%). PM, olivine and spinel compositions calculated through mass balance from the bulk silicate Earth of **McDonough and Sun (1995)** and **Johnson et al. (1990)** modes. Abyssal peridotite field and partial melting line from **Amhed et al. (2016).**

Fig. 4 - Elemental concentrations in mol/g of ^{3}He, ^{4}He, $^{40}Ar^{*}$, ^{36}Ar, $^{21}Ne^{*}$ and CO_2 measured in FI from La Grille ultramafic xenoliths.

Fig. 5 - R/Ra vs. $^{4}He/^{20}Ne$ ratios of FI in olivine and pyroxene phenocrysts extracted from La Grille xenoliths. The blue and green solid lines represent MORB (8 ± 1; **Graham, 2002**) and SCLM (6.1 ± 0.9; **Gautheron and Moreira 2002**) end-member, respectively. The dashed lines show mixing trends with addition of 20 and 50% of mantle component. European SCLM data (Eifel region, **Buikin et al. ,2005**, **Gautheron et al., 2005**, **Rizzo et al., 2021**; Pannonian Basin, **Buikin et al., 2005**; Lower Silesia, **Rizzo et al., 2018**), West Antarctic Rift System (WARS) data (**Correale et al., 2019**), Kenya Rift Graben data (**Halldórsson et al., 2014; Hopp et al., 2007**), Ethiopia (Afar) data (**Halldórsson et al., 2014**), La Reunion data (**Boudoire et al., 2020; Hopp and Trieloff, 2005**), and La Grille and Karthala olivine data (orange and purple crosses, respectively; **Class et al., 2005**) are shown for comparison. Data from summit fumaroles collected both in the pit crater and the Soufriere area at Karthala volcano (light green and white triangles, respectively) are also reported (**Liuzzo et al., 2021**). Symbols as in **Fig. 4**.

Fig. 6 - The Ne three-isotope diagram ($^{21}Ne/^{22}Ne$ versus $^{20}Ne/^{22}Ne$). The black, red and blue solid lines represent binary mixing between air ($^{21}Ne/^{22}Ne$ = 0.0290 and $^{20}Ne/^{22}Ne$ = 9.8) and MORB-like mantle ($^{21}Ne/^{22}Ne$ = 0.06 and $^{20}Ne/^{22}Ne$ = 12.5; **Moreira et al., 1998; Sarda et al., 1988**), SOLAR WIND ($^{21}Ne/^{22}Ne$ = 0.0328 and $^{20}Ne/^{22}Ne$ = 13.8; **Heber et al., 2009**) and CRUST [$^{21}Ne/^{22}Ne$ = 0.6145 (average value of 0.469–0.76) and $^{20}Ne/^{22}Ne$ = 0.3; **Ballentine, 1997** and references therein)], and, respectively. Symbols as in **Fig. 4**. Compositional ranges of European SCLM, West Antarctic Rift System (WARS), Kenya Rift Graben, Ethiopia (Afar) and La Reunion as in **Fig. 5**.

Fig. 7 - $^{40}Ar/^{36}Ar$ versus $^{3}He/^{36}Ar$ diagram. The black solid, dashed and dash-dot lines represent binary mixing between air [$^{40}Ar/^{36}Ar$ = 295,5, $^{3}He/^{36}Ar = 2.3 \times 10^{-7}$, and $^{4}He = 1{,}13 \times 10^{-16}$ (arbitrarily chosen to fit data) (**Lee et al., 2006**; **Ozima and Podosek, 2002**)] and MORB-like mantle [($^{40}Ar/^{36}Ar$ = 44,000 and $^{3}He/^{36}Ar$ = 2.45 and 0,002, and $^{4}He = 1.0 \times 10^{-9}$ and 8.0×10^{-13}, (arbitrarily chosen to fit data) assuming $^{3}He/^{4}He$ = 8, $^{4}He/^{40}Ar^{*}$= 5 and $^{4}He/^{40}Ar^{*}$= 0,004 (**Moreira et al., 1998**)] The range of typical fertile mantle (**Graham, 2002**; **Marty, 2012**) is also reported. Symbols as in **Fig. 4**. Compositional ranges of European SCLM, WARS, Kenya Rift Graben, Ethiopia (Afar) and La Reunion as in **Fig. 5**.

Fig. 8 - $^{4}He/^{40}Ar^{*}$ versus Rc/Ra ($^{3}He/^{4}He$ corrected for air contamination) measured in FI from La Grille mantle xenoliths. The light violet field represents the MORB-like compositions of $^{3}He/^{4}He$ ratios (8 ± 1, **Graham, 2002**) and $^{4}He/^{40}Ar^{*}$ mantle production ratio (1-5, **Graham, 2002**; **Marty, 2012**). Symbols as in **Fig. 4**.

Fig. 9 – Mg# versus (a) $^{4}He/^{40}Ar^{*}$ and (b) Rc/Ra ($^{3}He/^{4}He$ corrected for air contamination) showing the composition of ol, opx, and cpx from La Grille ultramafic xenoliths. The vertical dotted line indicates the Mg# threshold that separates mantle lithotypes from

cumulate rocks. The light violet field represents the MORB-like compositions of $^{4}He/^{40}Ar^{*}$ mantle production ratio (1-5, **Graham, 2002**; **Marty, 2012**) and $^{3}He/^{4}He$ ratios (8 ± 1**, Graham, 2002**). Symbols as in **Fig. 4**.

Fig. 10 –$^{4}He/^{40}Ar^{*}$ versus (a) He**,** (b) $^{40}Ar^{*}$, and (c) CO_2 concentrations. Batch and fractional melting curves were computed using the following formula (from **White, 2005**):

$$Batch\ melting: C_e^m = \frac{C_e^s}{\left[F + D_e^{\frac{cryst}{melt}} \cdot (1-F)\right]}\ ;\ Fractional\ melting: C_e^m = \left[C_e^s \cdot \left(\frac{1}{D_e^{\frac{cryst}{melt}}}\right) \cdot (1-F)^{\left(\frac{1}{D_e^{\frac{cryst}{melt}}}\right)}\right]$$

where *e* is the element of interest, c_e^m and c_e^s are the concentrations in the melt and solid phase, respectively; F is the melting fraction ranging from 0 to 1; $D_e^{\frac{cryst}{melt}}$ is the crystal-melt partitioning coefficient of the element of interest. The crystal-melt partitioning coefficients of He, Ar and CO_2 for Ol and Cpx are the following: $D_{He}^{Ol/melt}$= 1.7 x 10^{-4}, $D_{Ar}^{Ol/melt}$= 1.1 x 10^{-3}, $D_{CO2}^{Ol/melt}$= 7 x 10^{-4} (assumed to fit data), $D_{He}^{Cpx/melt}$= 2 x 10^{-4}, $D_{Ar}^{Cpx/melt}$=1.1 x 10^{-3}, $D_{CO2}^{Cpx/melt}$= 7 x 10^{-4} (assumed to fit data). The model starting compositions are as follows: He = 6.4 x 10^{-10} mol/g (**Ozima and Podosek, 2002**), $^{40}Ar^{*}$ = 2.5 x 10^{-10} mol/g, CO_2 = 1.4 x 10^{-5} mol/g, and He/Ar* = 2.5. Symbols as in **Fig. 4**.

Fig. 11 – ^{4}He concentrations versus $^{3}He/^{4}He$ (Rc/Ra) of crushed Ol, Opx and Cpx phenocrysts in FI from La Grille xenoliths. The light blue and red fields indicate the range of R/Ra ratios for a MORB-like (8 ± 1, **Graham, 2002**) and SCLM-like (6.1 ± 0.9, **Gautheron and Moreira, 2002**) mantle, respectively. La Grille and Karthala olivines from **Class et al., 2005** are shown for comparison. Symbols as in **Fig. 4**. Compositional ranges of European SCLM, WARS, Kenya Rift Graben, Ethiopia (Afar) and La Reunion as in **Fig. 5**.

Fig. 12 – Extrapolated Ne isotopes $(^{21}Ne/^{22}Ne)_{EX}$ versus He isotopes ($^{4}He/^{3}He$) for La Grille ultramafic xenoliths (**Halldórsson et al 2014**; **Hopp et al. 2004**). Dotted lines represent binary mixing between three endmembers: 1) a mantle plume component (PLUME) with $(^{21}Ne/^{22}Ne)_{EX}$ = 0.034 ± 0.001 (**Graham, 2002**) and $^{4}He/^{3}He$ value of ~36000 (20Ra), which corresponds to the highest He isotope ratio observed in the EARS (**Marty et al., 1996**), 2) MORB-like upper mantle at $(^{21}Ne/^{22}Ne)_{EX}$ = 0.06 ± 0.001 and 8 ± 1 Ra (**Graham, 2002**; **Hopp et al., 2004, 2007**), 3) SCLM with $(^{21}Ne/^{22}Ne)_{EX}$ = 0.07 ± 0.001 and 6.1 ± 0.9 Ra (**Gautheron and Moreira, 2002; Hopp et al., 2004, 2007**). Symbols as in **Fig. 4**. Compositional ranges of European SCLM, WARS, Kenya Rift Graben, Ethiopia (Afar) and La Reunion as in **Fig. 5**.

Fig. 13 a, b – a) $^{87}Sr/^{86}Sr$ vs. $^{143}Nd/^{144}Nd$ and **b)** $^{208}Pb/^{204}Pb$ vs. $^{206}Pb/^{204}Pb$ binary diagrams of Opx and Cpx of La Grille mantle xenoliths. Karthala whole-rock lavas (brown squares) from **Class et al., 1998**; La Grille whole-rock lavas (red squares) from **Class and Goldstein, 1997** and **Class et al., 1998**; Mayotte, Moheli and Anjouan whole-rock lavas (white, orange, and black triangles, respectively) from GEOROC Database (**http://georoc.mpch-mainz.gwdg.de/georoc/**); End-member values for DMM (Depleted Morb Mantle), HIMU (high-μ = $^{238}U/^{204}Pb$ ratio), EMI and EMII (Enriched Mantle) are from **Hoffman, 2014, Stracke, 2012 and Zindler and Hart,1986.**

Fig. 1 a,b,c – R/Ra vs **(a)** $^{87}Sr/^{86}Sr$, **(b)** $^{143}Nd/^{144}Nd$, and **(c)** $^{206}Pb/^{204}Pb$ isotope ratios measured in Opx and Cpx from La Grille mantle xenoliths. Sr-Nd-Pb data of Karthala and La Grille bulk lavas are from **Class et al., 1998**, and **Class and Goldstein, 1997** and **Class**

et al., 1998, respectively. He isotope composition (R/Ra) of Karthala and La Grille volcanoes are from olivine phenocrysts extracted from crushed whole-rock lavas (**Class et al., 2005**).

Fig. 15 - A, Sketches illustrating the processes experienced by La Grille Upper Mantle. Group 1 and Group 2 record metasomatism by a carbonated undersaturated silicate melt, similar to the La Grille lavas, that reacted with different lithospheric domains. In the harzburgitic domain, it caused the recrystallization of Cpx at the expenses of Opx to form Group 1 xenoliths. In the dunitic domain, it percolated and crystallized Cpx into a dunite matrix. From left to right, increasing degrees of metasomatic reactions. The opx-bearing cumulate wehrlites of Group 3 crystallized from a slightly oversaturated silicate melt at some point of the history of the lithosphere and have been then sampled by the uprising magmas. Color codes: olivine, white; cpx, green; opx, yellowish taupe; spinel, black; melt, yellow. **B**, Sketch (not to scale) of the sampled lithospheric section, with co-existing harzburgitic and dunitic domains crossed by layers of opx-bearing cumulate wehrlites. Black and grey channels represent Karthala and La Grille magmas, respectively. Blue, yellow and pink circles indicate the possible areas of provenance of the ultramafic xenoliths of the three Groups.

Figure 1

Click here to access/download;Figure;Fig.1.tiff

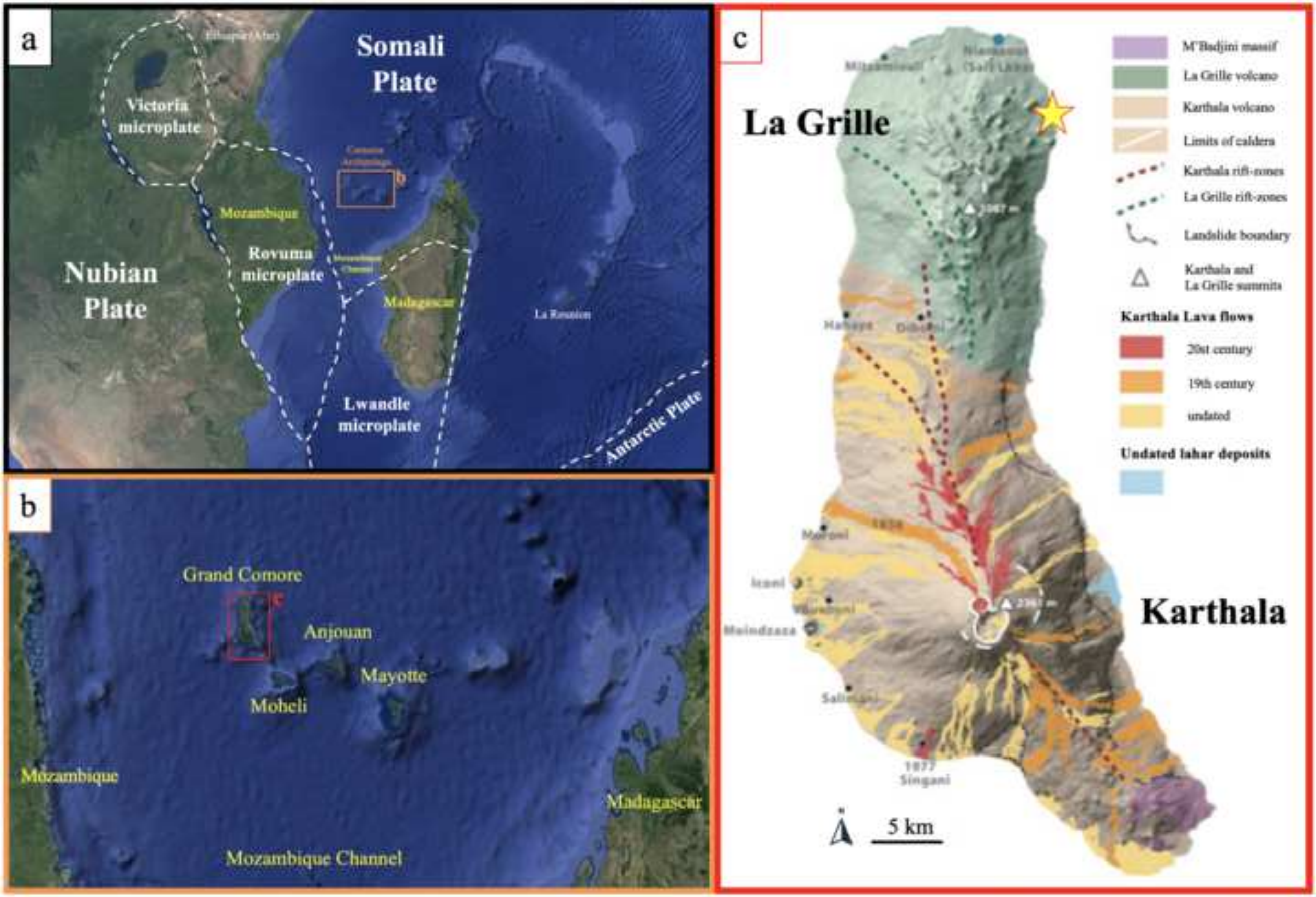

Figure 2

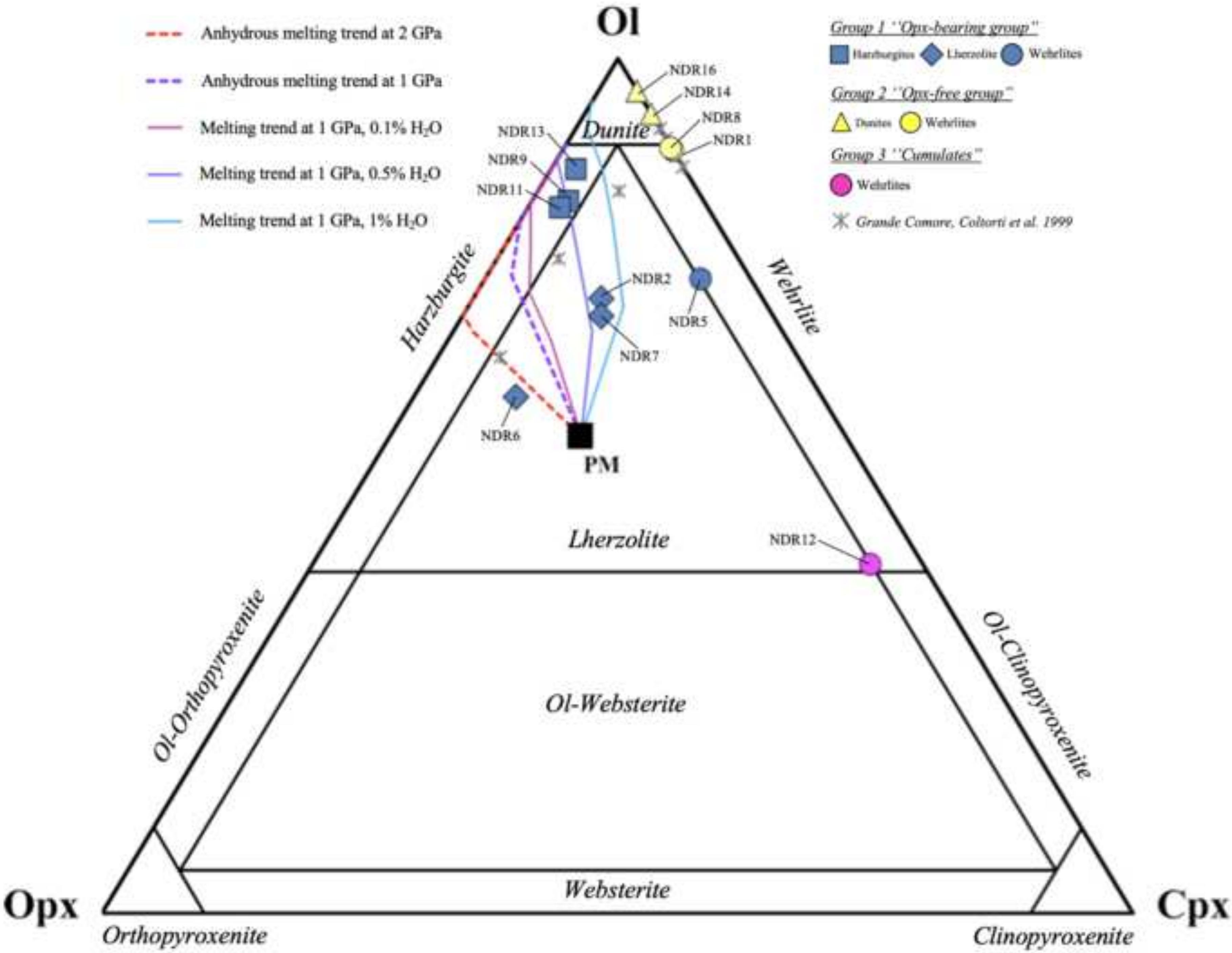

Ol
Opx
Cpx
Anhydrous melting trend at 2 GPa
Anhydrous melting trend at 1 GPa
Melting trend at 1 GPa, 0.1% H_2O
Melting trend at 1 GPa, 0.5% H_2O
Melting trend at 1 GPa, 1% H_2O
Group 1 "Opx-bearing group"
Harzburgites
Lherzolite
Wehrlites
Group 2 "Opx-free group"
Dunites
Wehrlites
Group 3 "Cumulates"
Wehrlites
Grande Comore, Coltorti et al. 1999
Dunite
Harzburgite
Wehrlite
Lherzolite
Ol-Orthopyroxenite
Ol-Clinopyroxenite
Ol-Websterite
Websterite
Orthopyroxenite
Clinopyroxenite
PM
NDR16
NDR14
NDR8
NDR1
NDR13
NDR9
NDR11
NDR2
NDR5
NDR7
NDR6
NDR12

Figure 3

Click here to access/download;Figure;Fig.3.tiff

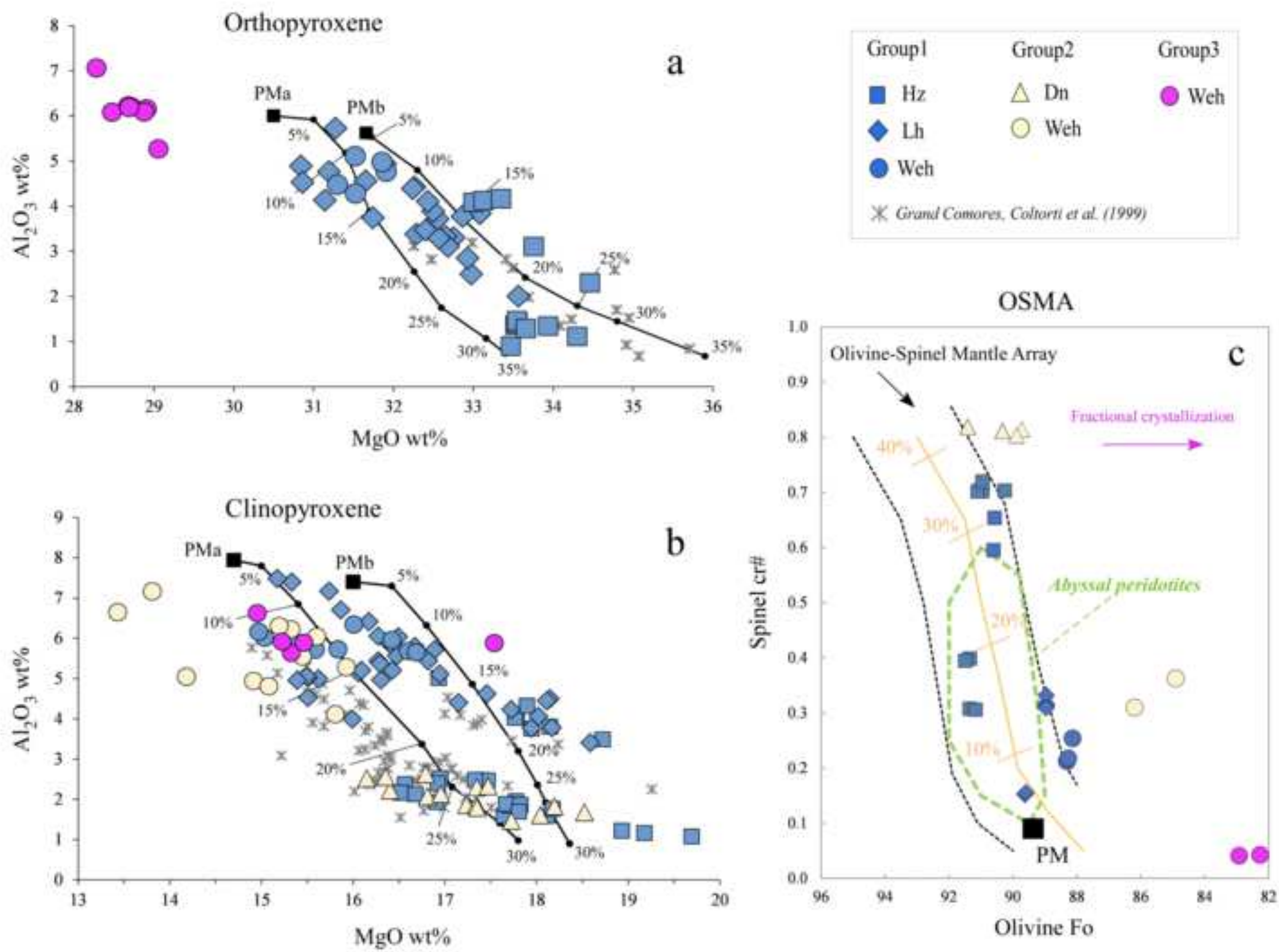

Figure 4

Click here to access/download;Figure;Fig.4.tiff

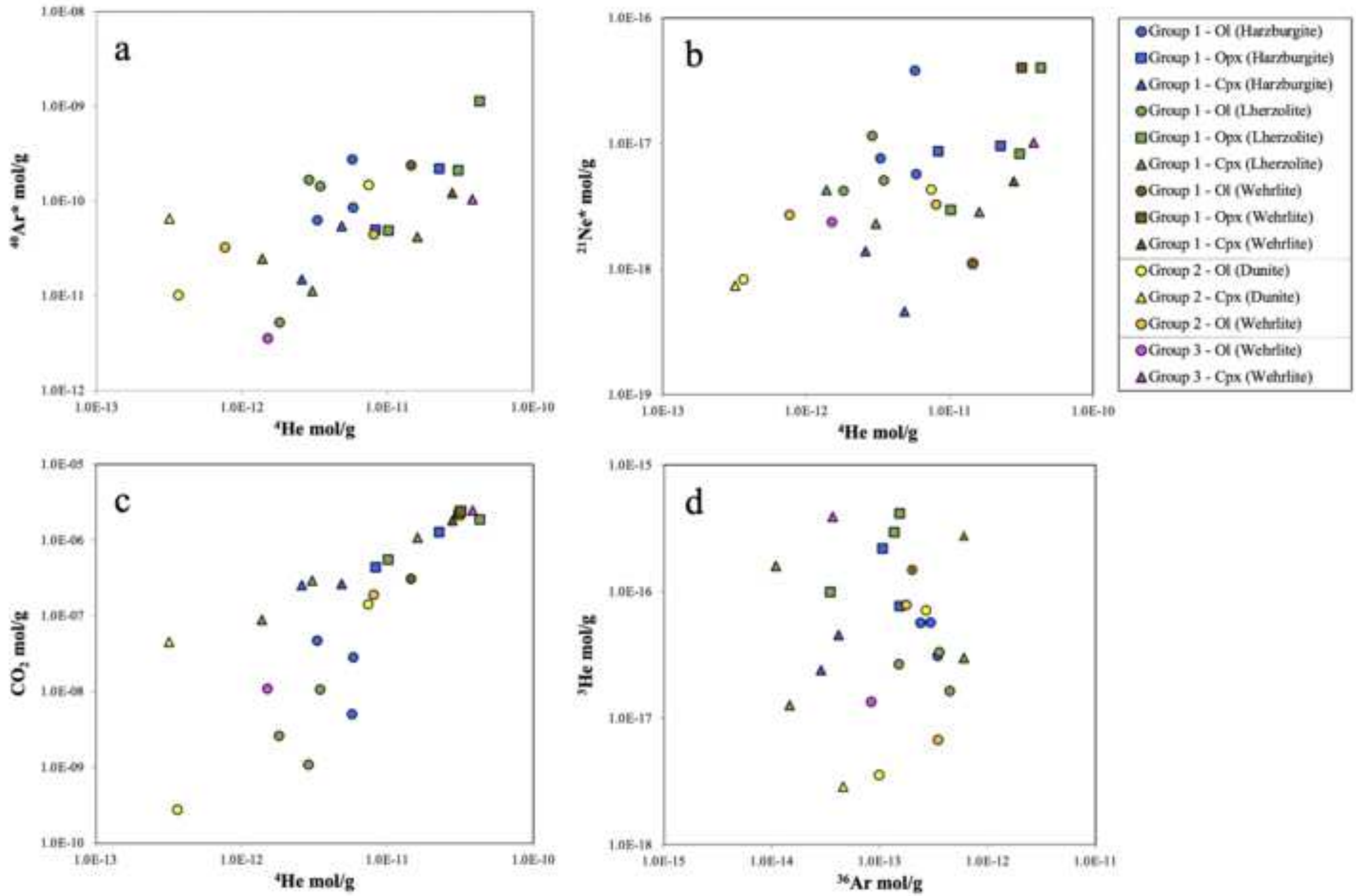

Figure 5

Click here to access/download;Figure;Fig.5.tiff

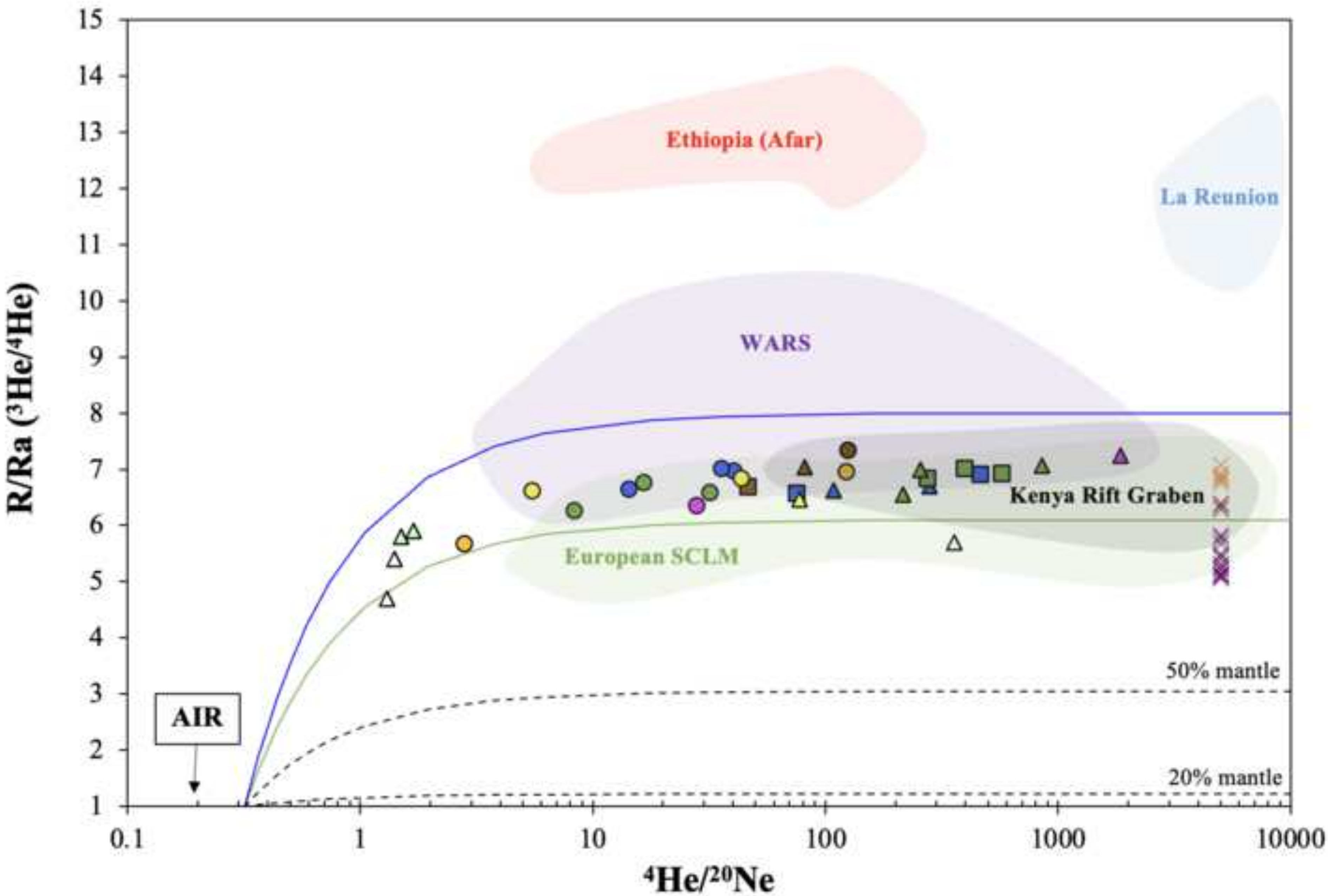

Figure 6

Click here to access/download;Figure;Fig.6.tiff

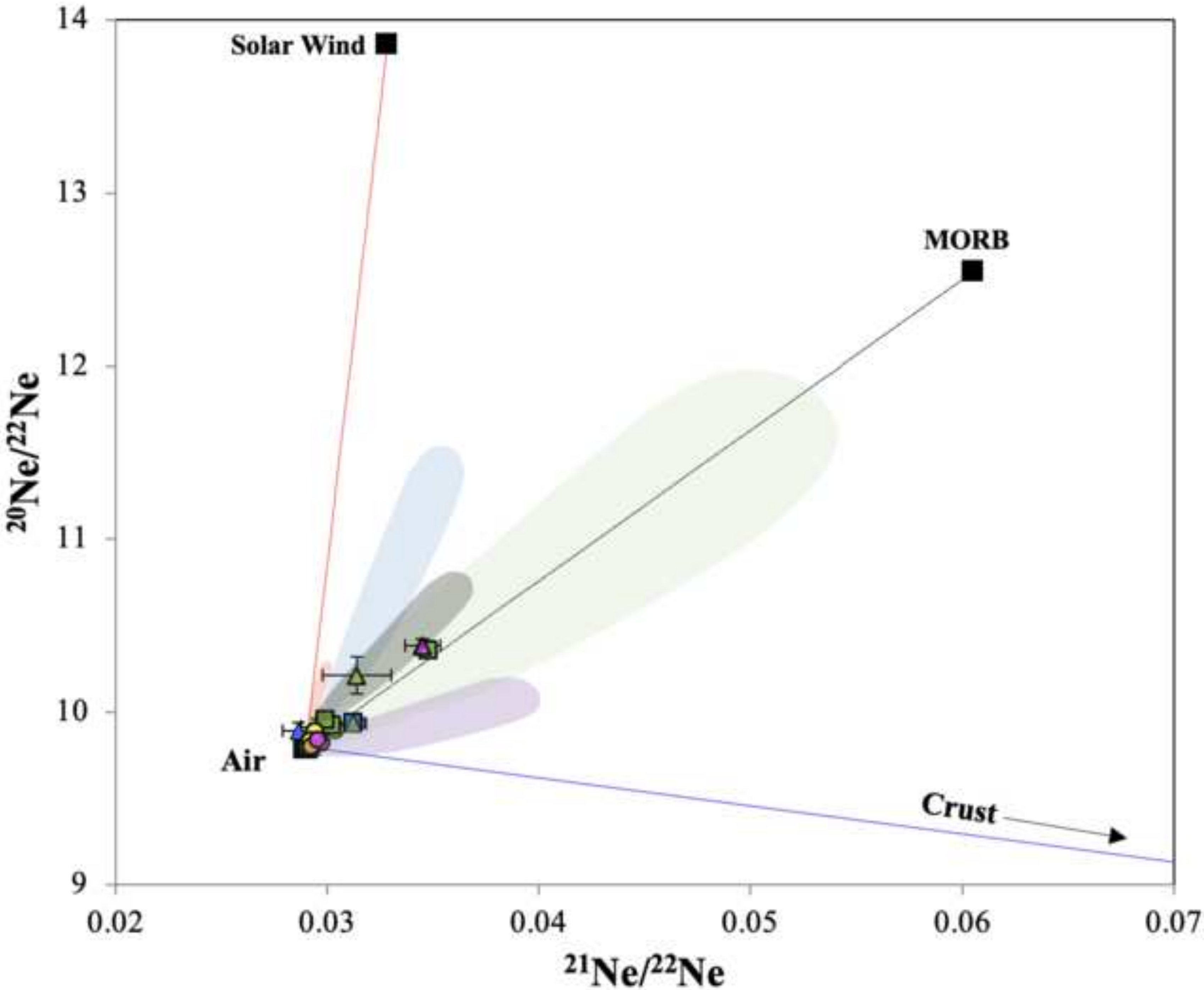

Figure 7

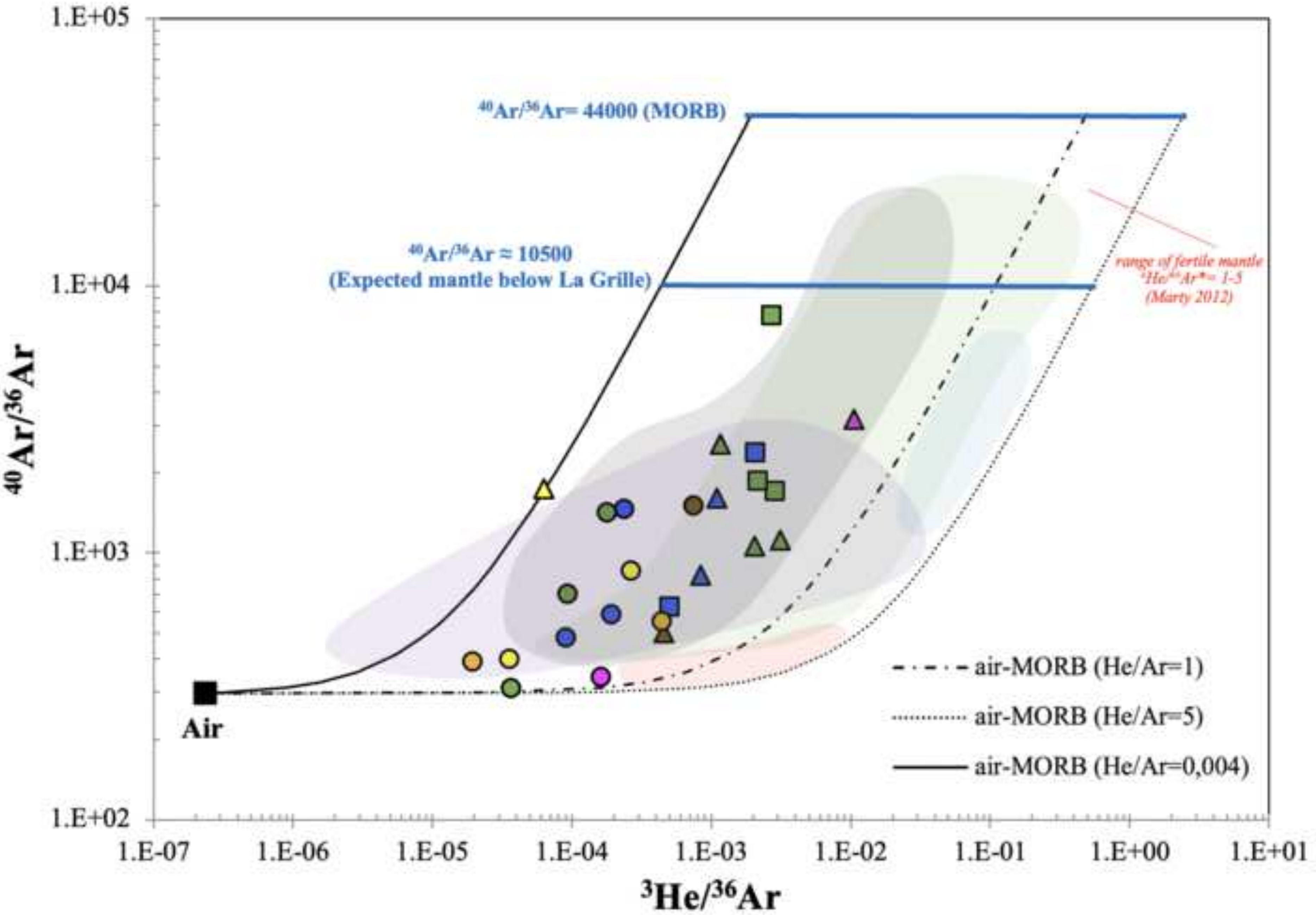

1.E+05
1.E+04
1.E+03
1.E+02
$^{40}Ar/^{36}Ar$
$^{40}Ar/^{36}Ar$= 44000 (MORB)
$^{40}Ar/^{36}Ar \approx$ 10500
(Expected mantle below La Grille)
range of fertile mantle
(Marty 2012)
Air
air-MORB (He/Ar=1)
air-MORB (He/Ar=5)
air-MORB (He/Ar=0,004)
1.E-07
1.E-06
1.E-05
1.E-04
1.E-03
1.E-02
1.E-01
1.E+00
1.E+01
$^{3}He/^{36}Ar$

Figure 8

Click here to access/download;Figure;Fig.8.tiff

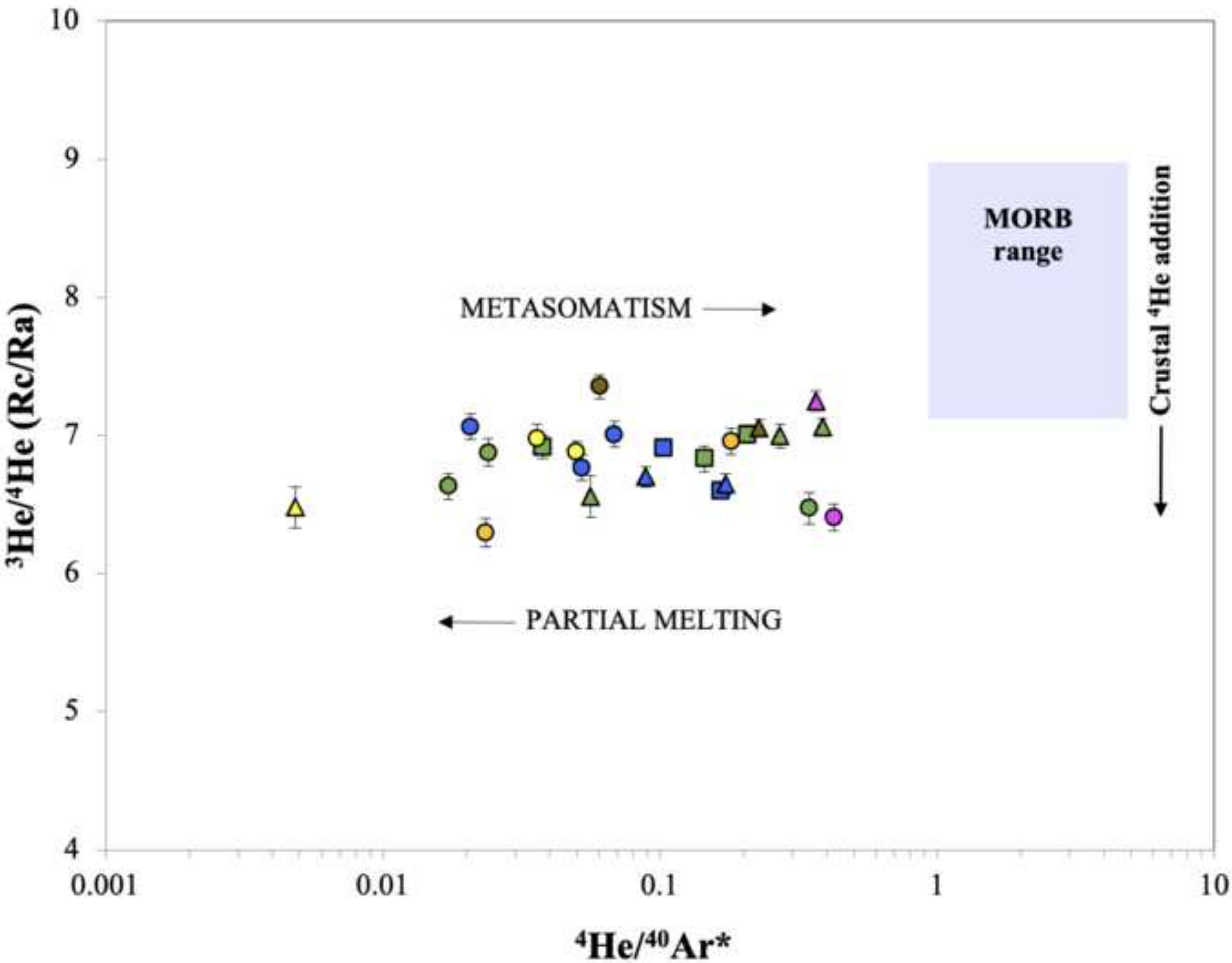

Figure 9

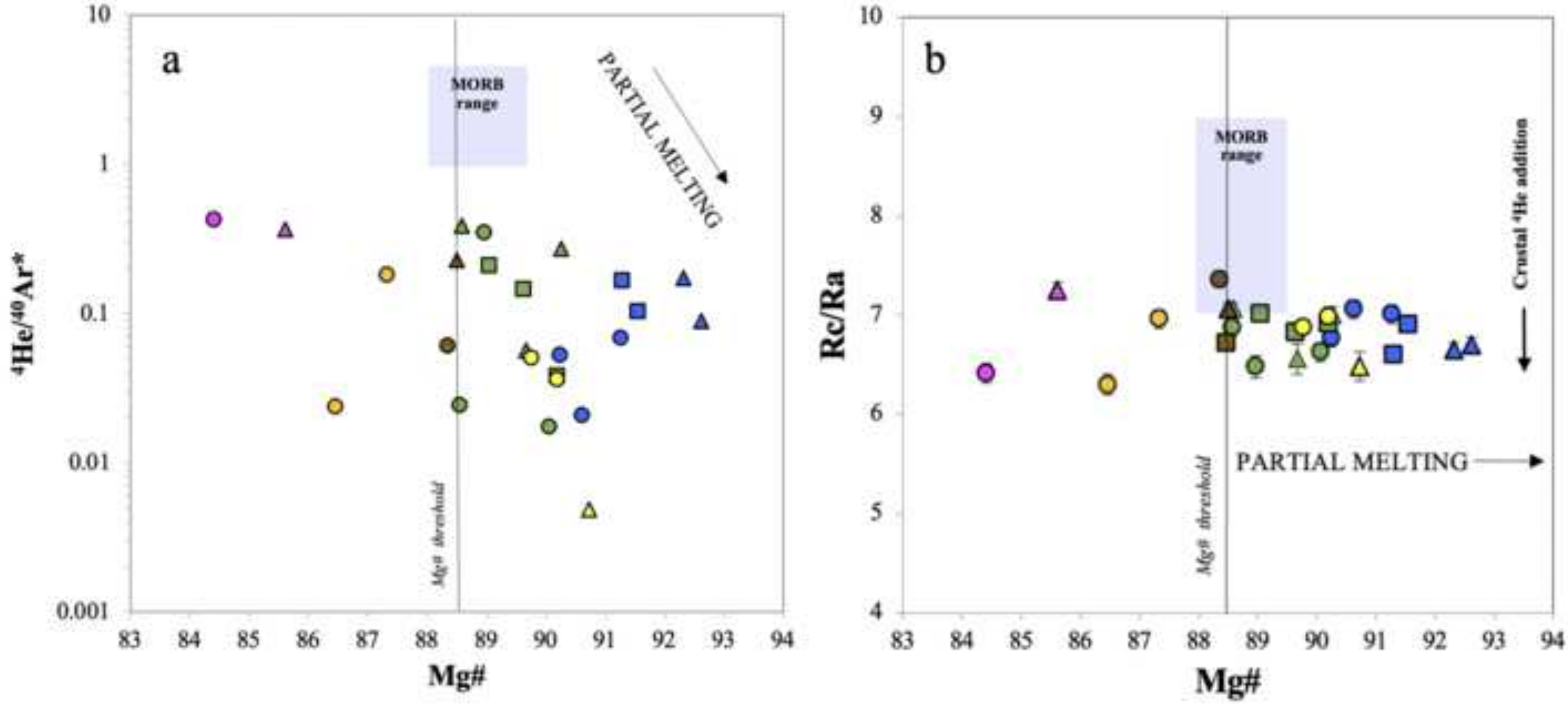
a
MORB range
PARTIAL MELTING
Mg# threshold
$^4He/^{40}Ar^*$
10
1
0.1
0.01
0.001
83 84 85 86 87 88 89 90 91 92 93 94
Mg#
b
MORB range
Crustal ^4He addition
PARTIAL MELTING
Mg# threshold
Rc/Ra
10
9
8
7
6
5
4
83 84 85 86 87 88 89 90 91 92 93 94
Mg#

Figure 10

Click here to access/download;Figure;Fig.10.tiff

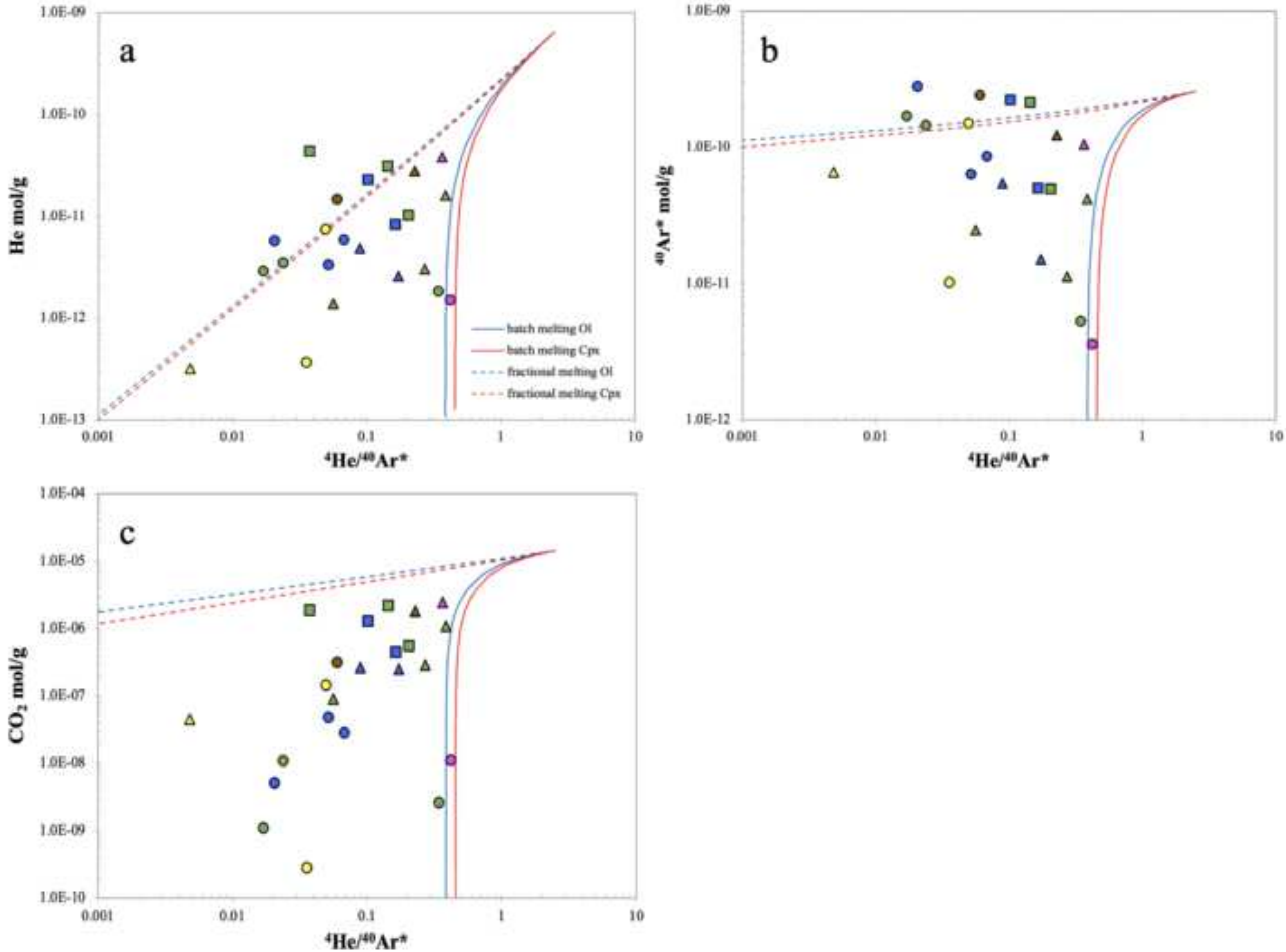

Figure 11 Click here to access/download;Figure;Fig.11.tiff

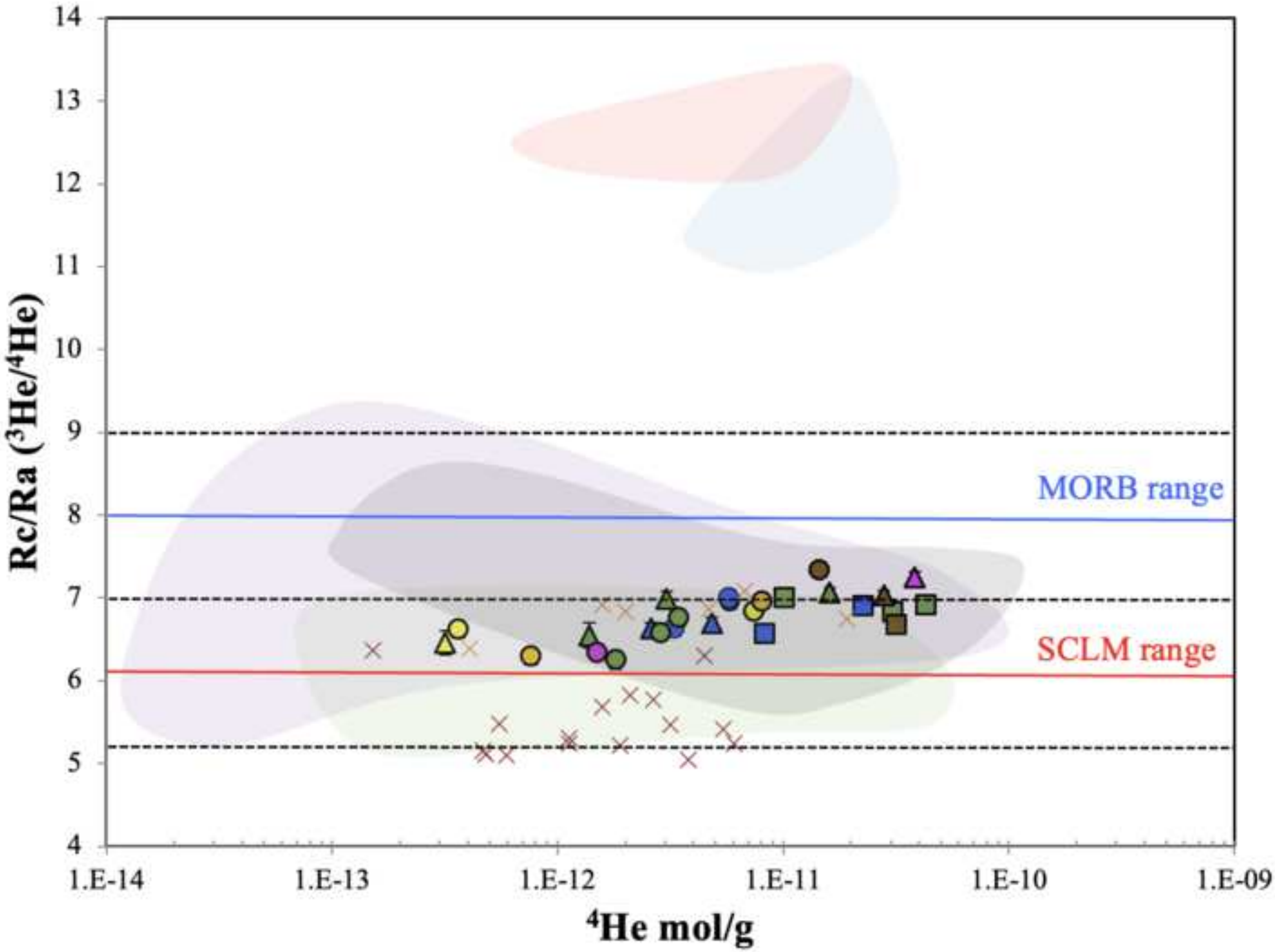

Figure 12

Click here to access/download;Figure;Fig.12.tiff

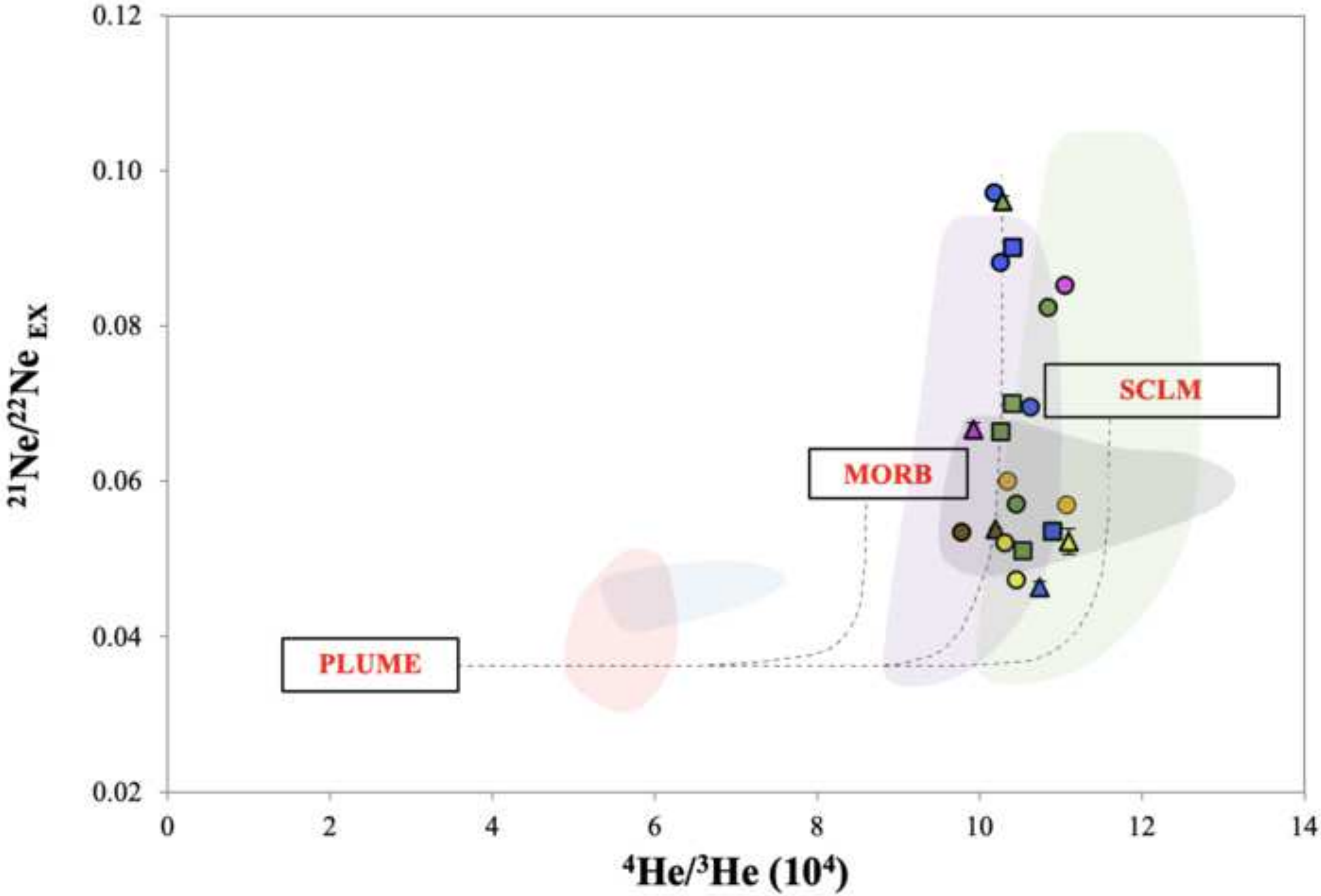

Figure 13a

Click here to access/download;Figure;Fig.13a.tiff

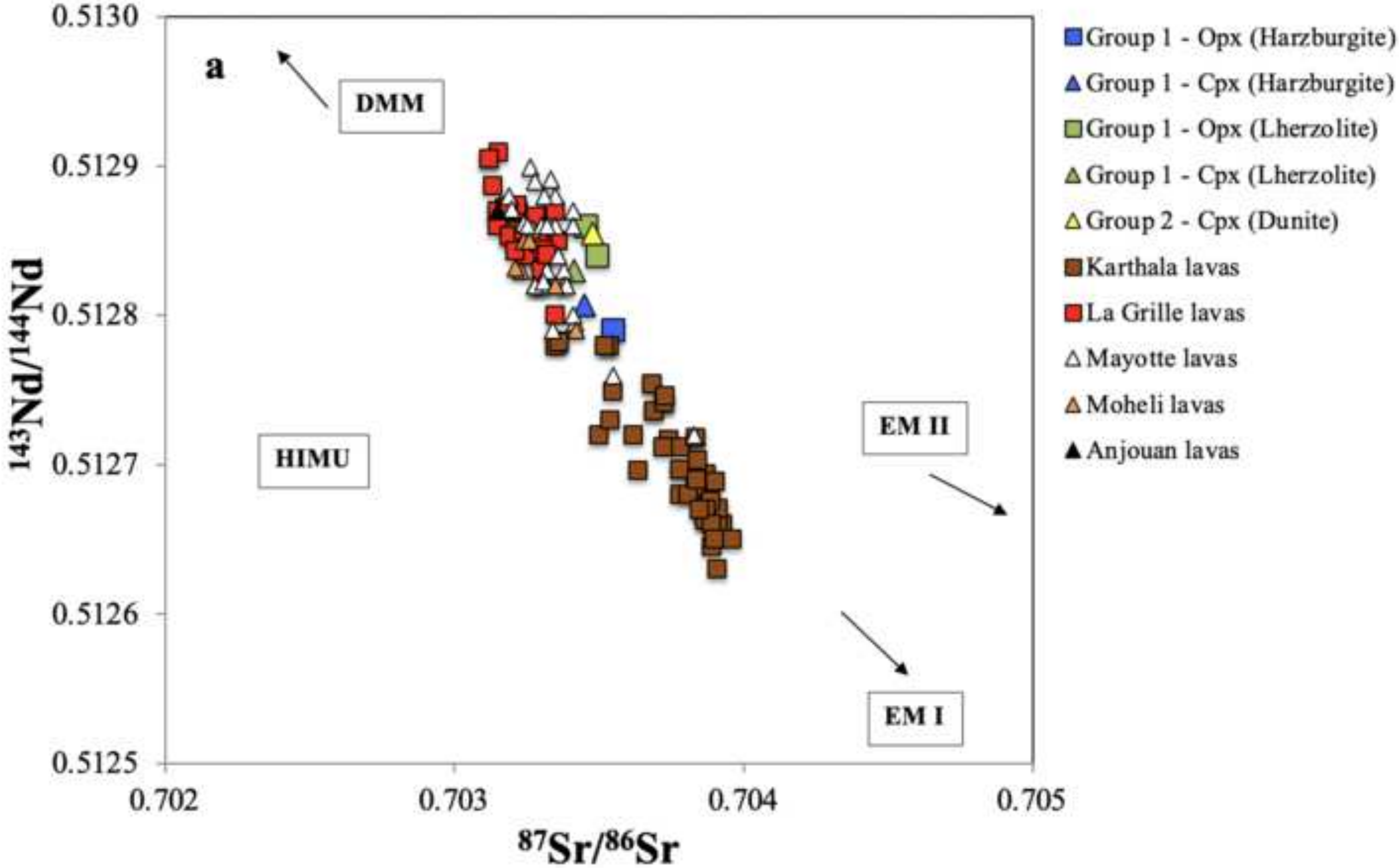

Figure 13b

Click here to access/download;Figure;Fig.13b.tiff

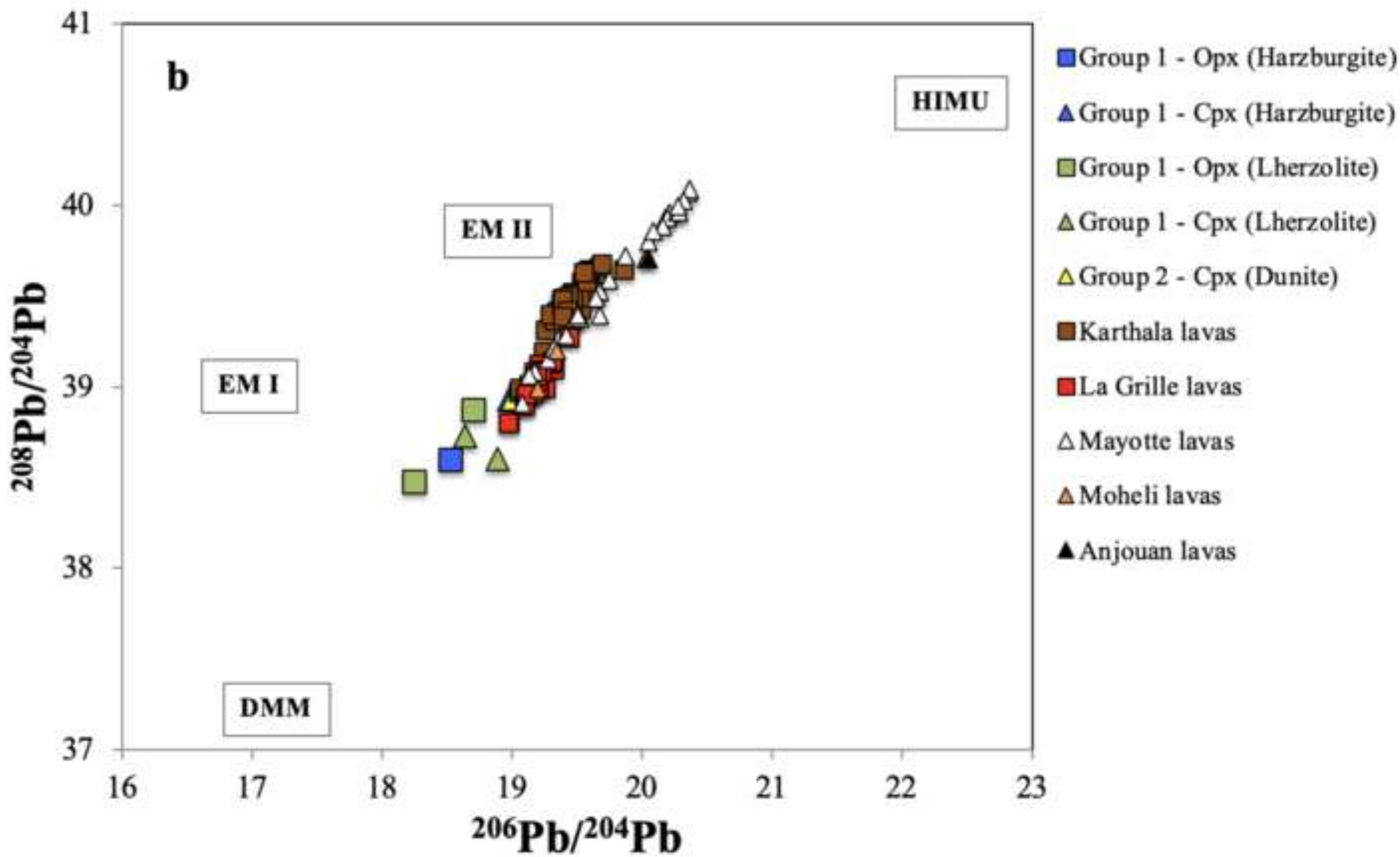

Figure 14a

Click here to access/download;Figure;Fig.14a.tiff

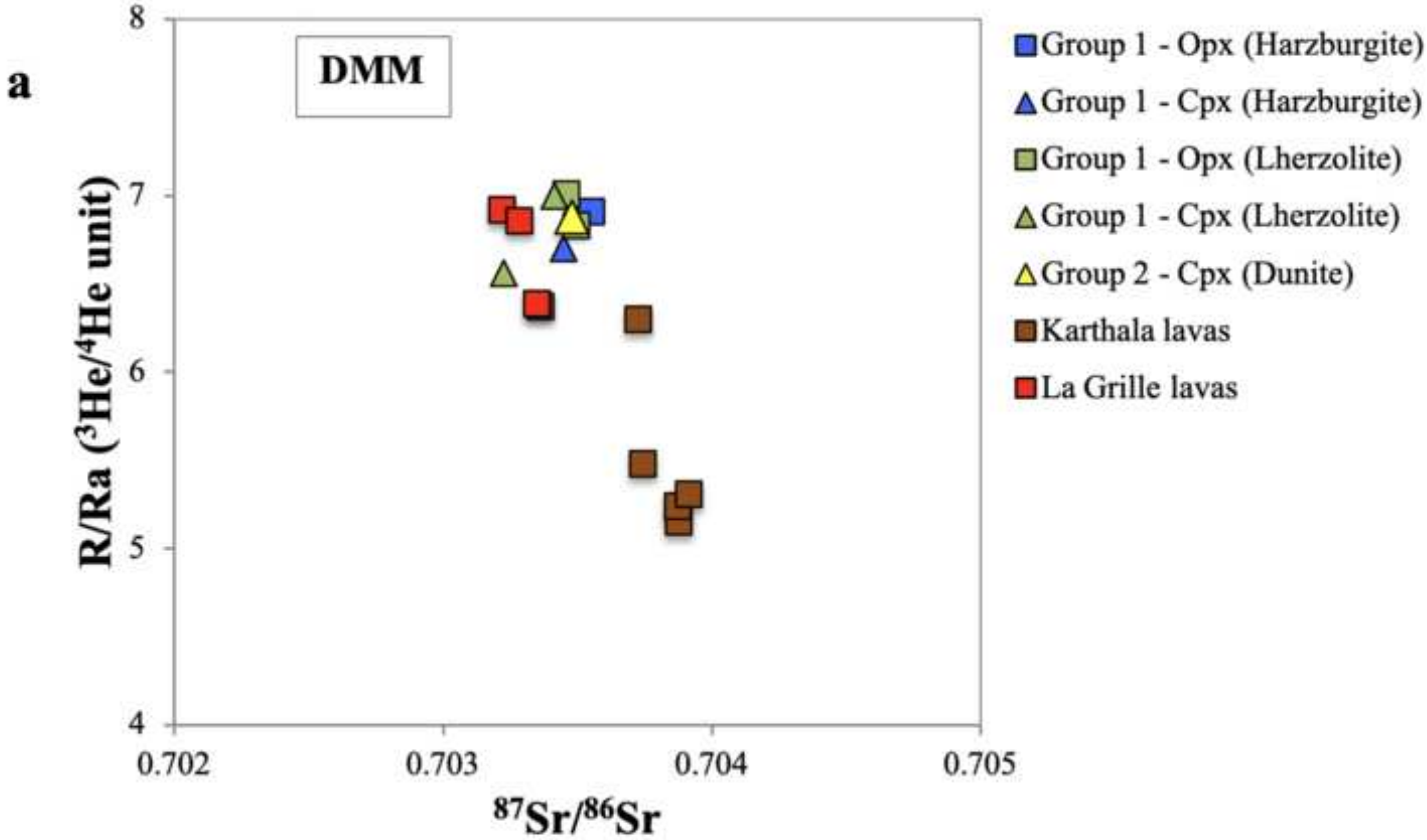

Figure 14b

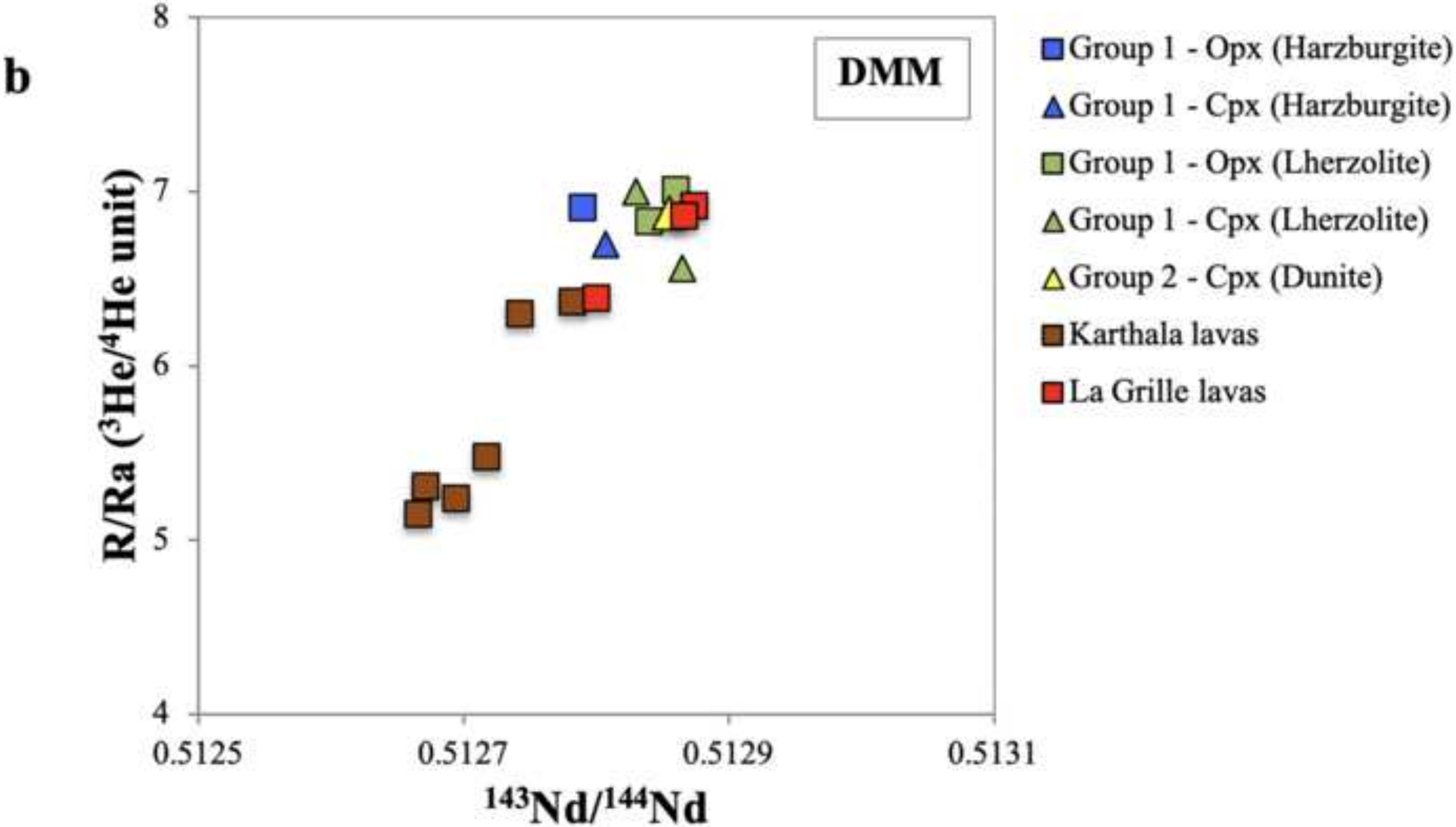

b
DMM
8
7
6
5
4
0.5125
0.5127
0.5129
0.5131
R/Ra ($^3He/^4He$ unit)
$^{143}Nd/^{144}Nd$
Group 1 - Opx (Harzburgite)
Group 1 - Cpx (Harzburgite)
Group 1 - Opx (Lherzolite)
Group 1 - Cpx (Lherzolite)
Group 2 - Cpx (Dunite)
Karthala lavas
La Grille lavas

Figure 14c

Click here to access/download;Figure;Fig.14c.tiff

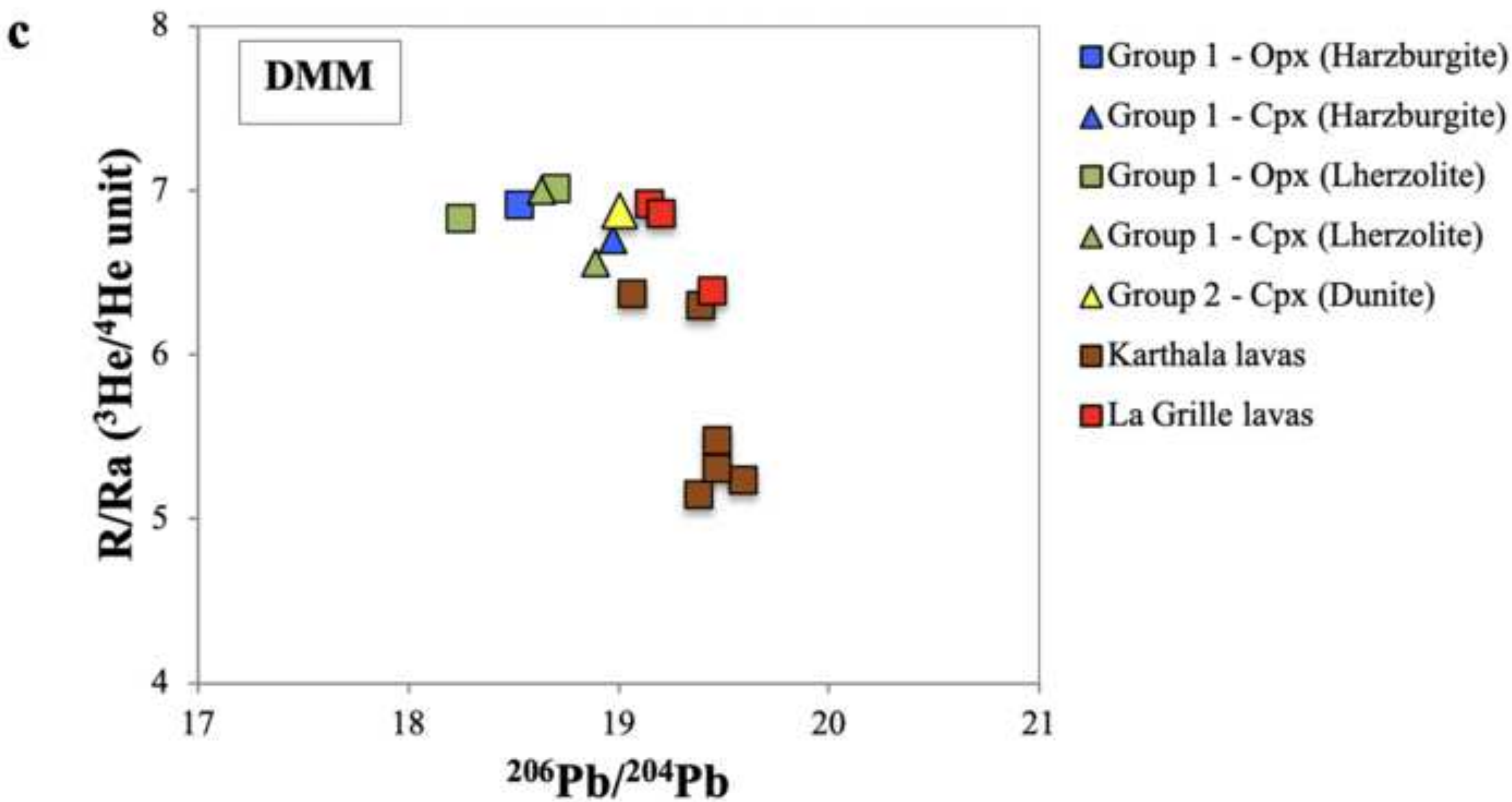

Figure 15

Click here to access/download;Figure;Fig.15.tiff

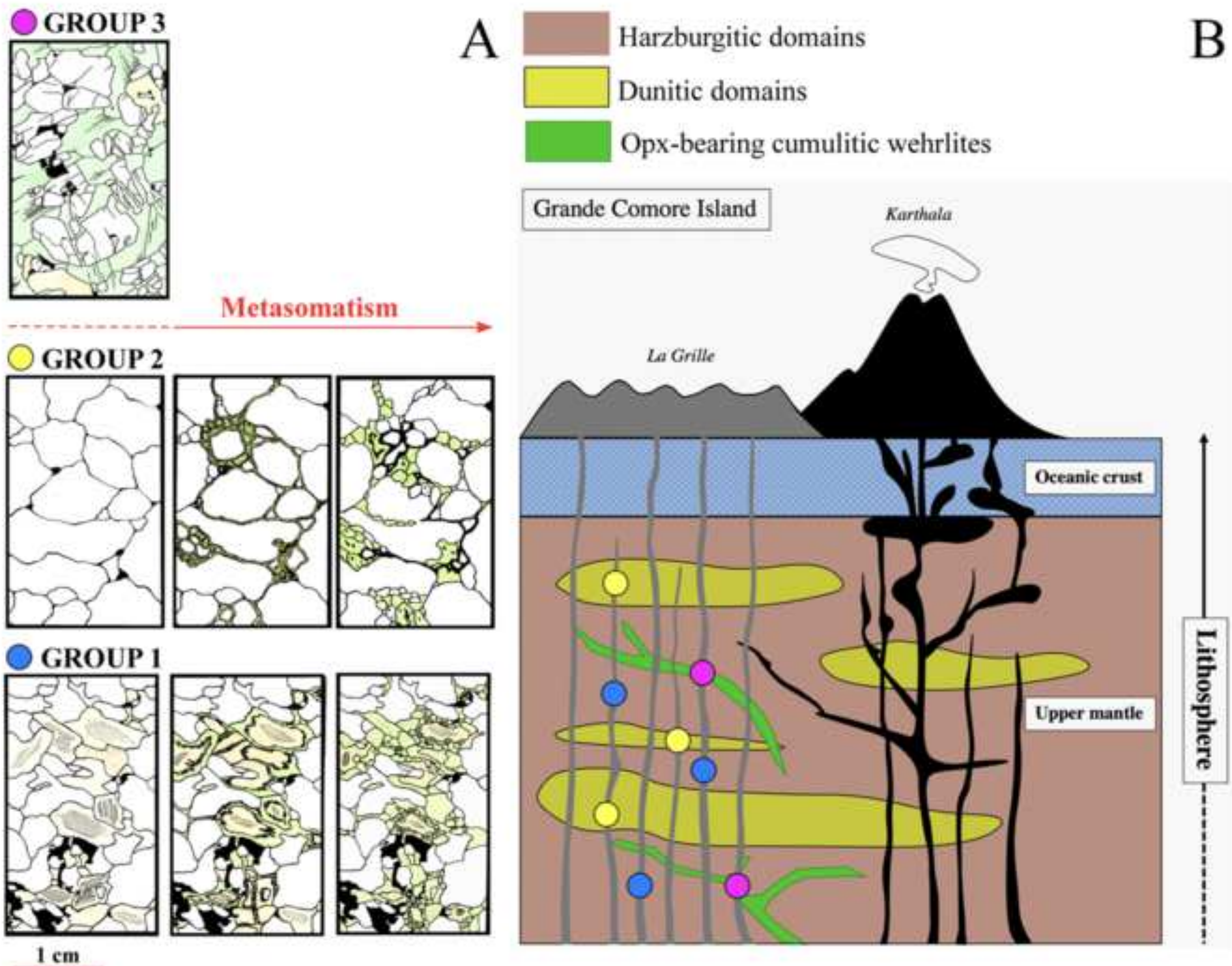

Table 1. Sample name, rock classification, group type, texture, modal estimates of La Grille ultramafic xenoliths. The equilibrium temperature and oxygen fugacity together with the standard deviation (StD) are reported for each sample. Temperature was calculated from [1]**Ballhaus et al., 1991** and [2]**Brey and Kohler, 1990** thermometers. Oxygen fugacity relative to the Fayalite-Magnetite-Quartz (FMQ) buffer was computed from [1]**Ballhaus et al., 1991** and [3]**Miller et al., 2016** oxybarometers. Hz, harzburgite; Lh, lherzolite; Whe, wehrlite; Dn, dunite; Ol, olivine; Opx, orthopyroxene; Cpx, clinopyroxene; Sp, spinel; Gl, glass.

Sample	Rock type	Group	Texture	Phase modal abudance					Thermal and redox state							
				Ol	Opx	Cpx	Sp	Gl	T°C[1]	Std	T°C[2]	Std	fO_2[1]	Std	fO_2[3]	Std
NDR1	Weh	2	Ad-cumulitic, infiltrated	86	0	11	2	1	1117	51			0.09			
NDR2	Lh	1	Coarse-grained protogranular	69	15	12	3	1	1061/1242	8/11	1129	26	-0.67/-0.37	0.02/0.02	-0.68	0.19
NDR5	Weh	1	Coarse-grained protogranular	70	5	20	4	1	1075	21	1033	14	-029	0.05	-0.25	0.03
NDR6	Lh	1	Coarse-grained protogranular	58	29	10	3	1	no spinel analyzed		1139	49				
NDR7	Lh	1	Coarse-grained protogranular-porphyroclastic	67	16	13	2	2	933	9	930	80	-0.93	0.03	-0.81	0.06
NDR8	Weh	2	Ad-cumulitic, infiltrated	87	0	10	2	1	no spinel analyzed							
NDR9	Hz	1	Coarse-grained protogranular	81	13	4	2	1	974	58	1110	10	-0.40	0.05	-0.17	0.04
NDR11	Hz	1	Coarse-grained protogranular	81	14	3	2	0	1142	13	1013	62	0.05	0.09	0.31	0.08
NDR12	Weh	3	Orthocumulitic	40	5	53	1	1	1091	27	1136	11	-0.65	0.11	-1.07	0.07
NDR13	Hz	1	Coarse-grained protogranular	85	10	2	1	1	1113	23	1093	44	-0.64	0.12	-0.35	0.11
NDR14	Dn	2	Ad-cumulitic, infiltrated	87	0	4	0	6	1180	76			0.71	0.13		
NDR16	Dn	2	Mosaic equigranular, infiltrated	91	0	4	0	5	no spinel analyzed							

Click here to access/download

Supplementary material/Appendix (Files for online publication only)

6. ESM Figures.pdf

Declaration of interests

☒The authors declare that they have no known competing financial interests or personal relationships that could have appeared to influence the work reported in this paper.

☐The authors declare the following financial interests/personal relationships which may be considered as potential competing interests: